

VIETNAM NATIONAL UNIVERSITY HO CHI MINH CITY
UNIVERSITY OF TECHNOLOGY
FACULTY OF TRANSPORTATION ENGINEERING
DEPARTMENT OF AEROSPACE ENGINEERING

-----oo-----



GRADUATION THESIS

**AERODYNAMICS STUDY OF VERTICAL AXIS WIND
TURBINE USING BLADE ELEMENT METHOD**

(Nghiên cứu tuabin gió trực đứng theo lý thuyết phần tử cánh)

Student. **Mai Nguyễn Văn**

Student ID. **G1304756**

Instructors. **Assoc. Prof. Nguyễn Thiện Tông**

Dr. Lê Thị Hồng Hiếu

Ho Chi Minh City, December 2017

(Intentionally left blank)

Commitment

I am MAI Nguyen Van. I commit that.

- This graduation thesis is completed by myself the work in it are my own
- Results presented in this thesis are truthful and they have not been published in any official work before.
- Quotations and results data used for comparison in this thesis are cited and has the highest accuracy in the range of my knowledge.

(Intentionally left blank)

Acknowledgements

This thesis marks the end of my study in Aerospace Engineering at the Department of Aerospace Engineering at Ho Chi Minh University of Technology. In this thesis, I work on aerodynamics aspect of vertical axis wind turbine and produce performance prediction of the turbine.

The creation of this thesis has been a long and challenging process, which would not have been possible without the help and support of some people. First, my sincere gratitude is for my thesis instructors Prof. Nguyen Thien Tong and Dr. Le Thi Hong Hieu for their valuable guidance, direction and providing invaluable pieces of advice throughout the progress of this thesis. Second, I wish to thank all lectures and members from Faculty of Transportation Engineering and Department of Aerospace Engineering, who have offered me opportunities to work with as well as provided healthy educational environment and sound knowledge to improve myself. Third, I am grateful to all of those with whom I have had the pleasure to work during this and other related projects. Finally, my acknowledgment goes to my fellow classmates Mr. Tran Hoai Bao and Mr. Tran Khanh Thien for sharing thoughts and cooperating in some parts of this thesis.

This thesis's formatting was based on the template of Mr. Bui Nha Dat's graduation thesis.

Mai Nguyen Van
Ho Chi Minh City, December 2017

Intentionally left blank

Abstract

The use of wind energy for energy generation is one of the oldest methods for harnessing renewable energy.

Renewable energy sources such as wind energy, tidal energy etc. is abundant and can help in reducing the dependency on fossil fuels. With increased concern for environment now days led to the research for more environment friendly sources of energy and with this considerations wind energy can be considered as a viable option in this regard. Though Horizontal Axis Wind Turbine (HAWT) is more popular but needs high wind speed to generate energy. On the other hand, Vertical Axis Wind Turbine (VAWT) needs low wind speed and can be installed in a larger range of venues. This thesis combines momentum theory and blade element method to investigate aerodynamics aspect of the turbine with three streamtube models in order to yield turbine performance predictions. Finite aspect ratio effect is also considered to enhance the prediction accuracy. The forecasted results will subsequently be compared with other numerical simulation and experimental results.

Keyword. wind energy, vertical axis wind turbine, double multiple streamtube, blade element method, momentum theory, multiple streamtube, single streamtube, power prediction...

Table of Contents

Commitment	iii
Acknowledgements	v
Abstract	vii
Table of Contents	viii
Nomenclature	x
Abbreviations	x
Symbols	xi
Subscripts	xii
List of Figures	xiii
List of Tables	xvii
Chapter 1. INTRODUCTION	1
1.1 Alternative Energy	1
1.2 Wind Energy	1
1.3 Wind Energy Utilization	2
1.4 Wind Energy in Asia	2
1.5 Wind Energy in Vietnam	4
1.6 Objectives of the Thesis	6
1.7 Outline of the Thesis	7
Chapter 2. LITERATURE REVIEW	8
2.1 Introduction	8
2.2 Configurations	10
2.2.1 Darrieus type wind turbine	10
2.2.2 Egg-beater type Darrieus wind turbine	10
2.2.3 Giromill (straight bladed type Darrieus wind) turbine	11
2.2.4 Twisted bladed (Helical) Darrieus rotor	12
2.3 Savonius Rotor	13
2.4 Combined Savonius and Darrieus Rotor	14
2.5 Design Techniques of Vertical Axis Wind Turbine	14
2.5.1 Efficiency	14
2.5.2 Aerodynamic load calculations	15
2.5.3 Flow field visualization and analysis	17
Chapter 3. AERODYNAMICS OF VAWT	18
3.1 Aerodynamics Principles of Straight Blade VAWT	18
3.2 Aerodynamics Prediction Model for VAWT	20
3.3 One-Dimensional Momentum Theory (Single Actuator Disk Theory) and the Betz Limit	22
3.4 Double Actuator Disk Theory	26
3.5 Blade Element Theory	29
3.6 Single Streamtube Model	31
3.7 Multiple Streamtube Model	37
3.8 Double-Multiple Streamtube Model	44

3.8.1	Aerodynamic Model	45
3.8.2	Upwind Half of the Rotor	46
3.8.3	Downwind Half of the Rotor	49
3.9	Finite Aspect Ratio Effect	55
Chapter 4.	RESULTS VALIDATION AND DISCUSSION	57
4.1	Comparison with Numerical Simulation	57
4.2	Comparison with CFD Simulation	63
4.3	Comparison with Experimental Force Data	65
4.3.1	The 12 kW turbine	65
4.3.2	Sandia 17-m VAWT	67
4.4	Comparison with Experimental Performance Data	72
4.4.1	Uppsala University VAWT H-rotor.....	72
4.4.2	VAWT Ltd 260H	75
4.4.3	VAWT Ltd 850H.....	77
Chapter 5.	PREDICTION CALCULATION FOR DESIGNING	80
5.1	Prediction Using Single Streamtube with Betz Limit	80
5.2	Power Prediction Using Two Multiple Streamtube Model	84
5.3	Effect of Pitch Angle.....	89
Chapter 6.	CONCLUSIONS.....	94
6.1	Achievements and Limitations	94
6.2	Suggestions for Future Work	94
References		96
Appendix		99

Nomenclature

Abbreviations

HAWT	Horizontal axis wind turbine
VAWT	Vertical axis wind turbine
Ltd	Limited
CFD	Computational fluid dynamics
FiT	Feed-in tariff
CAD	Computer-aided design
GW	Gigawatt
EVN	Electricity of Vietnam
MW	Megawatt
AR	Aspect ratio
2D	Two-dimensional
3D	Three-dimensional
TSR	Tip speed ratio
AOA	Angle of attack
DMST	Double multiple streamtube
MST	Multiple streamtube

Symbols

P	Power	W
P_i	Instantaneous power	W
Re	Reynolds number	--
ρ	Air density	kg/m ³
σ	Rotor solidity	--
V	Velocity at blade element	m/s
V_∞	Free stream velocity	m/s
V_w	Wake velocity	m/s
W	Blade relative velocity	m/s
t/c	Airfoil thickness chord ratio	--
c	Blade chord	m
N	Number of blades	--
H	Rotor height	m
D	Rotor diameter	m
θ	Azimuthal angle (position)	rad
$\Delta\theta$	Streamtube angular interval	rad
ω	Rotational velocity	rad/s or RPM
C_P	Power coefficient	--
C_{P_i}	Instantaneous power coefficient	--
C_L	Lift coefficient	--
C_D	Drag coefficient	--
C_N	Normal force coefficient	--
C_T	Tangential force coefficient	--
C_{Ti}	Instantaneous thrust coefficient	--
T_i	Instantaneous thrust	N

C_{Thrust}	Thrust coefficient	--
Q	Rotor torque	Nm
Q_i	Instantaneous torque	Nm
T_{mt}	Momentum theory thrust	N
$C_{T_{mt}}$	Momentum theory thrust coefficient	--
a	Induction/induced factor	--
ν	Air kinematic viscosity	m^2/s
η	Non-dimensional rotor height	--

Subscripts

- ∞ Far field free stream condition
- i Instantaneous value
- $'$ Downstream value

List of Figures

Figure 1.1. Global Cumulative Capacity of Wind Energy (GWEC 2012) [1]..	2
Figure 1.2. Annual Market Forecast By Region 2017-2021 [2].	3
Figure 1.3. Cumulative Market Forecast By Region 2017-2021 [2].	3
Figure 1.4. Target by technology in 2020, 2025 and 2030 [2].....	5
Figure 1.5. Vietnamese FiT for Wind and Solar Energy [3].....	6
Figure 2.1. An ancient windmill in the British Isles [5].....	8
Figure 2.2. Merits of vertical axis wind turbines over horizontal axis wind turbines [6].....	9
Figure 2.3. Original illustrations by G.J.M. Darrieus in 1931 patent [7].....	10
Figure 2.4. Darrieus rotor – egg beater shaped wind turbine [6].	11
Figure 2.5. Darrieus rotor – straight bladed wind turbine [6].	12
Figure 2.6. Helical H-rotor wind turbines by QuietRevolution and Turby [7].	13
Figure 2.7. Savonius rotor [6].	13
Figure 2.8. Combined Savonius and Darrieus rotor [6].	14
Figure 3.1. Straight blade Darrieus type VAWT [7].....	18
Figure 3.2. VAWT flow velocities and blade [8].....	18
Figure 3.3. Overview of the development of the streamtube models [9].....	22
Figure 3.4. Actuator disc model of a wind turbine (modified from [9])......	23
Figure 3.5. Operating parameters for a Betz turbine (modified from [10]). ...	26
Figure 3.6. A pair of actuator disks in tandem (modified from [9]).	27

Figure 3.7. Force coefficients of a blade element airfoil [8].	30
Figure 3.8. Forces on a blade element airfoil in a horizontal plane (modified from [8])......	31
Figure 3.9. Velocities diagram (modified from [10]).	32
Figure 3.10. Multiple streamtube geometry (modified from [10]).	37
Figure 3.11. Thrust force coefficient as a function of induced factor a	43
Figure 3.12. Plan view of VAWT [8].	45
Figure 3.13. Rotor element ABCD replaced by two actuator disks in tandem (modified from [8]).	46
Figure 3.14. Angles, forces and velocity vectors at the equator [8].	47
Figure 4.1. Tangential force coefficient from two calculation at $TSR = 4.6$	58
Figure 4.2. Tangential force coefficient from two calculation at $TSR = 3.7$	58
Figure 4.3. Normal force coefficient from two calculation at $TSR = 4.6$	59
Figure 4.4. Normal force coefficient from two calculation at $TSR = 3.7$	59
Figure 4.5. Normal force coefficient from two calculation at $TSR = 3.09$	60
Figure 4.6. Normal force coefficient from two calculation at $TSR = 2.49$	60
Figure 4.7. Local AOA from two calculation at $TSR = 4$, $\omega = 33 RPM$	62
Figure 4.8. Tangential force coefficient from two calculation at $TSR = 4$, $\omega = 33 RPM$	62
Figure 4.9. Power curves from reference data with thesis calculation with 2 model.....	63
Figure 4.10. Power curves comparision with CFD data	64
Figure 4.11. The 12 kW turbine, designed and built at the Division of Electricity at Uppsala University [13].	65

Figure 4.12. Comparison of measured data from [13] and simulations of <i>CFN</i> at $TSR = 3.44, \omega = 64.8 RPM$	66
Figure 4.13. Comparison of measured data from [18] and simulations of <i>CFN</i> at $TSR = 3.6, \omega = 50.6 RPM$	66
Figure 4.14. Comparison of measurement data from [18] and simulations of <i>CFN</i> at $TSR = 3.58, \omega = 64.67 RPM$	67
Figure 4.15. Tangential force coefficient at $TSR = 4.6$	68
Figure 4.16. Tangential force coefficient at $TSR = 3.7$	69
Figure 4.17. Tangential force coefficient at $TSR = 3.09$	69
Figure 4.18. Tangential force coefficient at $TSR = 2.49$	70
Figure 4.19. Normal force coefficient at $TSR = 4.6$	70
Figure 4.20. Normal force coefficient at $TSR = 3.7$	71
Figure 4.21. Normal force coefficient at $TSR = 3.09$	71
Figure 4.22. Normal force coefficient at $TSR = 2.49$	72
Figure 4.23. The 12 kW turbine, designed and built at the Division of Electricity at Uppsala University [13].	73
Figure 4.24. Power curves of Uppsala University VAWT H-rotor	74
Figure 4.25. Power curves of Uppsala University VAWT H-rotor with finite AR effect	74
Figure 4.26. Power curves of VAWT Ltd 260H	76
Figure 4.27. Power curves of VAWT Ltd 260H with finite AR effect	76
Figure 4.28. Power curves of VAWT Ltd 850H	78
Figure 4.29. Power curves of VAWT Ltd 850H with finite AR effect	78
Figure 5.1. Induction factor α in Betz's limit at different azimuthal position.	80

Figure 5.2. Optimum power coefficient at different TSR using Betz assumption	82
Figure 5.3. Optimum solidity at different TSR using Betz assumption	82
Figure 5.4. C_p curves with different CD characteristic	83
Figure 5.5. Solidity graphs wth different CD chacteristic	83
Figure 5.6. Power curves prediction with Double Multiple Streamtube model	84
Figure 5.7. Power curves prediction with Multiple Streamtube model	85
Figure 5.8. Solidity graphs wth different CD chacteristic with finite AR effect	86
Figure 5.9. Blade pitch angle's sign convention (modified from [17]).	89
Figure 5.10. Performance curves for varied pitch angle at $V\infty = 4 \text{ m/s}$	91
Figure 5.11. Performance curves for varied pitch angle at $V\infty = 6 \text{ m/s}$	91
Figure 5.12. Performance curves for varied pitch angle at $V\infty = 8 \text{ m/s}$	92
Figure 5.13. Performance curves for varied pitch angle at $V\infty = 10 \text{ m/s}$	92

List of Tables

Table 3.1. Notations	19
Table 3.2. Values of power coefficient versus induction factor.....	26
Table 3.3. Antonations	27
Table 3.4. Sign convention for forces on a blade element	30
Table 3.5. Synthesized equations and step for calculations	36
Table 3.6. Synthesized equations and step for calculations	43
Table 3.7. Synthesized equations and step for calculations for the whole turbine	54
Table 4.1. Sandia 17 m VAWT parameters [13], [14]	57
Table 4.2. VAWT H-260 parameters [11], [15].....	61
Table 4.3. Turbine parameters [9]	62
Table 4.4. Three-bladed wind turbine model parameter [16]	64
Table 4.5. 3D CFD simulation data (digitized form [17])	64
Table 4.6. Turbine parameters obtained from [13].	65
Table 4.7. Turbine parameters collected from [13], [14]	68
Table 4.8. Nominal properties of the wind turbines [19],[13].	73
Table 4.9. Power coefficient experimental data (digitized from [19]).....	73
Table 4.10. Geometry parameters of wind turbines [11],[15].....	75
Table 4.11. Power coefficient experimental data (digitized from [15])......	75
Table 4.12. Geometry parameters of wind turbines [11],[15].....	77
Table 4.13. Power coefficient experimental data (digitized from [15]).....	77

Table 5.1. Lift and drag coefficient characteristic	81
Table 5.2. Input parameters of designing turbine	84
Table 5.3. The result table for both methods.	86
Table 5.4. Advisable parameters for the turbine.....	86
Table 5.5. Final design parameter.....	87
Table 5.6. Turbine parameters	90
Table 5.7. Final parameters for the turbine.....	93

Chapter 1. INTRODUCTION

The continuous improvement of this world is based on technological advancement. And the technological advancement is directly related to the utilization of energy. The demand of energy is creeping up every day due to increase of population, industrial and agricultural advancement. But the conventional energy sources are becoming limited which is ultimately making them more expensive. In addition to this, everyone is concerned about global climate change. This whole scenario is pushing the world to find the alternative sources of energy.[1]

Technological corporations face the challenge of developing better technology, based on innovative solutions to reach those goals. Technology is our DNA. Changing the way energy is generated and consumed, being able to make a difference here, is our driving force.[2]

1.1 Alternative Energy

Solar and Wind power are the most popular among the various sources of renewable energy. Only these two kinds of alternative sources can generate most of the world's electricity within next 50 years, on the other hand which can also help the climate change condition. [1]

1.2 Wind Energy

Wind energy has the potential to resolve the power demand of the entire world if it can be converted into electricity efficiently. Wind is going to be the most popular alternative energy source; because of its availability throughout place and time. As a pollution free and sustainable source, wind is getting importance in energy policy too. The disadvantages are its lower efficiency and high installation cost. But the ultimate cost would be lowered if it operates continuously and small scale turbines can be installed in any corner of the world. [1]

1.3 Wind Energy Utilization

Wind is the generating electricity currently less than 3.5% of US and barely 4.5% of world electricity consumption. Though the popularity of wind as energy source is increasing rapidly but it will still generate a few portions of US and world electricity requirements by 2030. The scarcity of resources, increasing demand of energy and concern of global climate change is pushing hard to increase the efforts to find viable energy alternatives. Some of the renewable energies may not be achievable or sustainable, some are local and limited. Other than fossil fuel the only hope is solar and wind. To be the significantly larger contributor to generate global electricity, the wind power needed to be more efficient [1].

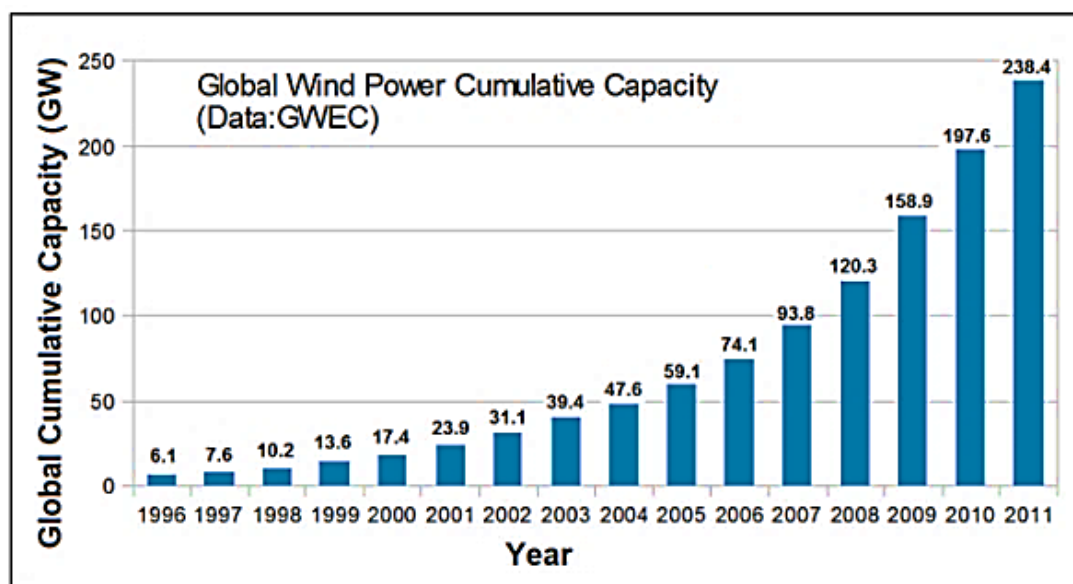


Figure 1.1. Global Cumulative Capacity of Wind Energy (GWEC 2012) [1]

1.4 Wind Energy in Asia

At 203.7 GW of installed capacity, the Asian region is the driver of the global industry, and we expect that to continue for the foreseeable future. While falling back from its record breaking 30 GW market in 2015, China posted strong installations of 23.4 GW, just ahead of 2014's market. While we expect the market to increase a bit in 2017 due to the imminent feed-in-tariff reduction (and a spurt in offshore), it is unlikely to repeat its 2015 achievement in the medium term. This is due to the heavy congestion and poor management of the overall power system

INTRODUCTION

which saw 17% of China's wind generated electricity curtailed in 2017; the flattening of demand growth in the country; and increasing solar installations. The Five-Year Plan for Energy (2016-2020) was finally published late last year, and calls for 210 GW of wind by 2020, which will almost certainly be surpassed, but not by as much as we had thought last year. While China has taken the political decision to transition away from a coal-based power system towards sustainable energy, it has some serious systemic and market issues to address before it can move much further forward. Overall, we expect the Asian market to add 154 GW in the next five years, for a total of 357 GW by the end of 2021.[2]

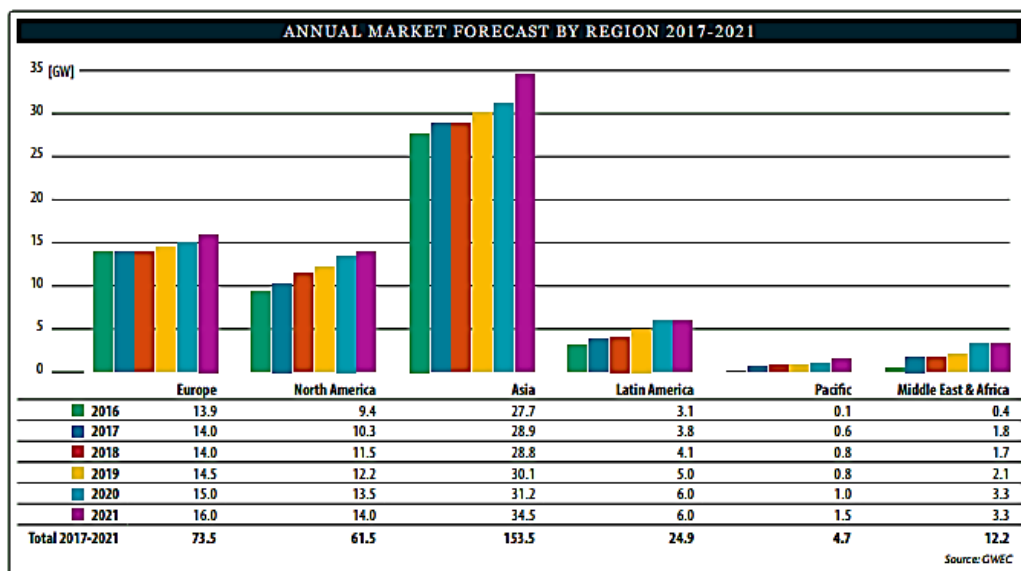


Figure 1.2. Annual Market Forecast By Region 2017-2021 [2]

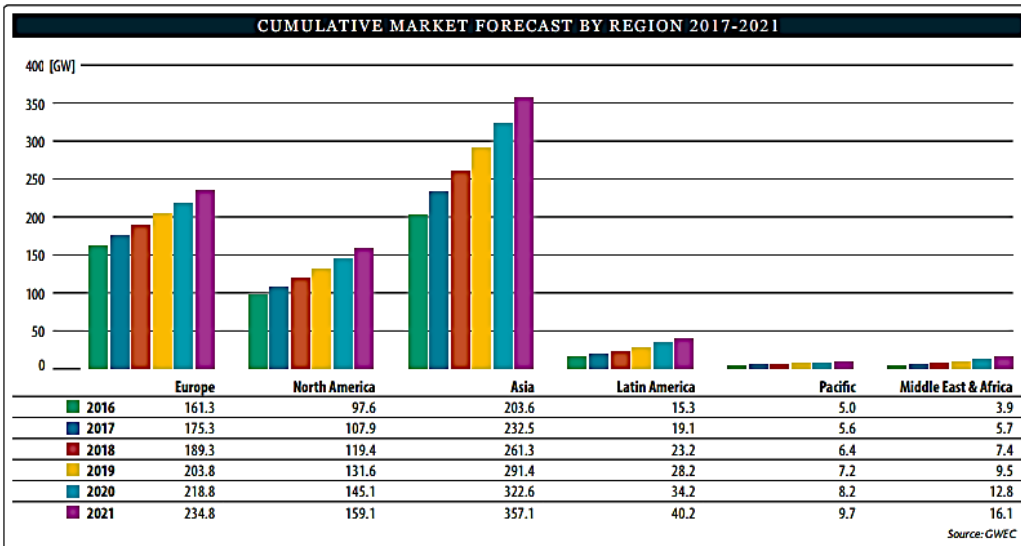


Figure 1.3. Cumulative Market Forecast By Region 2017-2021 [2]

1.5 Wind Energy in Vietnam

Vietnam's first near-shore/intertidal wind project, the 99.2 MW Bac Lieu wind farm, is Asia's first offshore wind farm in the Mekong Delta region, and came online in stages from 2013- 2015. Another nearshore wind project, the 800 MW Phu Cuong wind farm, also located in Mekong Delta, is now gearing up. The first phase, the Phu Cuong 1 Wind Farm (170 MW), is expected to reach financial close in 2018. In 2016, new projects, both onshore and offshore, were being developed in Soc Trang Province, which is emerging as the next hot spot for wind development in Vietnam. Despite slow progress to date, the Vietnamese wind market has started attracting world leading turbine manufacturers and investors. Vietnam may become the next gigawatt sized wind market in Asia, once the regulatory and financial conditions are corrected, which may come during the course of 2017.[2]

Vietnam has some of the most abundant wind resources in Southeast Asia. The country's more than 3,500 km the South China Sea, provide ideal conditions for wind power development. A study conducted by the World Bank has found that 8.6% of Vietnam's total land area has high to very high potential for large scale wind development, with average wind speeds exceeding 7 m/s. The overall onshore wind potential has been estimated at 24 GW [2].

Wind development in Vietnam is still at the early stages, with an overall capacity of 159 MW, up 24 MW from 2015. Vietnam has four wind farms. The 30 MW Tuy Phong, Phu Quy (6 MW) and Phu Lac (24 MW) wind farms in Binh Thuan province; and the 99 MW Bac Lieu wind farm in the Mekong Delta's Bac Lieu Province. The two most promising regions for wind power are Ninh Thuan and Binh Thuan provinces. Binh Thuan has a Master plan for wind power development for 2020, approved by the Ministry of Industry and Trade (MOIT).

The National Power Development Plan was introduced by the government in 2011 to enhance energy security, for the promotion of the use of renewable energy, and to further liberalize the power market. The goal of the plan is to increase electricity production from renewables to 4.5% in 2020 and 6% by 2030, from 3.5% in 2010.

This target was further revised in March 2016, introducing an interim target of 2 GW of wind by 2025

Target by technology in 2020, 2025 and 2030			
	2020 (MW)	2025 (MW)	2030 (MW)
Wind	800	2,000	6,000
Biomass	500	2,000	
Hydropower	21,600	24,600	27,800
(Pumped Storage)		1,200	2,400
Thermal Power	26,000	45,800	
Solar	850	4,000	12,000
Nuclear		46,000 (first reactor)	

Figure 1.4. Target by technology in 2020, 2025 and 2030 [2]

Estimations from an existing 2011 wind atlas cite around 24 GW of potential. Vietnam's annual electricity production increased more than tenfold, from 8.6 TWh in 1990 to 145.5 TWh in 2014 (World Bank, EVN, 2015). The annual increase in this period was between 12-15% - almost twice as high as the GDP growth rate. Vietnam's overall installed generation capacity was 34 GW in 2014.[3]

According to the National Power Development Plan (PDP VII), Vietnam aims to increase its renewable energy share in power production from 3.5% in 2010 to 4.5% in 2020 and 6% in 2030. This will bring the total wind power capacity from the current negligible level to around 1,000 MW by 2020 and around 6,200 MW by 2030.[4]

Feed-in tariff

According to the Renewable Energy Development Strategy 2016-2030, Vietnam will promote on-shore wind power until 2030 and assess the potential for offshore wind resources as an electricity solution for after 2030. Feed-in Tariffs (FiT) are proposed by the Ministry of Industry and Trade and decided on by the Prime Minister. The FiT are a crucial element in building a bankable proposition for new renewable energy projects. Vietnamese FiT are indicated in the table below.

Source	Decision	FiT	Remark
Solar	Decision No.: 11/2017/QD-TTg of April 11, 2017	VND 2,086/kWh (9.35 USD cents/kWh, excluding VAT)	<ul style="list-style-type: none"> • FiT only applicable if efficiency of solar cells is >16% or if efficiency of modules is >15% • In effect only until June 30, 2019
Wind	Decision No.: 37/2011/QD-TTg of June 29, 2011	VND 1,614/kWh (7.8 USD cents/kWh, excluding VAT)	For contract period of 20 years from the day of trading operation

Figure 1.5. Vietnamese FiT for Wind and Solar Energy [3]

According to Decision No. 37/2011 / QD-TTg on the mechanisms to support wind power. In which, the buyer (EVN) is responsible for purchasing all electricity output from wind power project at the price of 1,614 VND/kWh (excluding VAT value added tax equivalent to 7.8 cent/kWh) at the point of delivery of electricity. Electricity purchase prices are adjusted according to fluctuations in the exchange rate between VND and USD. In particular, the State provides a subsidy of 207 VND/kWh (equivalent to 1.0 cent/kWh) for the entire output of electricity purchased from wind power plants through Vietnam Environment Protection Fund. This means, the buyer or EVN only pay 6.8 cent/kWh.

In addition to the target set for wind development, the government has also issued a regulation (Decision No. 37/QD-TTg) introducing a feed-in tariff for the sector in 2011. The price is set at 1,614 VND/kWh (7.8 cent/kWh or 0.07 EUR/kWh) which includes a government subsidy of 207 VND/kWh (1.0 cent/kWh) through the Vietnamese Environmental Protection Fund. The rest of the 6.8 cent/kWh comes from the country's only grid operator and utility Vietnam Electricity (EVN). The tariff is valid for 20 years by a PPA signed between the wind developer and EVN.[2]

1.6 Objectives of the Thesis

The objective of this thesis is to study the aerodynamics of straight blade VAWT by using and combining Blade element theory with momentum theory to determine solidity and power coefficient versus tip speed ratio. In this thesis three prediction model will be introduced and use to compare with each other.

Study and integrate Tip loss and Finite aspect ratio effect in the three models to improve the results. Compare the result with CFD and experimental data to validate the outcomes. Using the result to find out the desired solidity and Tip speed ratio for another VAWT design thesis

1.7 Outline of the Thesis

This thesis includes six chapters.

Chapter 1 (Introduction) provides overall information about renewable wind energy in the world and in Vietnam.

Chapter 2 (Literature review) is a review into history of VAWT and relevant researches

Chapter 3 (Aerodynamics of VAWT) introduces actuator disk theory, blade element theory and the three aerodynamics models

Chapter 4 (Results validation and discussion) compares new numerical results with other existing numerical, experimental and CFD results.

Chapter 5 (Procedure of calculation for turbine design) presents procedure of calculation for turbine design: from initial geometry parameters, a set of power curves of the turbine are produced, from which the desired *TSR* and σ are determined.

Chapter 6 (Conclusions) gives a summary of some accomplishment that the thesis has achieved and suggestion of some future work for improvement.

Chapter 2. LITERATURE REVIEW

2.1 Introduction

In the history of mankind wind energy has played an important role. Among others wind energy was harnessed to grind grain. These so called wind mills are of the horizontal axis design (HAWT) and were also used for pumping water and later for sawing wood etc. Using multiple blades, the wind energy generated by the atmosphere is converted to kinetic energy inside the turbine. As more attention was put on the environmental aspect of traditional (fossil) fuels the development of wind turbines for generating electricity became more interesting.



Figure 2.1. An ancient windmill in the British Isles [5]

The focus on Renewable Energy Resources has been increasing. Different sources of renewable energy include biomass, solar, geothermal, hydroelectric, and wind. Among these resources wind has proved to be a cheaper alternative energy resource. Wind power is now the world's fastest growing energy resource. Although the vertical axis wind turbine (VAWT) was the first ever wind turbine to be used for harnessing wind energy, researchers of the modern era lost interest in it due to the initial perception that VAWT cannot be used for large scale electricity generation. Horizontal axis wind turbine (HAWT) remained the focus of all wind energy related research activity for last few decades.

Scientists and Engineers developed various wind turbine configurations and utilized different approaches for their analysis. Optimum conditions for the working of VAWTs were determined. The details of these techniques and configurations along with the major findings of researchers on vertical axis wind turbines are reviewed in this paper [6]. A closer look on the concepts leads towards the fact that VAWTs are suitable for electricity generation in the conditions where traditional HAWTs are unable to give reasonable efficiencies such as high wind velocities and turbulent wind flows. Another major advantage is that VAWTs are Omni-directional, accepting wind from any direction without any yawing mechanism.

	Vertical axis wind turbine (VAWT)	Horizontal axis wind turbine (HAWT)
Tower sway	Small	Large
Yaw mechanism	No	Yes
Self starting	No	Yes
Overall formation	Simple	Complex
Generator location	On ground	Not on ground
Height from ground	Small	Large
Blade's operation space	Small	Large
Noise produced	Less	Relatively high
Wind direction	Independent	Dependent
Obstruction for birds	Less	High
Ideal efficiency	More than 70%	50–60%

Figure 2.2. Merits of vertical axis wind turbines over horizontal axis wind turbines [6]

Currently, large scale VAWTs are not economically attractive; however, they offer energy solutions for remote places away from the main distribution lines and places where large wind farms cannot be installed due to environmental concerns and small scale dispersed generation units are preferred

2.2 Configurations

A great degree of design versatility exists in the vertical axis wind turbines. In the past few decades, the engineers came up with many new and innovative design approaches to resolve these issues associated with VAWTs.

2.2.1 Darrieus type wind turbine

Darrieus wind turbine designs were first patented in 1931. These types of turbines have highest values of efficiency among VAWTs. Darrieus type wind turbines have many variants all of which are Lift-type wind turbines, which mean lift forces acting on the blades of turbine cause the rotor to rotate and hence generate electricity.

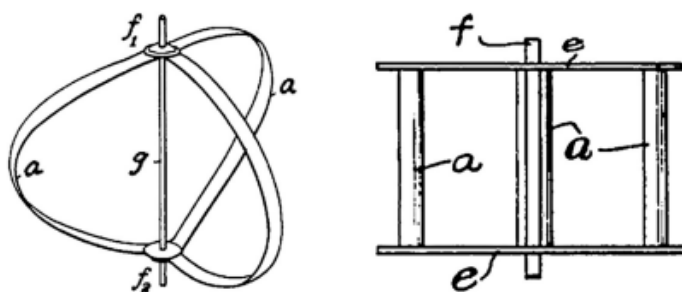


Figure 2.3. Original illustrations by G.J.M. Darrieus in 1931 patent [7]

2.2.2 Egg-beater type Darrieus wind turbine

It contains two or more blades arranged as arms of an egg-beater. Although this design is among the first ones to be produced for large scale power generation, the difficulty in manufacturing of complex geometry of blades and the associated high costs have limited its production at commercial scale. Various authors have contributed towards the designing and optimization of this turbine type. Brahimi and Paraschivoiu calculated structural loads on the Darrieus rotor wings in turbulent flow conditions. Rosen and Abramovich also carried out detailed study

on the structure of Darrieus rotor blades. They presented a theoretical model which can be used to analyze the behavior of blades under different loading configurations. The theoretical model was also tested experimentally. Bergeles et al. carried out flow field study of Darrieus wind turbine experimentally. The wake effect of the turbine blade rotor was studied in detail. Wakui et al. analyzed the wind turbine generator systems for this type of wind turbine configuration [6].

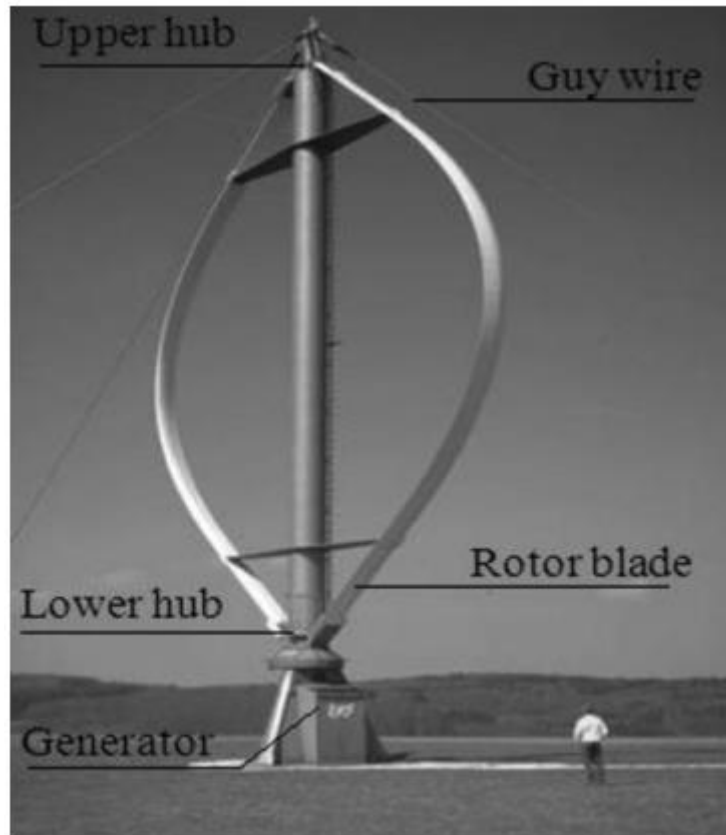


Figure 2.4. Darrieus rotor – egg beater shaped wind turbine [6]

2.2.3 Giromill (straight bladed type Darrieus wind) turbine

The curved egg-beater type blades are replaced by straight blades having airfoil cross-section as seen from the top of the turbine to give a new configuration of VAWT known as straight bladed Darrieus type. Commonly occurring configurations are two and three bladed which can have fixed or variable pitch.

Authors contributing to the designing and optimization include Vandenberghe and Dick who carried out a detailed aerodynamic study of this type of configuration.

Their results can be used for ‘parametric optimization’ of the wind turbines. Islam et al. also discussed various aerodynamic effects on this configuration such as dynamic stall and wake effect. Howell et al. performed aerodynamic analysis by using fluid flow simulations as well as wind tunnel testing. Their results indicate that the coefficient of power (C_p) increases till tip speed ratio ‘2’ and afterwards a declining trend is observed.

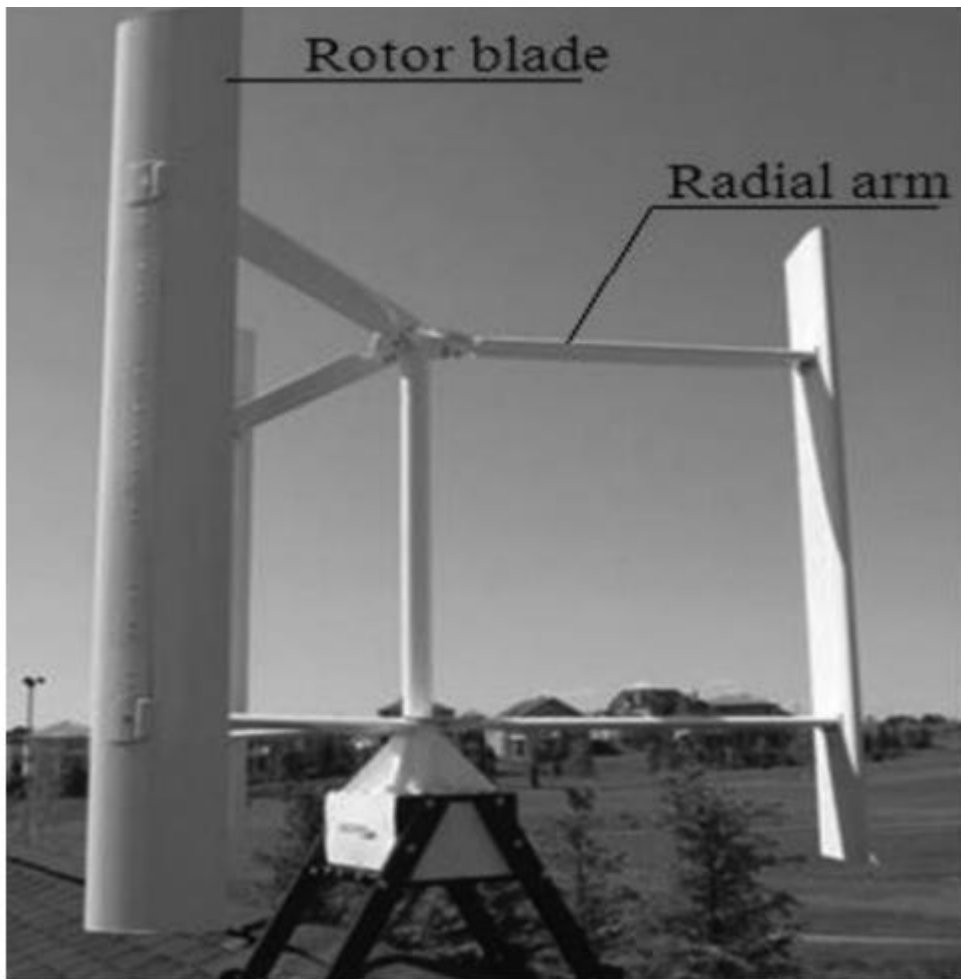


Figure 2.5. Darrieus rotor – straight bladed wind turbine [6]

2.2.4 Twisted bladed (Helical) Darrieus rotor

One of the main advantages of the twisted blades is that a twisted rotor blade helps reducing flow separation. The resulting rotor thus has a positive lift at zero angle of incidence enabling it to self-start at favorable wind conditions. The main drawback of this configuration is the complexity involved in the fabrication of

twisted blades that increases with the size of turbine and low power coefficient (0.128)



Figure 2.6. Helical H-rotor wind turbines by QuietRevolution and Turby [7]

2.3 Savonius Rotor

Savonius rotor consists of cup-shaped half, hollow cylinders fixed with a central rotating shaft. The torque is generated due to the drag force acting on the half cylinders. The flow energy utilization of Savonius rotor (20%) is lower than that of Darrieus rotor. The greatest advantage of a Savonius rotor is its ability to self-start in contrast to other ‘Lift type’ VAWTs. [6]

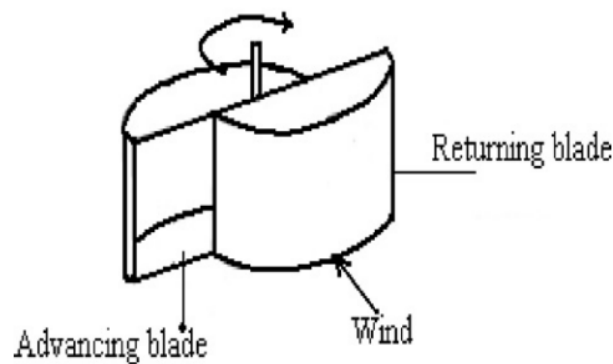


Figure 2.7. Savonius rotor [6]

2.4 Combined Savonius and Darrieus Rotor

In order to take advantage of the merits of both the configurations, a combination of the two rotors was suggested by Gavalda et al. Gupta and Biswas and Debnath et al. and is shown in Table 2. It was found that the coefficient of power can be as high as 0.35 for different overlap percentages. Moreover, a high torque coefficient was obtained which showed the ability of self-start at low wind velocity. Further study is however required to show the validity of these results for large scale commercial applications [6].

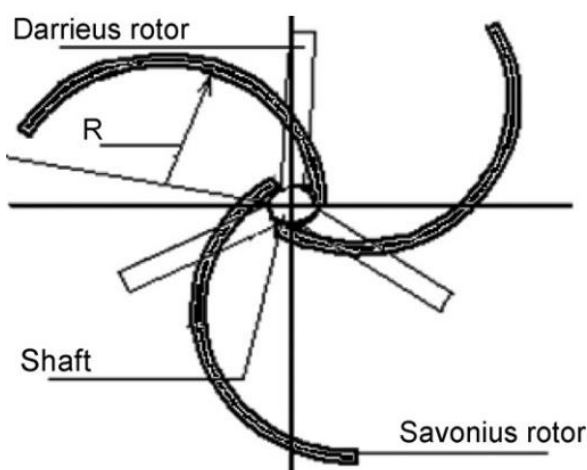


Figure 2.8. Combined Savonius and Darrieus rotor [6]

2.5 Design Techniques of Vertical Axis Wind Turbine

Prediction of aerodynamic performance of the wind turbines is crucial to their design optimization. Different parameters such as power and torque coefficients, and aerodynamic loads need to be determined and flow field around the rotor has to be visualized in order to carry out the performance analysis.

2.5.1 Efficiency

Efficiency of a wind turbine is expressed usually in terms of coefficient of power

2.5.1.1 Impulsive method

The aerodynamic coefficients, i.e. the lift coefficient, the drag coefficient and the power coefficient can be estimated by calculating the impulse loss of the flow

going through the area swept by the rotor and the averaged-in-time of total aerodynamic force which is applied to the blades

2.5.1.2 Buckingham Pi theorem

Pope et al. presented a new model which could predict the performance of drag type VAWT. They developed a power correlation using Buckingham-Pi theorem for vertical axis wind. The relation developed between coefficient of power (C_P) and tip speed ratio (TSR) is given below

$$C_P = a \cdot TSR^2 + b \cdot TSR + c \quad (2.1)$$

2.5.1.3 Computational fluid dynamics (CFD)

CFD has now become a powerful tool of fluid mechanics which analyzes and solves the problems related to fluid flows, utilizing numerical methods with the help of computers. CFD can save time as well as expensive experimentation and is also being employed for improvement in vertical axis wind turbine analysis. CFD analysis has been extensively used for the determination of coefficient of power for various wind turbine configurations. 2D or 3D models of wind turbine blade is created using CAD software and are meshed and solved. For Darrieus rotor, the C_P value increases up to an optimum value of TSR and then tends to decrease, which is in good agreement to the experimental results

2.5.2 Aerodynamic load calculations

The term ‘aerodynamic load’ refers to the forces acting and hence the stresses induced in the blades of a rotor as it rotates due to the wind flow around it.

2.5.2.1 Blade element method

The earliest and the most commonly used method for the calculation of aerodynamic loads on wind turbine blades is the blade element momentum method developed by Glauert in 1963. This method is a combination of blade element theory and momentum theory. The calculations are performed by considering each element of the rotor as an independent entity.

2.5.2.2 Actuator disc method

Actuator disc theory was proposed by Glauert, as described by Islam et al. [23], to calculate the drag forces and hence aerodynamic loads on the blades. Actuator disc methods were also used for the determination of loads on wind turbines.

2.5.2.3 Dynamic analysis

Basic angular momentum equations of Engineering Mechanics, shown as under, were used to calculate the forces acting on the blades of a Darrieus rotor

$$\left[\frac{dH_A}{dt} \right]_{XYZ} = \left[\frac{dI_A}{dt} \right]_{xyz} + I(\alpha) \left[\frac{d\omega}{dt} \right]_{xyz} + \Omega \times [[I(\alpha)][\omega]] \quad (2.2)$$

Eighteen equations were thus developed for the rotor, considering various degrees of freedom and were solved using computer codes. A reasonable agreement was observed between the calculated values and experimental data obtained previously by researchers.

2.5.2.4 Impulsive methods

Impulsive method of load calculation relies on the relation between impulse loss of the flow going through the area swept by the rotor and the averaged-in-time of total aerodynamic force which is applied to the blades.

2.5.2.5 Vortex methods

Vortex models for load calculations on rotor blade are modeling non-stationary structure of streamlines for every rotor blade using vortex lattice method. Another vortex Analytical Model for aerodynamic load calculations is developed by measuring vortices' circulation strength and location which was then used to estimate the velocity of air around the rotor at any point. The velocity measurements were then used to estimate the rotor performance under different flow conditions. The advantages of this model include its ability to determine blade-wake interactions, estimate results in unsteady flow conditions and for finite aspect ratios of rotor blades.

2.5.3 Flow field visualization and analysis

Visualization of flow field around the wind turbine facilitates in understanding and analyzing the aerodynamic behavior of wind turbine

2.5.3.1 Particle image velocimetry

Dye injection technique was used to visualize flow field in the region of a Darrieus rotor during dynamic stall. In this technique, a colored dye is bled into the flowing fluid and flow pattern is observed through the dye track. Researcher used particle image velocimetry (PIV) with a conditional imaging technique to measure phase averaged velocity distributions around the blade. They concluded that the phenomenon of dynamic stall appears due to shedding of two pairs of vortices from blade during one rotation of rotor.

2.5.3.2 Computational fluid dynamics (CFD)

CFD techniques have also been used for flow field visualization of a VAWT. Relatively low computational cost and reasonable accuracy are attractive features of CFD Operational modal analysis

Standard model testing technique was used which utilized artificial source of excitation such as step relaxation. In 1986, the idea of utilizing natural wind for excitation of wind turbines or other large structures was presented. In 1993, a cross correlation function was developed which compared the output values without any need of input values. This cross correlation function could be directly used in the software for calculation of modal parameters.

2.5.3.3 Wind tunnel testing

A prototype of straight blade VAWT for wind tunnel test and measured forces on the blades and power absorbed.

Chapter 3. AERODYNAMICS OF VAWT

3.1 Aerodynamics Principles of Straight Blade VAWT

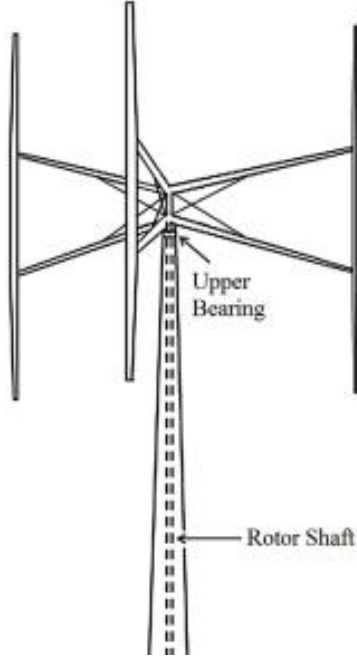


Figure 3.1. Straight blade Darrieus type VAWT [7]

First of all, there are a number of different approaches to define the origin of the azimuthal angle and the wind flow direction. In this thesis the wind and the origin of azimuthal angle to have the same direction as shown in Figure 3.2.

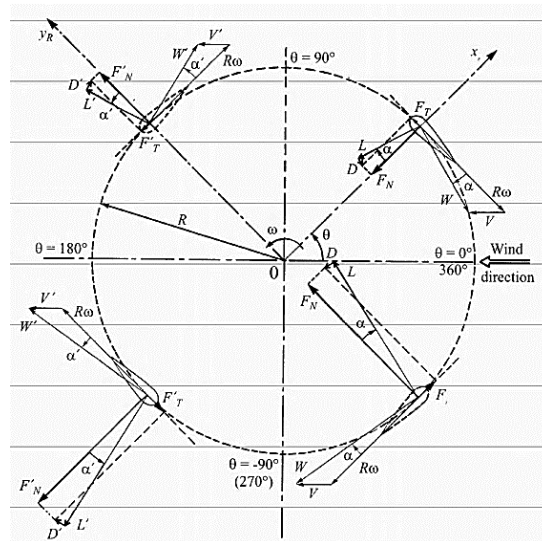


Figure 3.2. VAWT flow velocities and blade [8]

The figure above show the view from above of the turbine. As the blade is straight, just a slide of the rotor is needed and seen as a blade element. While the turbine is operation it is rotating, thus there are 2 main velocity constitute to the relative velocity of the blade.

- Tangential velocity form the angle velocity
- Wind velocity at the blade

The relative velocity can be used Pythagorean equation and expressed as.

$$W^2 = (R\omega - V \sin \theta)^2 + V^2 \cos^2 \theta \quad (3.1)$$

$$\frac{W^2}{V_\infty^2} = \left(\frac{R\omega}{V_\infty} - \frac{V}{V_\infty} \sin \theta \right)^2 + \left(\frac{V}{V_\infty} \right)^2 \cos^2 \theta \quad (3.2)$$

Table 3.1. Notations

W	Relative velocity at blade element
ω	Angular velocity of the turbine rotor
$R\omega$	Rotational speed at blade element (rotor radius)
V_∞	Free stream wind velocity
θ	Azimuthal angle
TSR	Tip speed ration

Define tip speed ratio of the turbine as the fraction of rotational speed and the free stream wind velocity

$$TSR = \frac{R\omega}{V_\infty} \quad (3.3)$$

$$\frac{W^2}{V_\infty^2} = \left(TSR - \frac{V}{V_\infty} \sin \theta \right)^2 + \left(\frac{V}{V_\infty} \right)^2 \cos^2 \theta \quad (3.4)$$

$$\frac{W}{V_\infty} = \sqrt{\left(TSR - \frac{V}{V_\infty} \sin \theta \right)^2 + \left(\frac{V}{V_\infty} \right)^2 \cos^2 \theta} \quad (3.5)$$

The angle of attack of the blade element is the angle between \vec{W} direction and the chord line of the element

$$\tan \alpha = \frac{\frac{V}{V_\infty} \cos \theta}{TSR - \frac{V}{V_\infty} \sin \theta} \quad (3.6)$$

$$\alpha = \text{atan} \frac{\frac{V}{V_\infty} \cos \theta}{TSR - \frac{V}{V_\infty} \sin \theta} \quad (3.7)$$

The forces on the blade elements can be based on available experimental 2D airfoil data or form theoretical extrapolation.

$$C_N = C_L \cos \alpha + C_D \sin \alpha \quad (3.8)$$

$$C_T = C_L \sin \alpha - C_D \cos \alpha \quad (3.9)$$

Thrust (or drag) by one element (in the direction of the airflow)

$$C_{Thrust} = C_N \sin \theta - C_T \cos \theta \quad (3.10)$$

Total thrust for a turbine with N blades, chord on the complete revolution.

$$Thrust = \frac{Nc}{2\pi} \int_{-H/2}^{H/2} \int_0^{2\pi} q C_{Thrust} d\theta dz \quad (3.11)$$

3.2 Aerodynamics Prediction Model for VAWT

Various computational models exist, each with their own strengths and weaknesses that attempt to accurately predict the performance of a wind turbine.

There are three categories of analytical model in complexity order.

- The Single Streamtube Model: which supposes that the entire rotor is enclosed in one streamtube
- The Multiple Streamtube Model: in which the swept volume of the rotor is divided into a series of adjacent streamtubes
- The Double-Multiple Streamtube Model: which is the upwind and downwind rotor halves model, which considers the VAWT as replaced by two rotor halves in aerodynamically independent series.

All the three all use momentum theory combined with blade element theory to forecast the power output of the turbine. In order to comprehend the three primary models, first need to revised 2 momentum theory (single disk and double disk) and blade element theory.

The major difference between these streamtube models is in the calculation of the induced velocities. The first two types consider the constant induced velocities through the rotor, which is replaced by an equivalent actuator disk.

In the upwind and downwind aerodynamic model authors such as Lapin have estimated the variation in induced velocity on both the upwind and downwind halves of the rotor using different assumptions.

Another analytical model that considers a multiple streamtube system divided into two parts was developed by Paraschivoiu for determining the aerodynamic blade loads and rotor performance on the Darrieus wind turbine with straight and curved blades. This so-called “double-multiple streamtube” (DMS) model uses two constant interference factors in the induced velocities, which are calculated by a double iteration, and accounts for vertical variations in the freestream velocity.

Continuing the development of the two-actuator disk theory, the previous DMS model of I. Paraschivoiu was improved by considering the variation in the upwind and downwind induced velocities as a function of the azimuthal angle for each streamtube. The new model which is referred to as the DMSV model using CARDAAV computer code considers the influence of all secondary effects including streamtube expansion, the blade geometry and airfoil type, rotating tower, and the presence of struts and aerodynamic spoilers on the Darrieus turbine. Finally, a semi-empirical dynamic-stall model is now included in the DMS method. This calculation is made by using Gormont's mode.

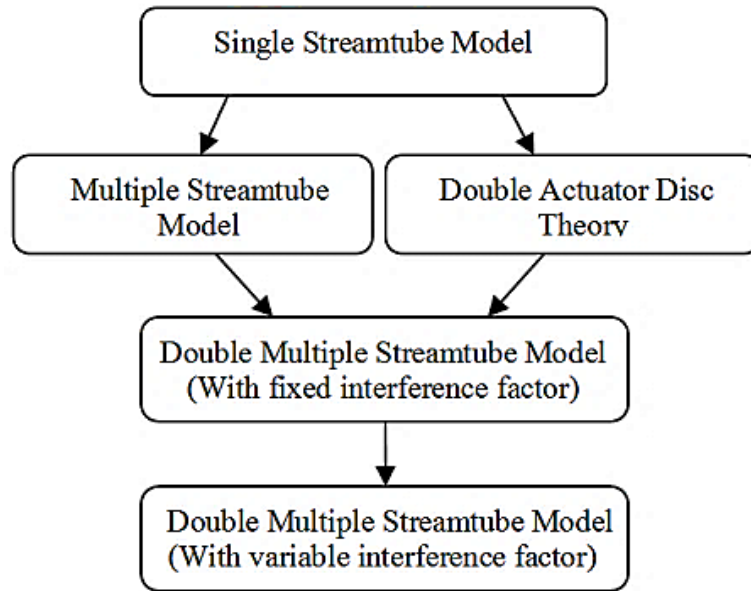


Figure 3.3. Overview of the development of the streamtube models [9]

3.3 One-Dimensional Momentum Theory (Single Actuator Disk Theory) and the Betz Limit

A simple model, generally attributed to Betz (1926), can be used to determine the power from an ideal turbine rotor, the thrust of the wind on the ideal rotor, and the effect of the rotor operation on the local wind field. This simple model is based on a linear momentum theory developed over 100 years ago.

This analysis is not limited to any particular type of wind turbine. The analysis assumes a control volume, in which the control volume boundaries are the surface of a stream tube and two cross-sections of the stream tube. The only flow is across the ends of the stream tube. The turbine is represented by a uniform ‘actuator disc’.

Assumptions:

- Homogenous, incompressible, steady state fluid flow;
- No frictional drag;
- An infinite number of blades;
- Uniform thrust over the disc or rotor area;
- A non-rotating wake;
- The static pressure far upstream and far downstream of the rotor is equal to the undisturbed ambient static pressure

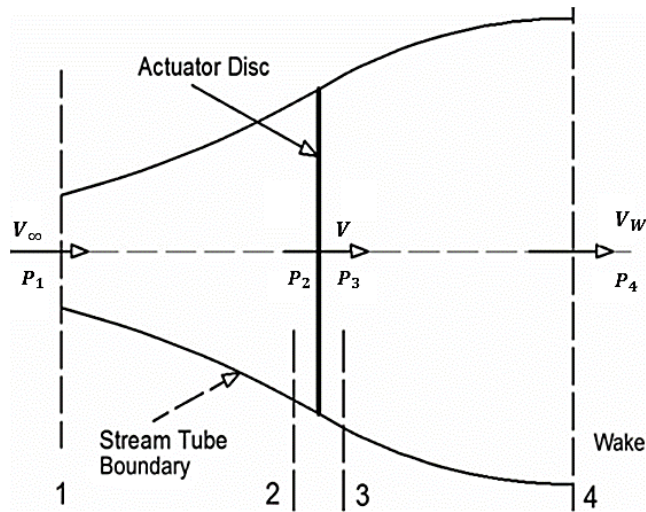


Figure 3.4. Actuator disc model of a wind turbine (modified from [9])

Conservation of linear momentum. T , which is the force of the wind on the wind turbine is equal and opposite to the rate of change of momentum of the air stream.

$$T = V_{\infty} \dot{m}_1 - V_W \dot{m}_4 \quad (3.12)$$

Since steady flow, $\dot{m} = \rho A V = \text{const}$ throughout the air stream

$$T = \dot{m}(V_{\infty} - V_W) \quad (3.13)$$

$$T > 0 \Rightarrow V_{\infty} > V_W \quad (3.14)$$

No work is done on either side of the turbine rotor. Thus the Bernoulli function can be used in either side of the actuator disc.

Assuming that from the far of either side, pressures are equal to atmosphere and velocity remains constant through the disc which is V

$$P_1 = P_4 = P_{\infty} \quad (3.15)$$

Upstream of the disc

$$P_1 + \frac{1}{2} \rho V_{\infty}^2 = P_2 + \frac{1}{2} \rho V^2 \quad (3.16)$$

Downstream of the disc

$$P_3 + \frac{1}{2} \rho V^2 = P_W + \frac{1}{2} \rho V_W^2 \quad (3.17)$$

Take Equation (3.16) – Equation (3.17)

$$\begin{aligned} & \left(P_1 + \frac{1}{2} \rho V_\infty^2 \right) - \left(P_W + \frac{1}{2} \rho V_W^2 \right) \\ &= \left(P_2 + \frac{1}{2} \rho V^2 \right) - \left(P_3 + \frac{1}{2} \rho V^2 \right) \end{aligned} \quad (3.18)$$

$$\frac{1}{2} \rho (V_\infty^2 - V_W^2) = P_2 - P_3 \quad (3.19)$$

The thrust can also be expressed as the net sum of the forces on each side of the actuator disc.

$$T = A(p_2 - p_3) \quad (3.20)$$

Substitutes Equation (3.19) into Equation (3.20).

$$T = \frac{1}{2} A \rho (V_\infty^2 - V_W^2) \quad (3.21)$$

Equating Equation (3.21) and Equation (3.13), the equation obtains.

$$\frac{1}{2} A \rho (V_\infty^2 - V_W^2) = \dot{m} (V_\infty - V_W) \quad (3.22)$$

$$\frac{1}{2} A \rho (V_\infty^2 - V_W^2) = \rho A V (V_\infty - V_W) \quad (3.23)$$

$$(V_\infty^2 - V_W^2) = 2V(V_\infty - V_W) \quad (3.24)$$

$$V = \frac{V_\infty + V_W}{2} \quad (3.25)$$

Introducing factor a , the axial induction factor.

$$a = \frac{V_\infty - V}{V_\infty} \quad (3.26)$$

$$V = V_\infty (1 - a) \quad (3.27)$$

$$V_W = V_\infty (1 - 2a) \quad (3.28)$$

As the axial induction factor increases from 0, the wind speed behind the rotor more and more slows. If $a = 1/2$, the wind has slowed to zero velocity behind the rotor and the simple theory is no longer applicable

The power out, P , is equal to the thrust times the velocity at the disc.

$$\begin{aligned}
 P &= \frac{1}{2} A \rho (V_\infty^2 - V_W^2) V \\
 &= \frac{1}{2} A \rho (V_\infty^2 - V_\infty^2 (1 - 2a)^2) V_\infty (1 - a) \\
 &= \frac{1}{2} A \rho V_\infty^3 (1 - (1 - 2a)^2) (1 - a) \\
 P &= \frac{1}{2} A \rho V_\infty^3 4a(1 - a)^2
 \end{aligned} \tag{3.29}$$

Power coefficient

$$C_P = \frac{P}{\frac{1}{2} \rho A V_\infty^3} = \frac{\text{Rotor power}}{\text{Power in the wind}} \tag{3.31}$$

$$C_P = \frac{\frac{1}{2} A \rho V_\infty^3 4a(1 - a)^2}{\frac{1}{2} \rho A V_\infty^3} = 4a(1 - a)^2 \tag{3.32}$$

Taking the derivative of the power coefficient and setting it equal to zero

$$C'_P = 4(1 - a)^2 + 4a \cdot 2(1 - a)(-1) = 0 \tag{3.33}$$

$$a = 1/3 \tag{3.34}$$

And

$$C_{P,max} = \frac{16}{27} = 59.26 \% \tag{3.35}$$

Thrust on the disc is.

$$T = \frac{1}{2} A \rho (V_\infty^2 - V_W^2) = \frac{1}{2} \rho A V_\infty^2 4a(1 - a) \tag{3.36}$$

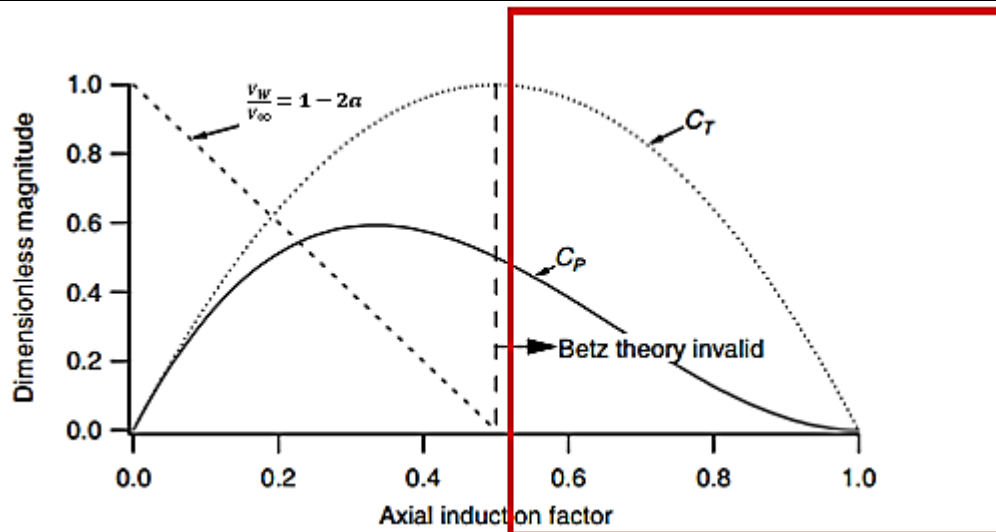
Thrust coefficient

$$C_T = \frac{T}{\frac{1}{2} \rho A V_\infty^2} = \frac{\text{Thrust force}}{\text{Dynamic force}} = \frac{\frac{1}{2} \rho A V_\infty^2 4a(1 - a)}{\frac{1}{2} \rho A V_\infty^2} \tag{3.37}$$

$$C_T = 4a(1 - a) \quad (3.38)$$

Table 3.2. Values of power coefficient versus induction factor

Induction factor	Power coefficient	Thrust coefficient
$a = 1/3$	$C_{P,max} = \frac{16}{27}$	$C_T = \frac{8}{9}$
$a = 1/2$	$C_P = \frac{1}{2}$	$C_{T,max} = 1$

**Figure 3.5. Operating parameters for a Betz turbine (modified from [10])**

The Betz limit is the maximum theoretically possible rotor power coefficient. In practice, there are other effects lead to a decrease in the maximum achievable power coefficient, overall turbine efficiency is a function of both the rotor power coefficient and the mechanical (including electrical) efficiency of the wind turbine.

$$\eta_{overall} = \frac{P_{out}}{\frac{1}{2} \rho A V_\infty^2} = \eta_{mech} C_P \quad (3.39)$$

3.4 Double Actuator Disk Theory

In vertical-axis wind turbines, the wind passes twice through the rotor swept area and the induced velocities differ on the upstream half of the swept surface and the

down-stream half. The Darrieus vertical-axis wind turbine could be represented by a pair of actuator disks in tandem at each level of the rotor. The first disk represents the upstream half of the surface swept by the blades, and the second disk the down-stream of the rotor [8].

The double actuator disk theory represents an improvement with respect to the single actuator disk theory or the multiple streamtube model but at the same time more unknowns have to be solved than equations. This difficulty can be overcome by using blade element theory.

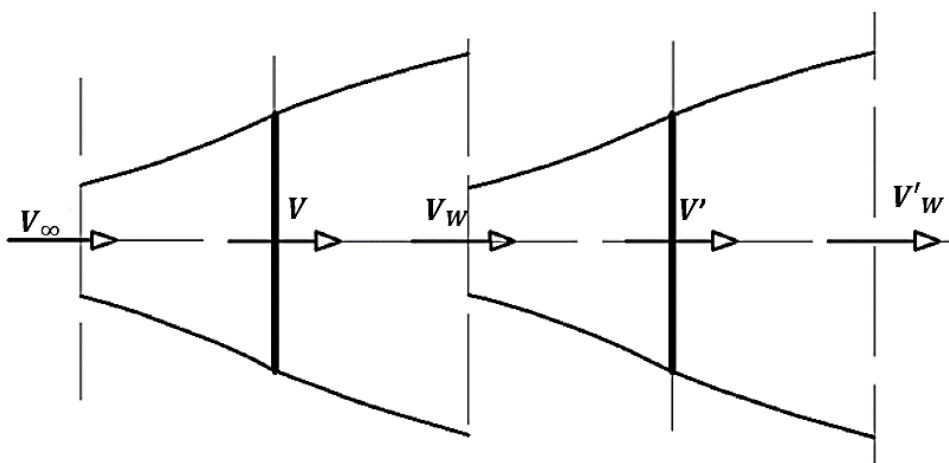


Figure 3.6. A pair of actuator disks in tandem (modified from [9])

In this case, each disk is treated as a single actuator disk, thus equations of single actuator disk theory can be used to apply for this case.

Table 3.3. Antonations

A	area of each disk
V	induced velocity at the first disk
V'	induced velocity at the second disk
V_w	Wake velocity of the first disk which is also the input velocity of the second disk
V'_w	Wake velocity of the second disk
a	First disk's induction factor
a'	Second disk's induction factor

Disk 1

From 1D momentum theory

$$V = V_\infty(1 - a) \quad (3.40)$$

$$V_W = V_\infty(1 - 2a) \quad (3.41)$$

Thrust on disk 1

$$T_1 = \frac{1}{2} \rho A V_\infty^2 4a(1 - a) \quad (3.42)$$

Thrust coefficient on disk 1

$$C_{T_1} = \frac{T_1}{\frac{1}{2} \rho A V_\infty^2} = 4a(1 - a) \quad (3.43)$$

Power on disk 1

$$P = \frac{1}{2} A \rho V_\infty^3 4a(1 - a)^2 \quad (3.44)$$

Power coefficient on disk 1

$$C_{P_1} = \frac{P_1}{\frac{1}{2} \rho A V_\infty^3} = 4a(1 - a)^2 \quad (3.45)$$

Disk 2

From 1D momentum theory

$$V' = V_W(1 - a') \quad (3.46)$$

$$V'_W = V_W(1 - 2a') \quad (3.47)$$

Thrust on disk 2

$$T_2 = \frac{1}{2} \rho A V_W^2 4a'(1 - a') \quad (3.48)$$

Thrust coefficient on disk 2

$$C_{T_2} = \frac{T_2}{\frac{1}{2} \rho A V_\infty^2} = \frac{V_W^2}{V_\infty^2} 4a'(1-a') \quad (3.49)$$

$$C_{T_2} = (1-2a)^2 4a'(1-a') \quad (3.50)$$

Power on disk 2

$$P_2 = \frac{1}{2} A \rho V_W^3 4a'(1-a')^2 \quad (3.51)$$

Power coefficient on disk 1

$$C_{P_2} = \frac{P_2}{\frac{1}{2} \rho A V_\infty^3} = \frac{V_W^3}{V_\infty^3} 4a'(1-a')^2 \quad (3.52)$$

$$C_{P_2} = (1-2a)^3 4a'(1-a') \quad (3.53)$$

Total thrust coefficient

$$C_T = C_{T_1} + C_{T_2} = 4a(1-a) + (1-2a)^2 4a'(1-a') \quad (3.54)$$

Total power coefficient

$$C_P = C_{P_1} + C_{P_2} = 4a(1-a)^2 + (1-2a)^3 4a'(1-a') \quad (3.55)$$

3.5 Blade Element Theory

Airfoil Characteristics

Assuming that two dimensional airfoil characteristics can be used for the local blade element lift and drag coefficients. Care must be taken to use airfoil characteristics appropriate to the wind turbine blade Reynolds number. It is convenient for further calculations to resolve the respective drag and lift coefficients into a normal force coefficient C_N and a thrust force coefficient C_T as shown in Figure 3.7

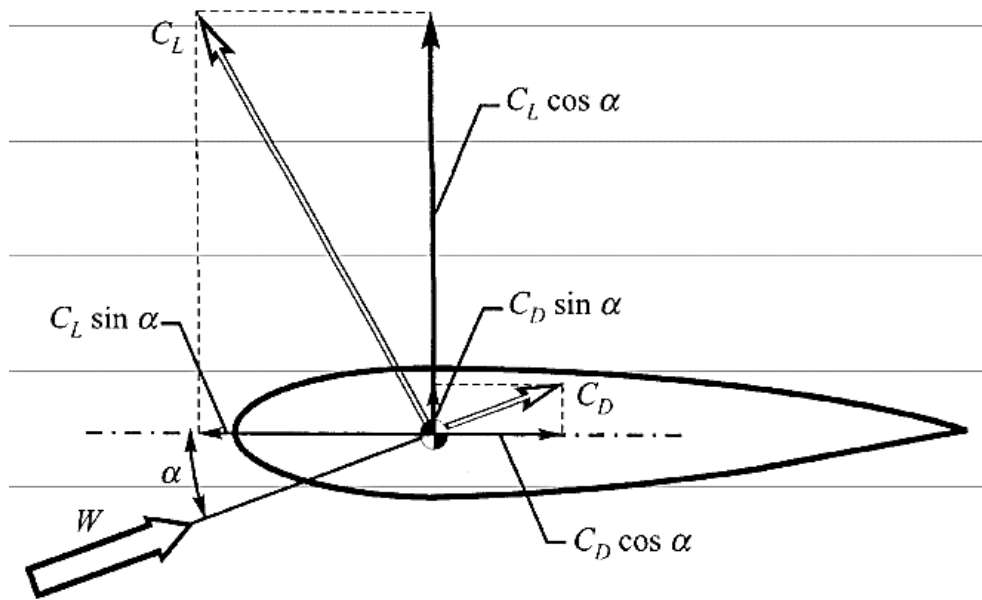


Figure 3.7. Force coefficients of a blade element airfoil [8]

$$C_N = C_L \cos \alpha + C_D \sin \alpha \quad (3.56)$$

$$C_T = C_L \sin \alpha - C_D \cos \alpha \quad (3.57)$$

$C_T > 0$ when directed forward along the airfoil chord

A blade element of chord c and height dh has a plan area $c \cdot dh$. This area is subjected to a normal force F_N and tangential force F_T

$$F_N = \frac{1}{2} \rho W^2 C_N \cdot c \cdot dh \quad (3.58)$$

$$F_T = \frac{1}{2} \rho W^2 C_T \cdot c \cdot dh \quad (3.59)$$

Table 3.4. Sign convention for forces on a blade element

Normal force F_N	Positive when heading to rotation center
Tangential force F_T	Positive when heading toward rotation direction

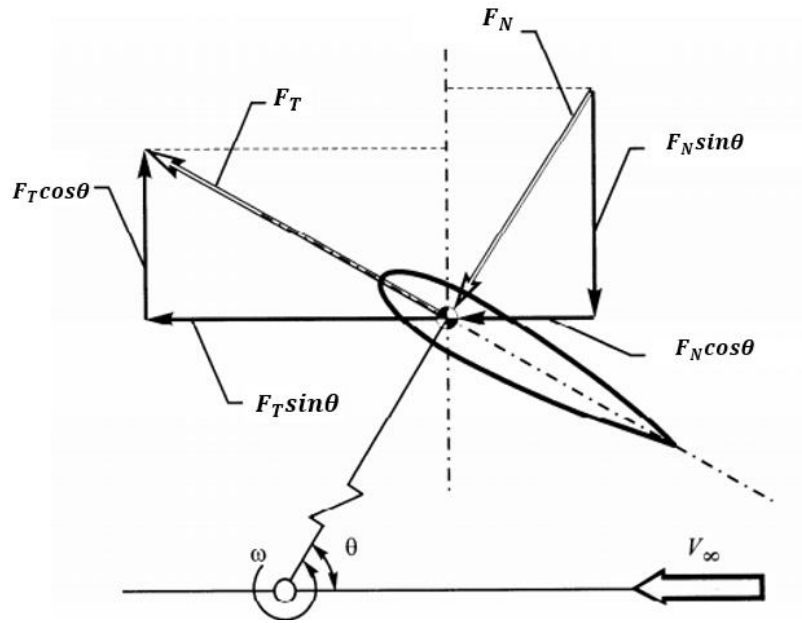


Figure 3.8. Forces on a blade element airfoil in a horizontal plane (modified from [8])

The instantaneous thrust and side-force, when the forces are resolved into directions parallel and perpendicular to the ambient wind direction (Figure 3.8), are.

$$\text{Thrust (parallel to } V_{\infty}) = F_N \cos\theta + F_T \sin\theta \quad (3.60)$$

$$\begin{aligned} \text{Side - force (perpendicular to } V_{\infty}) \\ = -F_N \sin\theta + F_T \cos\theta \end{aligned} \quad (3.61)$$

Instantaneous thrust and side-force coefficients

$$C_{Th} = C_N \cos\theta + C_T \sin\theta \quad (3.62)$$

$$C_{SF} = -C_N \sin\theta + C_T \cos\theta \quad (3.63)$$

The instantaneous thrust and side-force vary as the blade makes a full revolution, hence the total drag and side-force is obtained by integration over a full cycle and over the full height of the rotor

3.6 Single Streamtube Model

This model was first developed by Templin for the VAWT. It is based on the actuator disk theory and is the most basic model based on the momentum theory. The flow through the turbine is assumed to have one constant velocity. This simplest aerodynamic model yields the poorest agreement with experimental data.

The simplest momentum model takes the rotor to be enclosed in a single stream-tube. Wind velocity across the area swept by the rotor is assumed constant. By choosing some value of this velocity, a combination of the simple actuator-disc momentum model and blade element theory would give the far-field wind speed, turbine power, torque, and thrust for a turbine with given blade characteristics, rotational speed, and geometry.

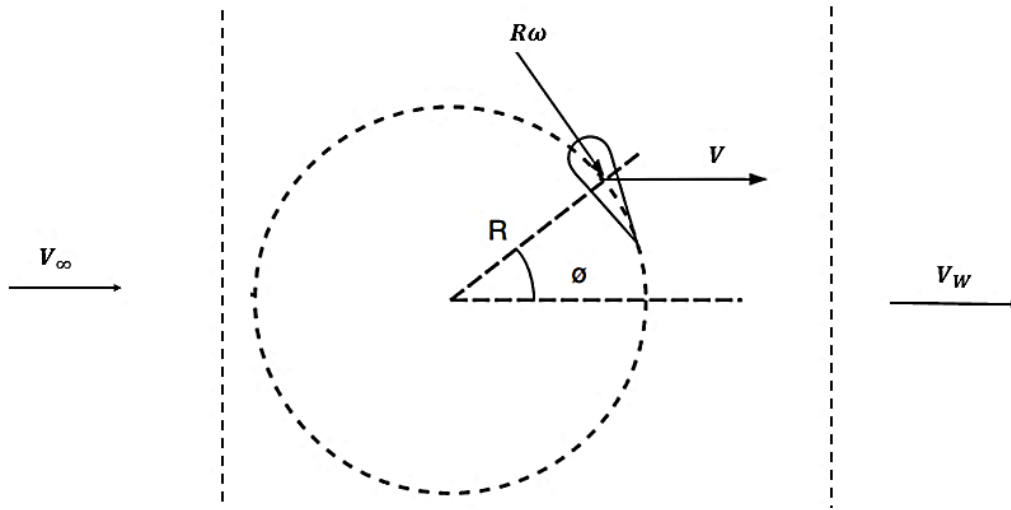


Figure 3.9. Velocities diagram (modified from [10])

In this model, wind velocity V is assumed to be constant for all the location of the blade on flight path

Applying momentum theory, assuming that the wind at blade element is induced by an induction factor a

$$V = V_\infty(1 - a) \quad (3.64)$$

$$V_w = V_\infty(1 - 2a) \quad (3.65)$$

Blade element relative velocity

$$W = \sqrt{(R\omega - V\sin\theta)^2 + V^2\cos^2\theta} \quad (3.66)$$

$$\frac{W}{V_\infty} = \sqrt{\left(TSR - \frac{V}{V_\infty}\sin\theta\right)^2 + \left(\frac{V}{V_\infty}\right)^2\cos^2\theta} \quad (3.67)$$

$$\frac{W}{V_\infty} = \sqrt{(TSR - (1 - a)\sin\theta)^2 + (1 - a)^2\cos^2\theta} \quad (3.68)$$

$$\alpha = \text{atan} \frac{(1 - a)\cos\theta}{TSR - (1 - a)\sin\theta} \quad (3.69)$$

Local Reynolds number

$$Re = \frac{Wc}{\nu} \quad (3.70)$$

Form AOA together with Re, which is used to interpolate lift and drag coefficient C_L, C_D of the blade element

Normal force coefficient C_N and tangential force coefficient C_T

$$C_N = C_L \cos\alpha + C_D \sin\alpha \quad (3.71)$$

$$C_T = C_L \sin\alpha - C_D \cos\alpha \quad (3.72)$$

Instantaneous thrust coefficient

$$C_{Ti} = C_N \cos\theta + C_T \sin\theta \quad (3.73)$$

Instantaneous thrust for one blade

$$T_i(\theta) = C_{Ti} \frac{1}{2} \rho W^2 H c \quad (3.74)$$

Average thrust (on the direction of V_∞) of the whole turbine calculated by integrating instantaneous thrust with dt for a revolution and then divided by period time $T = 2\pi/\omega$ and subsequently multiplied with number of blades N

$$dt = \frac{d\theta}{\omega} \quad (3.75)$$

$$\begin{aligned} Thrust &= N \frac{1}{T} \int_0^T T_i(\theta) dt = N \frac{1}{2\pi} \int_0^{2\pi} T_i d\theta \\ &= N \frac{1}{2\pi} \int_0^{2\pi} C_{Ti} \frac{1}{2} \rho W^2 H c d\theta \end{aligned} \quad (3.76)$$

$$Thrust = N \frac{\frac{1}{2} \rho W^2 dhc}{2\pi} \int_0^{2\pi} C_{Ti} d\theta \quad (3.77)$$

Average thrust coefficient

$$C_{Thrust} = \frac{Thrust}{\frac{1}{2} \rho V_\infty^2 DH} = \frac{N \frac{1}{2} \rho W^2 Hc}{\frac{1}{2} \rho V_\infty^2 DH} \int_0^{2\pi} C_{Ti} d\theta \quad (3.78)$$

$$C_{Thrust} = \frac{W^2 NHc}{V_\infty^2 2\pi DH} \int_0^{2\pi} C_{Ti} d\theta \quad (3.79)$$

Set wind turbine solidity $\sigma = Nc/D$

$$C_{Thrust} = \frac{\sigma}{2\pi} \left(\frac{W}{V_\infty} \right)^2 \int_0^{2\pi} C_{Ti} d\theta \quad (3.80)$$

Torque of the blade come from tangential force

$$C_T = C_L \sin \alpha - C_D \cos \alpha \quad (3.81)$$

Instantaneous tangential force

$$F_T = \frac{1}{2} \rho W^2 C_T cH \quad (3.82)$$

Instantaneous torque

$$Q_i = F_T R \quad (3.83)$$

Instantaneous power

$$P_i = Q_i \omega = \frac{1}{2} \rho W^2 C_T cH R \omega \quad (3.84)$$

Instantaneous power coefficient

$$C_{P_i} = \frac{P_i}{\frac{1}{2} \rho W^3 cH} = C_T \frac{R \omega}{W} = C_T TSR \frac{V_\infty}{W} \quad (3.85)$$

Average power of the whole turbine calculated by integrating instantaneous power with dt for a revolution and then divided by period time $T = 2\pi/\omega$ and subsequently multiplied with number of blades N

$$P = N \frac{1}{T} \int_0^T P_i(\theta) dt = N \frac{1}{2\pi} \int_0^{2\pi} P_i d\theta \quad (3.86)$$

$$P = N \frac{1}{2\pi} \int_0^{2\pi} \frac{1}{2} \rho W^3 c H C_{P_i} d\theta = N \frac{\frac{1}{2} \rho W^3 c H}{2\pi} \int_0^{2\pi} C_{P_i} d\theta \quad (3.87)$$

Average power coefficient

$$C_P = \frac{P}{\frac{1}{2} \rho V_\infty^3 D H} = \frac{N \frac{\frac{1}{2} \rho W^3 c H}{2\pi} \int_0^{2\pi} C_{P_i} d\theta}{\frac{1}{2} \rho V_\infty^3 D H} \quad (3.88)$$

$$C_P = \frac{N W^3 c}{V_\infty^3 D 2\pi} \int_0^{2\pi} C_{P_i} d\theta \quad (3.89)$$

$$C_P = \frac{\sigma}{2\pi} \left(\frac{W}{V_\infty} \right)^3 \int_0^{2\pi} C_{P_i} d\theta \quad (3.90)$$

On the other hand, thrust coefficient from momentum theory

$$C_{T_{mt}} = 4a(1 - a) \quad (3.91)$$

Equating these two thrust to obtain the iteration equation.

$$4a(1 - a) = \frac{\sigma}{2\pi} \left(\frac{W}{V_\infty} \right)^2 \int_0^{2\pi} C_{Ti} d\theta \quad (3.92)$$

Let

$$\frac{\sigma}{2\pi} \left(\frac{W}{V_\infty} \right)^2 \int_0^{2\pi} C_{Ti} d\theta = d \quad (3.93)$$

Iteration condition becomes.

$$4a^2 - 4a + d = 0 \quad (3.94)$$

Table 3.5. Synthesized equations and step for calculations

Single streamtube model
$a_{initial} = 0$
TSR, σ are needed
$\frac{W}{V_\infty} = \sqrt{(TSR - (1 - a)\sin\theta)^2 + (1 - a)^2\cos^2\theta}$
$\alpha = \text{atan} \frac{(1 - a)\cos\theta}{TSR - (1 - a)\sin\theta}$
$Re = \frac{Wc}{\nu}$
C_L, C_D
$C_N = C_L \cos\alpha + C_D \sin\alpha$
$C_T = C_L \sin\alpha - C_D \cos\alpha$
$C_{Ti} = C_N \cos\theta + C_T \sin\theta$
$C_{P_i} = \frac{C_T TSR}{\left(\frac{W}{V_\infty}\right)}$
$C_{Thrust} = \frac{\sigma}{2\pi} \left(\frac{W}{V_\infty}\right)^2 \int_0^{2\pi} C_{Ti} d\theta$
$C_P = \frac{\sigma}{2\pi} \left(\frac{W}{V_\infty}\right)^3 \int_0^{2\pi} C_{P_i} d\theta$
$d = \frac{\sigma}{2\pi} \left(\frac{W}{V_\infty}\right)^2 \int_0^{2\pi} C_{Ti} d\theta = C_{Thrust}$
$4a_{new}^2 - 4a_{new} + d = 0$
a_{new}
$a_{converged}$
C_{Thrust}
C_P

3.7 Multiple Streamtube Model

Another approach, known as the multiple stream tube theory. In this approach it is assumed that the induction factor may vary in the direction perpendicular to the wind, but is constant in the direction of the wind. Each stream tube of constant a is parallel to the wind.

The total span of the single streamtube is divided in multiple streamtube using a fixed angle $\Delta\theta$ as width. For each of these streamtube the momentum equations and blade elements have to be calculated, resulting in N induced factors

$$\Delta\theta = \frac{2\pi}{N_\theta} \quad (3.95)$$

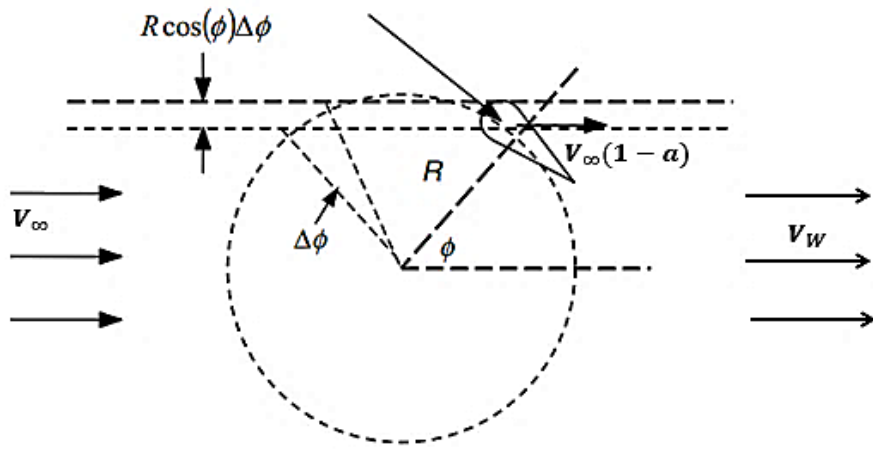


Figure 3.10. Multiple streamtube geometry (modified from [10])

During any given rotation, the blade passes through the stream tube twice at 2 azimuthal angles and these two angle have a relationship

$$\theta_1 + \theta_2 = \pm\pi \quad (3.96)$$

So that

$$\sin(\theta_1) = \sin(\theta_2) \quad (3.97)$$

$$\cos(\theta_1) = -\cos(\theta_2) \quad (3.98)$$

The force on the blade is found from blade element theory.

Applying momentum theory, assuming that the wind at blade element is induced by an induction factor a

$$V = V_\infty(1 - a) \quad (3.99)$$

$$V_W = V_\infty(1 - 2a) \quad (3.100)$$

Blade element relative velocity for the first time

$$W_1 = \sqrt{(R\omega - V\sin\theta_1)^2 + V^2\cos^2\theta_1} \quad (3.101)$$

$$\frac{W_1}{V_\infty} = \sqrt{\left(TSR - \frac{V}{V_\infty}\sin\theta_1\right)^2 + \left(\frac{V}{V_\infty}\right)^2\cos^2\theta_1} \quad (3.102)$$

$$\frac{W_1}{V_\infty} = \sqrt{(TSR - (1 - a)\sin\theta_1)^2 + (1 - a)^2\cos^2\theta_1} \quad (3.103)$$

$$\alpha_1 = \text{atan}\left(\frac{(1 - a)\cos\theta_1}{TSR - (1 - a)\sin\theta_1}\right) \quad (3.104)$$

Blade element relative velocity for the second time

$$\frac{W_2}{V_\infty} = \sqrt{(TSR - (1 - a)\sin\theta_2)^2 + (1 - a)^2\cos^2\theta_2} \quad (3.105)$$

So that

$$\frac{W_1}{V_\infty} = \frac{W_2}{V_\infty} \quad (3.106)$$

$$\alpha_2 = \text{atan}\left(\frac{(1 - a)\cos\theta_2}{TSR - (1 - a)\sin\theta_2}\right) \quad (3.107)$$

Hence,

$$\alpha_2 = -\alpha_1 \quad (3.108)$$

Thus,

$$\cos\alpha_1 = \cos\alpha_2 \quad (3.109)$$

$$\sin\alpha_1 = -\sin\alpha_2 \quad (3.110)$$

Local Reynolds number

$$Re_1 = Re_2 = \frac{W_1 c}{\nu} \quad (3.111)$$

Form AOA together with Re, lift and drag coefficient C_L, C_D of the blade element are interpolated.

Normal force coefficient C_N and tangential force coefficient C_T

$$C_{L1} = -C_{L2} \quad (3.112)$$

$$C_{D1} = C_{D2} \quad (3.113)$$

For the first time

$$C_{N1} = C_{L1} \cos \alpha_1 + C_{D1} \sin \alpha_1 \quad (3.114)$$

$$C_{T1} = C_{L1} \sin \alpha_1 - C_{D1} \cos \alpha_1 \quad (3.115)$$

$$C_{Ti1} = C_{N1} \cos \theta_1 + C_{T1} \sin \theta_1 \quad (3.116)$$

For the second time

$$\begin{aligned} C_{N2} &= C_{L2} \cos \alpha_2 + C_{D2} \sin \alpha_2 = -C_{L1} \cos \alpha_1 + C_{D1} (-\sin \alpha_1) \\ C_{N1} &= -C_{N2} \end{aligned} \quad (3.117)$$

$$\begin{aligned} C_{T2} &= C_{L2} \sin \alpha_2 - C_{D2} \cos \alpha_2 = -C_{L1} (-\sin \alpha_1) - C_{D1} \cos \alpha_1 \\ C_{T1} &= C_{T2} \end{aligned} \quad (3.118)$$

$$P_{i1} = P_{i2}$$

$$\begin{aligned} C_{Ti2} &= C_{N2} \cos \theta_2 + C_{T2} \sin \theta_2 = -C_{N1} (-\cos \theta_1) + C_{T1} \sin \theta_1 \\ C_{Ti1} &= C_{Ti2} \end{aligned} \quad (3.119)$$

$$F_{Ti1} = F_{Ti2}$$

It turns out that the instantaneous thrust and instantaneous power on the blade at both the first and second time crossing position is the same. So that at each stream-tube, only calculation for the azimuthal angles for the first time is needed.

From the beginning for. $-\pi/2 < \theta < \pi/2$

Blade element relative velocity

$$\frac{W}{V_\infty} = \sqrt{(TSR - (1-a)\sin\theta)^2 + (1-a)^2\cos^2\theta} \quad (3.120)$$

$$\alpha = \text{atan}\left(\frac{(1-a)\cos\theta}{TSR - (1-a)\sin\theta}\right) \quad (3.121)$$

Local Reynolds number

$$Re = \frac{Wc}{\nu} \quad (3.122)$$

From AOA together with Re, lift and drag coefficient C_L, C_D of the blade element are interpolated

Normal force coefficient C_N and tangential force coefficient C_T

$$C_N = C_L \cos\alpha + C_D \sin\alpha \quad (3.123)$$

$$C_T = C_L \sin\alpha - C_D \cos\alpha \quad (3.124)$$

Instantaneous thrust coefficient

$$C_{Ti} = C_N \cos\theta + C_T \sin\theta \quad (3.125)$$

Instantaneous thrust for one blade 1 time passing the tube

$$T_i(\theta) = C_{Ti} \frac{1}{2} \rho W^2 H c \quad (3.126)$$

Instantaneous power for one blade 1 time passing the tube

$$P_i = Q_i \omega = \frac{1}{2} \rho W^2 C_T c H R \omega \quad (3.127)$$

$$C_{Pi} = \frac{P_i}{\frac{1}{2} \rho W^3 c H} = \frac{C_T R \omega}{W} = C_T T S R \frac{V_\infty}{W} \quad (3.128)$$

Average power

$$P = N \frac{1}{2\pi} \int_{-\pi/2}^{\pi/2} 2P_i d\theta = N \frac{1}{\pi} \frac{1}{2} \rho W^3 c H \int_{-\pi/2}^{\pi/2} C_{Pi} d\theta \quad (3.129)$$

Average power coefficient

$$C_P = \frac{P}{\frac{1}{2} \rho V_\infty^3 D H} = \frac{N \frac{1}{\pi} \frac{1}{2} \rho W^3 c H \int_{-\pi/2}^{\pi/2} C_{Pi} d\theta}{\frac{1}{2} \rho V_\infty^3 D H} \quad (3.130)$$

$$C_P = \frac{\sigma}{\pi} \left(\frac{W}{V_\infty} \right)^3 \int_{-\pi/2}^{\pi/2} C_{Pi} d\theta \quad (3.131)$$

For N blade and for one revolution one blade pass through a tube twice with a total time of $2\Delta\theta$

$$T_{ni}(\theta) = \frac{NT_i(\theta) \cdot 2\Delta\theta}{2\pi} = \frac{N \cdot \Delta\theta}{2\pi} C_{Ti} \rho W^2 H c \quad (3.132)$$

Average thrust

$$Thrust = \frac{N}{2\pi} \int_{-\pi/2}^{\pi/2} 2T_i(\theta) d\theta \quad (3.133)$$

Average thrust coefficient

$$\begin{aligned} C_{Thrust} &= \frac{Thrust}{\frac{1}{2} \rho V_\infty^2 D H} = \frac{\frac{N}{2\pi} \int_{-\pi/2}^{\pi/2} 2T_i(\theta) d\theta}{\frac{1}{2} \rho V_\infty^2 D H} \\ &= \frac{\frac{N}{2\pi}}{\frac{1}{2} \rho V_\infty^2 D H} \int_{-\pi/2}^{\pi/2} 2T_i(\theta) d\theta \end{aligned} \quad (3.134)$$

$$= \frac{\frac{N}{2\pi} \rho W^2 H c}{\frac{1}{2} \rho V_\infty^2 D H} \int_{-\pi/2}^{\pi/2} C_{Ti} d\theta = \frac{2Nc}{2\pi D} \left(\frac{W}{V_\infty} \right)^2 \int_{-\pi/2}^{\pi/2} C_{Ti} d\theta \quad (3.135)$$

$$C_{Thrust} = \frac{\sigma}{\pi} \left(\frac{W}{V_\infty} \right)^2 \int_{-\pi/2}^{\pi/2} C_{Ti} d\theta \quad (3.136)$$

Thrust from momentum theory at a streamtube

$$T_{mt} = \rho(RH\Delta\theta|\cos\theta|)V(V_\infty - V_W) \quad (3.137)$$

$$= \rho(RH\Delta\theta|\cos\theta|)V_\infty(1-a)(V_\infty - V_\infty(1-2a)) \quad (3.138)$$

$$F = V_\infty^2(RH\Delta\theta|\cos\theta|)\rho 2a(1-a) \quad (3.139)$$

The thrust equating equation is.

$$V_\infty^2\rho(RH\Delta\theta|\cos\theta|)2a(1-a) = \frac{N\Delta\theta}{\pi}\frac{1}{2}\rho W^2 H c C_{Ti} \quad (3.140)$$

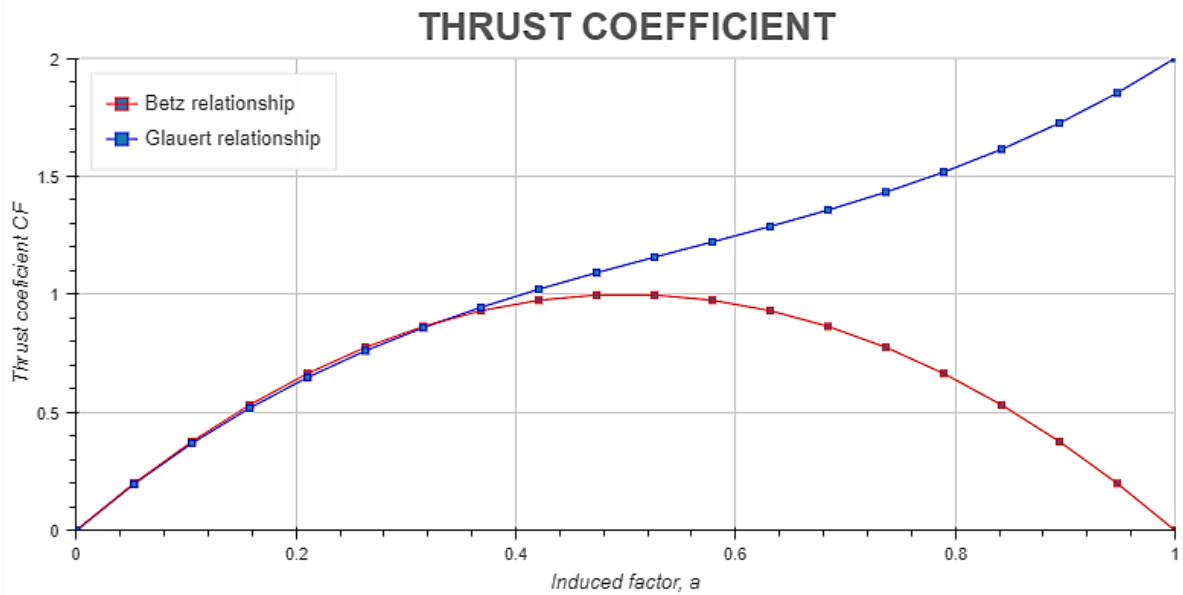
$$4a(1-a) = \frac{Nc}{\pi R} \left(\frac{W}{V_\infty}\right)^2 \frac{C_{Ti}}{|\cos\theta|} \quad (3.141)$$

$$4a(1-a) = \frac{2\sigma}{\pi} \left(\frac{W}{V_\infty}\right)^2 \frac{C_{Ti}}{|\cos\theta|} \quad (3.142)$$

From this equation, new induction factor a can be obtained and repeat the procedure until getting the converged value of a .

Momentum theory is not valid at axial induced factors greater than 0.5 because the wind velocity in the far wake would be negative. However, in practice, as the axial induced factor increases above 0.5 and thrust coefficients increase up to 2.0 [10]. Thus, experimental thrust coefficient by Glauert is used.

$$C_{T_{mt}} = 4a \left[1 - \frac{1}{4}(5 - 3a)a \right] \quad (3.143)$$

**Figure 3.11. Thrust force coefficient as a function of induced factor a**

Ultimately, the thrust equating equation is.

$$4a \left[1 - \frac{1}{4}(5 - 3a)a \right] = \frac{2\sigma}{\pi} \left(\frac{W}{V_\infty} \right)^2 \frac{C_{Ti}}{|\cos \theta|} \quad (3.144)$$

Set

$$d = \frac{2\sigma}{\pi} \left(\frac{W}{V_\infty} \right)^2 \frac{C_{Ti}}{|\cos \theta|} \quad (3.145)$$

Iteration condition becomes.

$$3a^3 - 5a^2 + 4a - d = 0 \quad (3.146)$$

Table 3.6. Synthesized equations and step for calculations

MULTIPLE STREAMTUBE MODEL
$a_{initial} = 0$
TSR, σ are needed
$-\pi/2 < \theta < \pi/2$
$\frac{W}{V_\infty}$ $= \sqrt{(TSR - (1 - a)\sin\theta)^2 + (1 - a)^2\cos^2\theta}$
$\alpha = \text{atan} \frac{(1 - a)\cos\theta}{TSR - (1 - a)\sin\theta}$
$Re = \frac{Wc}{\nu}$
C_L, C_D
$C_N = C_L \cos\alpha + C_D \sin\alpha$
$C_T = C_L \sin\alpha - C_D \cos\alpha$
$C_{Ti} = C_N \cos\theta + C_T \sin\theta$
$C_{Pi} = \frac{C_T TSR}{\left(\frac{W}{V_\infty}\right)}$
$d = \frac{2\sigma}{\pi} \left(\frac{W}{V_\infty}\right)^2 \frac{C_{Ti}}{ \cos\theta }$
$3a^3 - 5a^2 + 4a - d = 0$
a_{new}
a_{final}
$C_{Thrust} = \frac{\sigma}{\pi} \left(\frac{W}{V_\infty}\right)^2 \int_{-\pi/2}^{\pi/2} C_{Ti} d\theta$
$C_P = \frac{\sigma}{\pi} \left(\frac{W}{V_\infty}\right)^3 \int_{-\pi/2}^{\pi/2} C_{Pi} d\theta$

3.8 Double-Multiple Streamtube Model

Aerodynamic streamtube models are based on the conservation of momentum principle in a quasi-steady flow

forces on the rotor blades = changes in streamwise momentum through the turbine

3.8.1 Aerodynamic Model

The freestream velocity profile is assumed uniform with height. The upwind velocity component is less than the local ambient wind velocity, $V < V_{\infty i}$, and in the middle plane between the upstream and the down-stream zone there is an equilibrium induced velocity, $V_w < V$; thus the induced velocity decreases in the axial streamtube direction so that the downwind component is less than the equilibrium velocity, $V' < V_w$

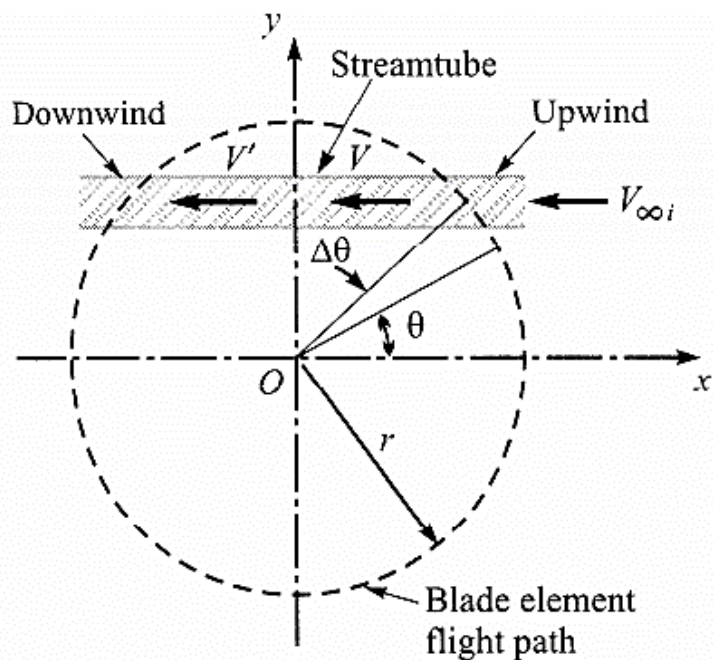


Figure 3.12. Plan view of VAWT [8]

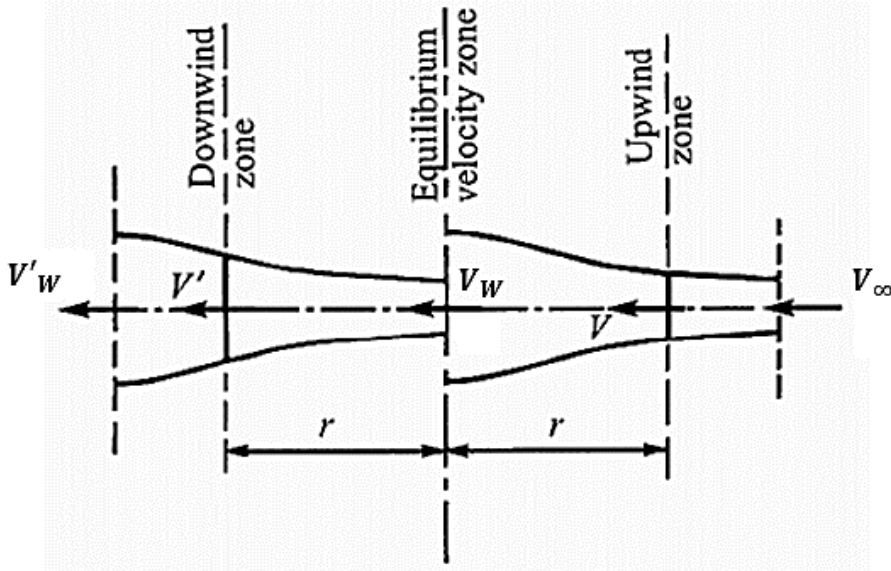


Figure 3.13. Rotor element ABCD replaced by two actuator disks in tandem (modified from [8])

For the upstream half-cycle of the rotor, the local wind velocity decreases by an interference factor of $a < 1$

$$V = V_{\infty}(1 - a) \quad (3.147)$$

Equilibrium-induced velocity

$$V_W + V_{\infty} = 2V \Leftrightarrow V_W + V_{\infty} = 2V_{\infty}(1 - a) \quad (3.148)$$

$$V_W = V_{\infty}(1 - 2a) \quad (3.149)$$

For the down-stream half-cycle of the rotor, V_W is the input velocity and, at the end of the streamtube, and the second interference factor for this part of the rotor is a' , induced velocity would be

$$V' = V_W(1 - a') = V_{\infty}(1 - 2a)(1 - a') \quad (3.150)$$

3.8.2 Upwind Half of the Rotor

The local relative velocity for the upstream half-cycle of the rotor, $-\frac{\pi}{2} < \theta < \frac{\pi}{2}$

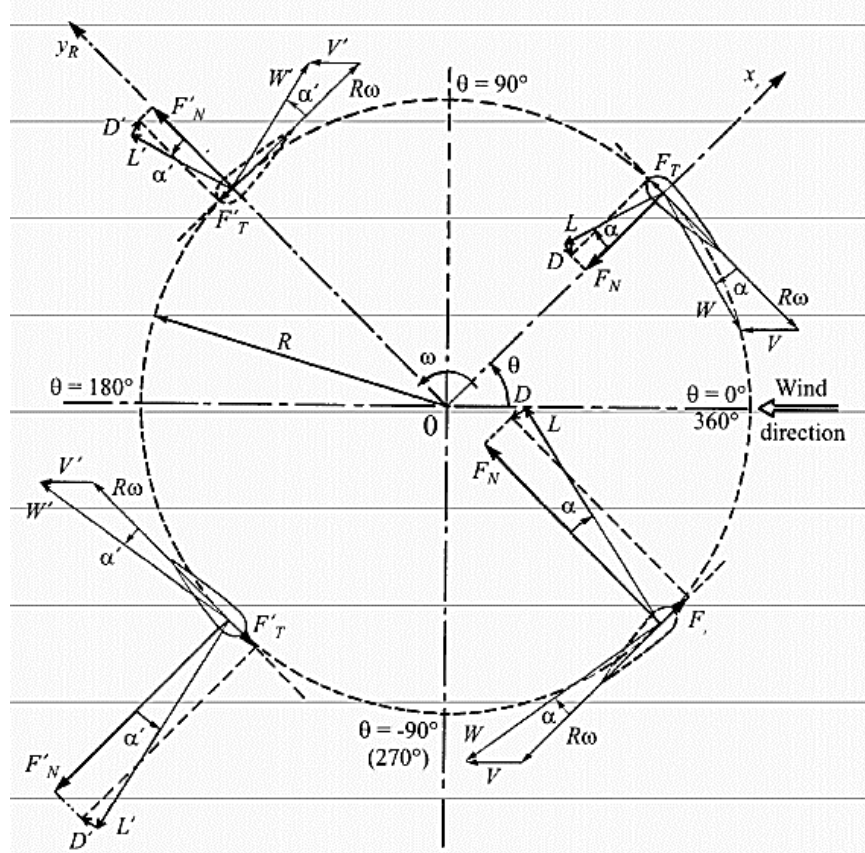


Figure 3.14. Angles, forces and velocity vectors at the equator [8]

From aerodynamics of VAWT, blade element relative velocity

$$W = \sqrt{(R\omega - V\sin\theta)^2 + V^2\cos^2\theta} \quad (3.151)$$

$$\frac{W}{V_\infty} = \sqrt{\left(TSR - \frac{V}{V_\infty}\sin\theta\right)^2 + \left(\frac{V}{V_\infty}\right)^2\cos^2\theta} \quad (3.152)$$

$$\frac{W}{V_\infty} = \sqrt{(TSR - (1-a)\sin\theta)^2 + (1-a)^2\cos^2\theta} \quad (3.153)$$

The expression for the local angle of attack may be derived.

$$\alpha = \text{atan} \left(\frac{\frac{V}{V_\infty}\cos\theta}{TSR - \frac{V}{V_\infty}\sin\theta} \right) \quad (3.154)$$

$$\alpha = \text{atan} \left(\frac{(1-a)\cos\theta}{TSR - (1-a)\sin\theta} \right) \quad (3.155)$$

Local Reynolds number

$$Re = \frac{Wc}{\nu} \quad (3.156)$$

Form AOA together with Re, lift and drag coefficient C_L, C_D of the blade element are interpolated

Normal force coefficient C_N and tangential force coefficient C_T

$$C_N = C_L \cos \alpha + C_D \sin \alpha \quad (3.157)$$

$$C_T = C_L \sin \alpha - C_D \cos \alpha \quad (3.158)$$

Instantaneous thrust coefficient

$$C_{Ti} = C_N \cos \theta + C_T \sin \theta \quad (3.159)$$

Instantaneous thrust for one blade

$$T_i(\theta) = C_{Ti} \frac{1}{2} \rho W^2 H c \quad (3.160)$$

thrust from momentum theory at a streamtube

$$T_{mt} = \rho (RH \Delta \theta |\cos \theta|) V (V_\infty - V_W) \quad (3.161)$$

$$T_{mt} = V_\infty^2 (RH \Delta \theta |\cos \theta|) \rho 2a(1-a) \quad (3.162)$$

the thrust equating equation is.

$$V_\infty^2 (RH \Delta \theta |\cos \theta|) \rho 2a(1-a) = \frac{N \Delta \theta}{2\pi} C_{Ti} \frac{1}{2} \rho W^2 H c \quad (3.163)$$

$$4a(1-a) = \frac{Nc}{2\pi R} \left(\frac{W}{V_\infty} \right)^2 \frac{C_{Ti}}{|\cos \theta|} \quad (3.164)$$

$$4a(1-a) = \frac{\sigma}{\pi} \left(\frac{W}{V_\infty} \right)^2 \frac{C_{Ti}}{|\cos \theta|} \quad (3.165)$$

thrust equating equation with Glauert correction

$$4a \left[1 - \frac{1}{4} (5 - 3a)a \right] = \frac{\sigma}{\pi} \left(\frac{W}{V_\infty} \right)^2 \frac{C_{Ti}}{|\cos \theta|} \quad (3.166)$$

Let

$$d = \frac{\sigma}{\pi} \left(\frac{W}{V_\infty} \right)^2 \frac{C_{Ti}}{|\cos \theta|} \quad (3.167)$$

Iteration condition becomes.

$$3a^3 - 5a^2 + 4a - d = 0 \quad (3.168)$$

Average up wind thrust coefficient

$$C_{Thrust} = \frac{\sigma}{2\pi} \left(\frac{W}{V_\infty} \right)^2 \int_{-\pi/2}^{\pi/2} C_{Ti} d\theta$$

Instantaneous power coefficient

$$C_{P_i} = \frac{P_i}{\frac{1}{2} \rho W^3 c H} = C_T \frac{R\omega}{W} \quad (3.169)$$

$$C_{P_i} = C_T TSR \frac{V_\infty}{W} \quad (3.170)$$

Average upwind power coefficient

$$C_P = \frac{\sigma}{2\pi} \left(\frac{W}{V_\infty} \right)^3 \int_{-\pi/2}^{\pi/2} C_{P_i} d\theta \quad (3.171)$$

3.8.3 Downwind Half of the Rotor

For the second half of the rotor in the stream flow direction $\pi/2 \leq 0 \leq 3\pi/2$, the local relative velocity W' calculated the same way as upwind the local relative velocity W

$$W' = \sqrt{(R\omega - V' \sin \theta)^2 + V'^2 \cos^2 \theta} \quad (3.172)$$

$$\frac{W'}{V_w} = \sqrt{\left(\frac{R\omega}{V_w} - \frac{V'}{V_w} \sin \theta \right)^2 + \left(\frac{V'}{V_w} \right)^2 \cos^2 \theta} \quad (3.173)$$

Set

$$TSR' = \frac{R\omega}{V_W} = \frac{R\omega}{V_\infty} \frac{V_\infty}{V_W} = \frac{TSR}{1 - 2a} \quad (3.174)$$

$$\frac{W'}{V_W} = \sqrt{(TSR' - (1 - a')\sin\theta)^2 + (1 - a')^2\cos^2\theta} \quad (3.175)$$

Similarly, downwind local angle of attack α' is calculated on the basis of geometric consideration in a comparable manner to upwind local angle of attack α

$$\alpha' = \tan^{-1} \left(\frac{\frac{V'}{V_W} \cos\theta}{\frac{R\omega}{V_W} - \frac{V'}{V_W} \sin\theta} \right) \quad (3.176)$$

$$\alpha' = \tan^{-1} \left(\frac{(1 - a') \cos\theta}{TSR' - (1 - a')\sin\theta} \right) \quad (3.177)$$

Local Reynolds number

$$Re' = \frac{W' c}{\nu} \quad (3.178)$$

Form AOA together with Re, lift and drag coefficient C_L', C_D' of the blade element are interpolated

Normal force coefficient C'_N and tangential force coefficient C'_T

$$C'_N = C_L' \cos\alpha + C_D' \sin\alpha \quad (3.179)$$

$$C'_T = C_L' \sin\alpha - C_D' \cos\alpha \quad (3.180)$$

Instantaneous thrust coefficient

$$C'_{Ti} = C'_N \cos\theta + C'_T \sin\theta \quad (3.181)$$

Instantaneous thrust for one blade

$$T_i'(\theta) = C'_{Ti} \frac{1}{2} \rho W'^2 H c \quad (3.182)$$

Thrust from momentum theory at a streamtube

$$\begin{aligned} T_{mt} &= \rho(RH\Delta\theta|\cos\theta|)V'(V_W - V'_W) \\ &= \rho(RH\Delta\theta|\cos\theta|)V_W(1 - a')(V_W - V_W(1 - 2a')) \end{aligned} \quad (3.183)$$

$$T_{mt} = V_W^2(RH\Delta\theta|\cos\theta|)\rho 2a'(1 - a') \quad (3.184)$$

The thrust equating equation is.

$$V_W^2(RH\Delta\theta|\cos\theta|)\rho 2a'(1 - a') = \frac{N\Delta\theta}{2\pi} C_{Ti}' \frac{1}{2} \rho W'^2 H c \quad (3.185)$$

$$4a'(1 - a') = \frac{\sigma}{\pi} \left(\frac{W'}{V_W} \right)^2 \frac{C'_{Ti}}{|\cos\theta|} \quad (3.186)$$

Thrust equating equation with Glauert correction

$$4a' \left[1 - \frac{1}{4}(5 - 3a')a' \right] = \frac{\sigma}{\pi} \left(\frac{W'}{V_W} \right)^2 \frac{C'_{Ti}}{|\cos\theta|} \quad (3.187)$$

Set

$$d' = \frac{\sigma}{\pi} \left(\frac{W'}{V_W} \right)^2 \frac{C'_{Ti}}{|\cos\theta|} \quad (3.188)$$

Iteration condition becomes.

$$3a'^3 - 5a'^2 + 4a' - d' = 0 \quad (3.189)$$

Average down wind thrust coefficient

$$C_{Thrust}' = \frac{\sigma}{2\pi} \left(\frac{W'}{V_\infty} \right)^2 \int_{\pi/2}^{3\pi/2} C_{Ti}' d\theta \quad (3.190)$$

$$C_{Thrust}' = \frac{\sigma}{2\pi} \left(\frac{V_W}{V_\infty} \frac{W'}{V_W} \right)^2 \int_{\frac{\pi}{2}}^{\frac{3\pi}{2}} C_{Ti}' d\theta \quad (3.191)$$

$$C_{Thrust}' = \frac{\sigma}{2\pi} \left((1 - 2a) \frac{W'}{V_W} \right)^2 \int_{\pi/2}^{3\pi/2} C_{Ti}' d\theta \quad (3.192)$$

Instantaneous tangential force

$$F_T' = \frac{1}{2} \rho W'^2 C_T' c H \quad (3.193)$$

Instantaneous torque

$$Q_i' = F_T' R \quad (3.194)$$

Instantaneous power

$$P_i' = Q_i' \omega = \frac{1}{2} \rho W'^2 C_T' c H R \omega \quad (3.195)$$

Instantaneous downwind power coefficient

$$C_{P_i}' = \frac{P_i'}{\frac{1}{2} \rho W'^3 c H} = C_T' \frac{R \omega}{W'} \quad (3.196)$$

$$C_{P_i}' = C_T' \frac{R \omega}{V_W} \frac{V_W}{W'} = C_T' \frac{R \omega}{V_W} \frac{V_W}{W'} \quad (3.197)$$

$$C_{P_i}' = \frac{C_T' TSR'}{\left(\frac{W'}{V_W}\right)} \quad (3.198)$$

Average downwind power

$$P' = N \frac{1}{T} \int_{\frac{T}{4}}^{\frac{3T}{4}} P_i'(\theta) dt = N \frac{1}{2\pi} \int_{\frac{\pi}{2}}^{\frac{3\pi}{2}} P_i' d\theta \quad (3.199)$$

$$P' = N \frac{\frac{1}{2} \rho W'^3 c H}{2\pi} \int_{\pi/2}^{3\pi/2} C_{P_i}' d\theta \quad (3.200)$$

Average downwind power coefficient

$$C_P' = \frac{P'}{\frac{1}{2} \rho V_\infty^3 D H} = \frac{\frac{1}{2} N \rho W'^3 c H}{\frac{1}{2} \rho V_\infty^3 D H} \int_{\pi/2}^{3\pi/2} C_{P_i}' d\theta \quad (3.201)$$

$$C'_P = \frac{Nc}{D2\pi} \left(\frac{W'}{V_\infty} \right)^3 \int_{\frac{\pi}{2}}^{\frac{3\pi}{2}} C'_{P_i} d\theta \quad (3.202)$$

$$C'_P = \frac{\sigma}{2\pi} \left(\frac{W'}{V_\infty} \right)^3 \int_{\frac{\pi}{2}}^{\frac{3\pi}{2}} C'_{P_i} d\theta \quad (3.203)$$

$$C'_P = \frac{\sigma}{2\pi} \left(\frac{W'}{V_W(1 - 2a)} \right)^3 \int_{\frac{\pi}{2}}^{\frac{3\pi}{2}} C'_{P_i} d\theta \quad (3.204)$$

Total wind turbine thrust coefficient

$$C_{Thrust_{total}} = C_{Thrust} + C_{Thrust}' \quad (3.205)$$

Total wind turbine thrust coefficient

$$C_{P_{total}} = C_P + C_P' \quad (3.206)$$

Table 3.7. Synthesized equations and step for calculations for the whole turbine

DOUBLE-MULTIPLE STREAMTUBE MODEL	
UPWIND	DOWNDOWN
$a_{initial} = 0$	$a'_{initial} = a_{converged}$ $= a(\text{final upwind value})$
TSR	$TSR' = \frac{TSR}{1 - 2a}$
$\frac{W}{V_\infty} = \sqrt{(TSR - (1 - a)\sin\theta)^2 + (1 - a)^2 \cos^2\theta}$	$\frac{W'}{V_W} = \sqrt{(TSR' - (1 - a')\sin\theta)^2 + (1 - a')^2 \cos^2\theta}$
$\alpha = \tan^{-1}\left(\frac{(1 - a) \cos\theta}{TSR - (1 - a)\sin\theta}\right)$	$\alpha' = \tan^{-1}\left(\frac{(1 - a') \cos\theta}{TSR' - (1 - a')\sin\theta}\right)$
$Re = \frac{Wc}{\nu}$	$Re' = \frac{W'c}{\nu}$
C_L, C_D	C'_L, C'_D
$C_N = C_L \cos\alpha + C_D \sin\alpha$	$C'_N = C'_L \cos\alpha + C'_D \sin\alpha$
$C_T = C_L \sin\alpha - C_D \cos\alpha$	$C'_T = C'_L \sin\alpha - C'_D \cos\alpha$
$C_{Ti} = C_N \cos\theta + C_T \sin\theta$	$C'_{Ti} = C'_N \cos\theta + C'_T \sin\theta$
$C_{P_i} = \frac{C_T TSR}{\left(\frac{W}{V_\infty}\right)}$	$C'_{P_i} = \frac{C'_T TSR'}{\left(\frac{W'}{V_W}\right)}$
$d = \frac{\sigma}{\pi} \left(\frac{W}{V_\infty}\right)^2 \frac{C_{Ti}}{ \cos\theta }$	$d' = \frac{\sigma}{\pi} \left(\frac{W'}{V_W}\right)^2 \frac{C'_{Ti}}{ \cos\theta }$
$3a_{new}^3 - 5a_{new}^2 + 4a_{new} - d = 0$	$3a'_{new}^3 - 5a'_{new}^2 + 4a'_{new} - d = 0$
a_{new}	a'_{new}
$a_{converged}, a'_{converged}$	
$C_{Thrust} = \frac{\sigma}{2\pi} \left(\frac{W}{V_\infty}\right)^2 \int_{-\pi/2}^{\pi/2} C_{Ti} d\theta$	$C'_{Thrust} = \frac{\sigma}{2\pi} \left((1 - 2a) \frac{W'}{V_W}\right)^2 \int_{\pi/2}^{3\pi/2} C'_{Ti} d\theta$
$C_P = \frac{\sigma}{2\pi} \left(\frac{W}{V_\infty}\right)^3 \int_{-\pi/2}^{\pi/2} C_{P_i} d\theta$	$C'_{P_i} = \frac{\sigma}{2\pi} \left(\frac{W'}{V_W} (1 - 2a)\right)^3 \int_{\pi/2}^{3\pi/2} C'_{P_i} d\theta$
$C_{Thrust_{total}} = C_{Thrust} + C'_{Thrust}$	
$C_{P_{total}} = C_P + C'_{P_i}$	

3.9 Finite Aspect Ratio Effect

Straight blade wind turbine performance prediction is significantly affected by blade tips and finite aspect ratio effects [11]. The blade tips of the straight-bladed rotor induce a velocity that can be broken down into two components [8].

- Spanwise component along the length of the blade
- Downwash component in the plane of the blade airfoil

The spanwise component varies along the entire length of the blade, the air passing through the rotor flows toward the tips of the blade, and the streamtubes passing near the blade tips consequently transfer less momentum to the airfoil than those passing at the equator. The blade tips are consequently less efficient than the rest of the blade. To evaluate this effect a method developed by Prandtl for propellers is used.

The downwash component (finite aspect ratio) affects the angle of attack α , which consequently impacts the lift and drag coefficients C_L and C_D respectively. Prandtl's finite wing theory is used to correct this.

For spanwise component

A new F factor was introduced.

$$F = \frac{2}{\pi} \cos^{-1}(e^{-f}) \quad (3.207)$$

Where,

$$f = \frac{N}{2} \frac{1 - |\eta|}{|\eta \sin \alpha|} \quad (3.208)$$

With $-1 \leq \eta \leq 1$. non-dimensional rotor height

N . number of blades

α . local angle of attack when $F = 1$

Consequently, relative velocity and angle of attack can be recalculated as:

$$\frac{W}{V_\infty} = \sqrt{(TSR - (1 - a)\sin\theta)^2 + (1 - a)^2 F^2 \cos^2 \theta} \quad (3.209)$$

$$\alpha = \text{atan} \left(\frac{(1 - a)F \cos \theta}{TSR - (1 - a)\sin\theta} \right) \quad (3.210)$$

Also, for the left hand site of the iteration equation, F is multiplied into.

$$3Fa^3 - 5Fa^2 + 4Fa - d = 0 \quad (3.211)$$

For downwash component

After getting $C_{L(2D)}$, $C_{D(2D)}$ from the interpolation form the drag polars

$$C_{L(3D)} = \frac{C_{L(2D)}}{1 + \frac{a_0}{\pi AR}} \quad (3.212)$$

$$C_{D(3D)} = C_{D(2D)} + \frac{C_{L(3D)}^2}{\pi AR} \quad (3.213)$$

Where,

$$a_0 = 1.8\pi \left(1 + 0.8 \frac{t}{c} \right) \quad (3.214)$$

t/c . airfoil thickness over chord

$$AR = b^2/S = H/c$$

Chapter 4. RESULTS VALIDATION AND DISCUSSION

4.1 Comparison with Numerical Simulation

In this section, in order to validate the calculation process, simulation results of this thesis is compared with other numerical simulation results which was also calculated using the same Double Multiple Streamtube model. All the airfoil aerodynamic characteristics used for calculation process are obtained from I. Paraschivoiu's Wind Turbine Design book [8], and a publication from R. E. Sheldahl and P. C. Klimas [12].

Sandia 17 m VAWT

Eduard Dyachuk, from Uppsala University, Sweden, he used both vortex model and double multiple streamtube model to calculate some aerodynamic parameters at the equator of the turbine rotor in his thesis [13]. It is important to emphasize that the data on this turbine are in 2D

Table 4.1. Sandia 17 m VAWT parameters [13], [14]

Sandia 17-m VAWT	
Rotor maximum diameter (m)	16.72
Rotor height (m)	16.72
Swept area (m^2)	187
Blade airfoil	2 x NACA0015
Blade chord (m)	0.612
Solidity	0.11
Rotational speed (rpm)	38.7
ω (rad/s)	4.05

Reference simulation data is obtain from [13] with different operation conditions are illustrated in the following graphs together with this thesis computation.

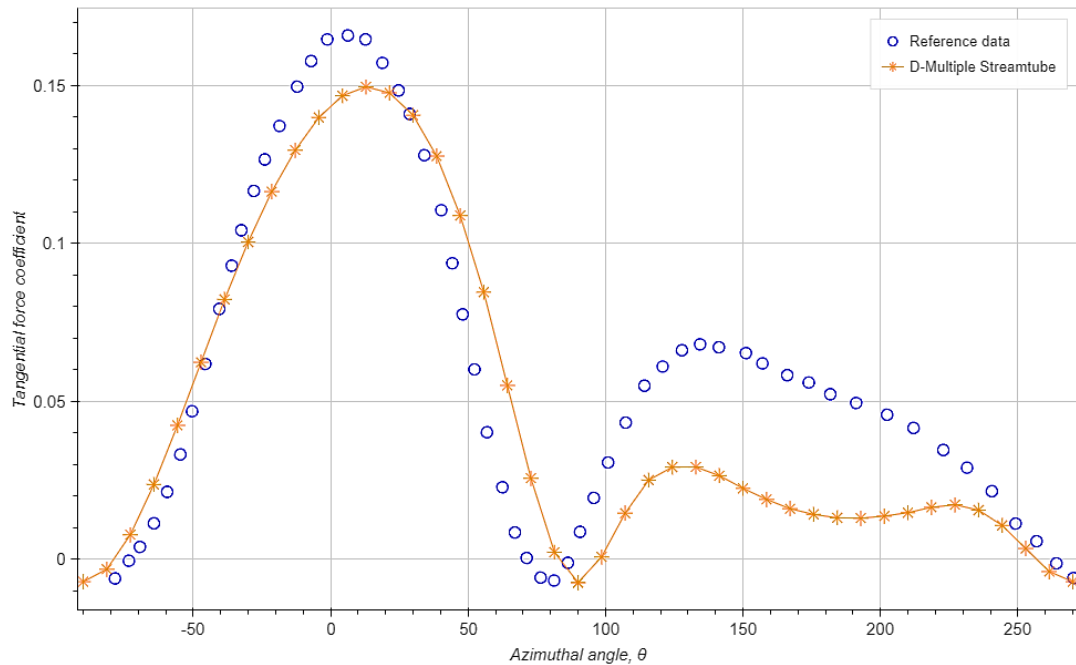


Figure 4.1. Tangential force coefficient from two calculation at $TSR = 4.6$

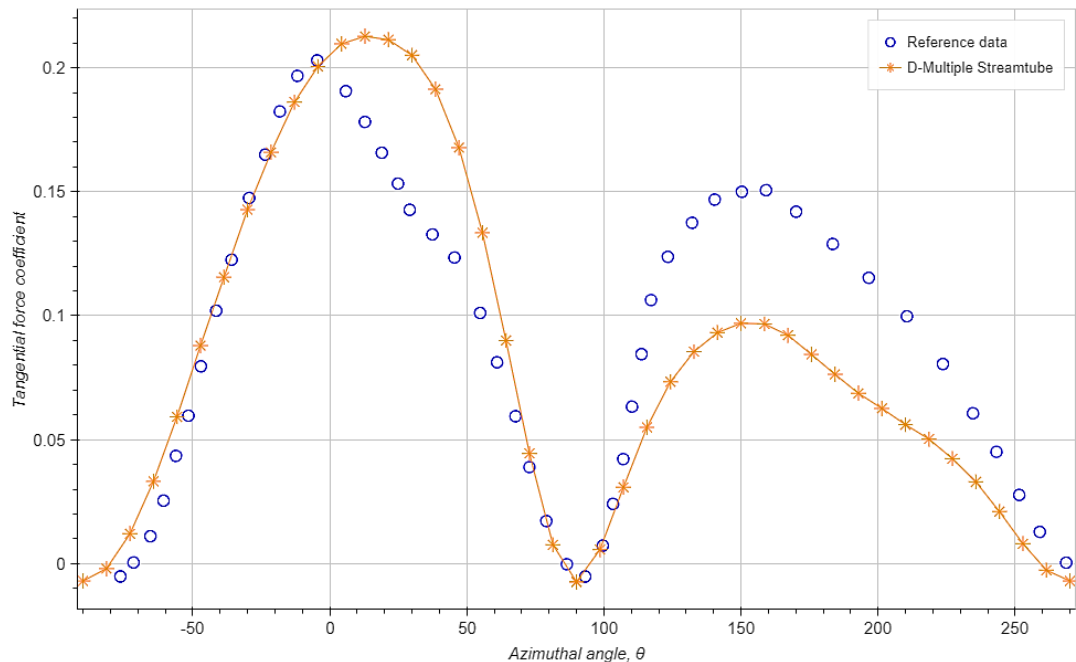


Figure 4.2. Tangential force coefficient from two calculation at $TSR = 3.7$

There is a good agreement of the two tangential force graph in the upwind half of the rotor, while in the downwind half of the rotor, this thesis simulation under predict the force compared to the reference simulation data.

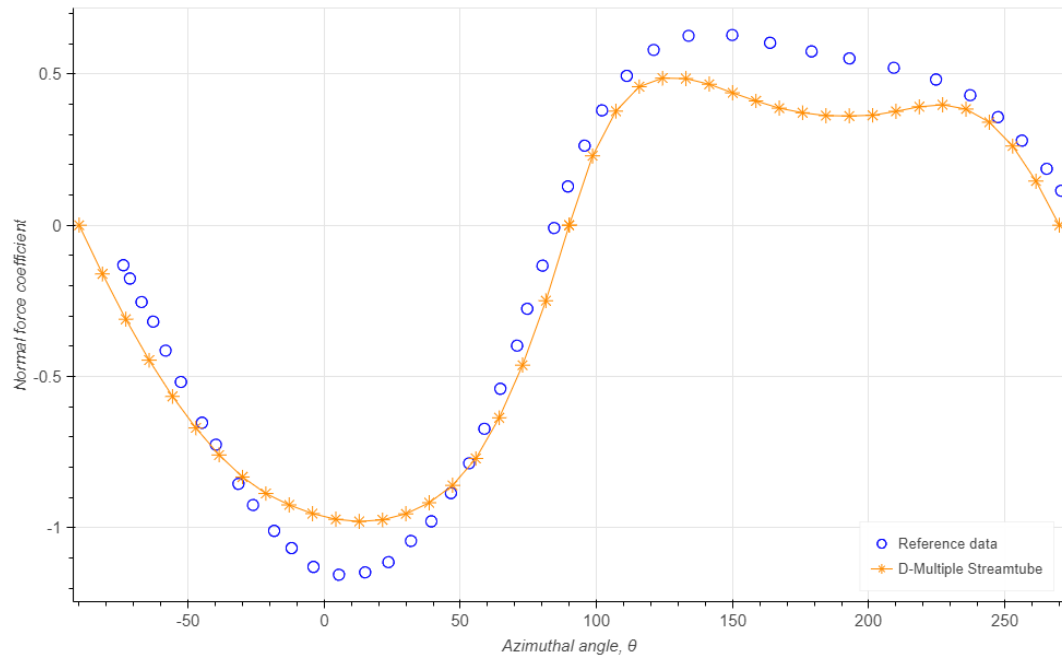


Figure 4.3. Normal force coefficient from two calculation at $TSR = 4.6$

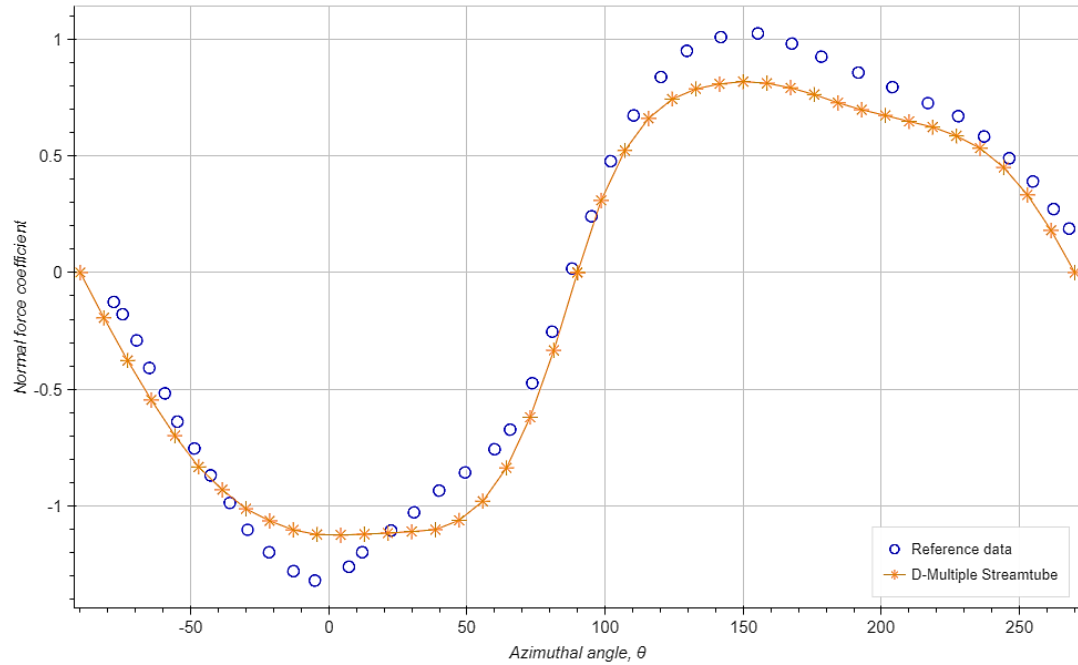


Figure 4.4. Normal force coefficient from two calculation at $TSR = 3.7$

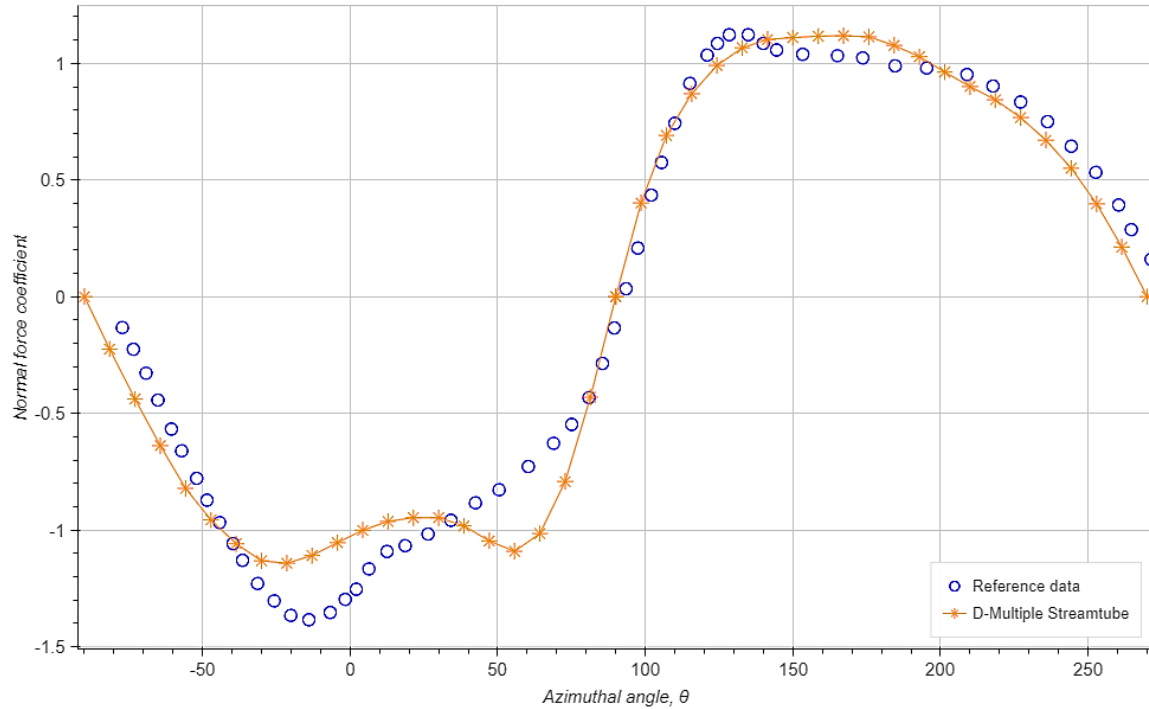


Figure 4.5. Normal force coefficient from two calculation at $TSR = 3.09$

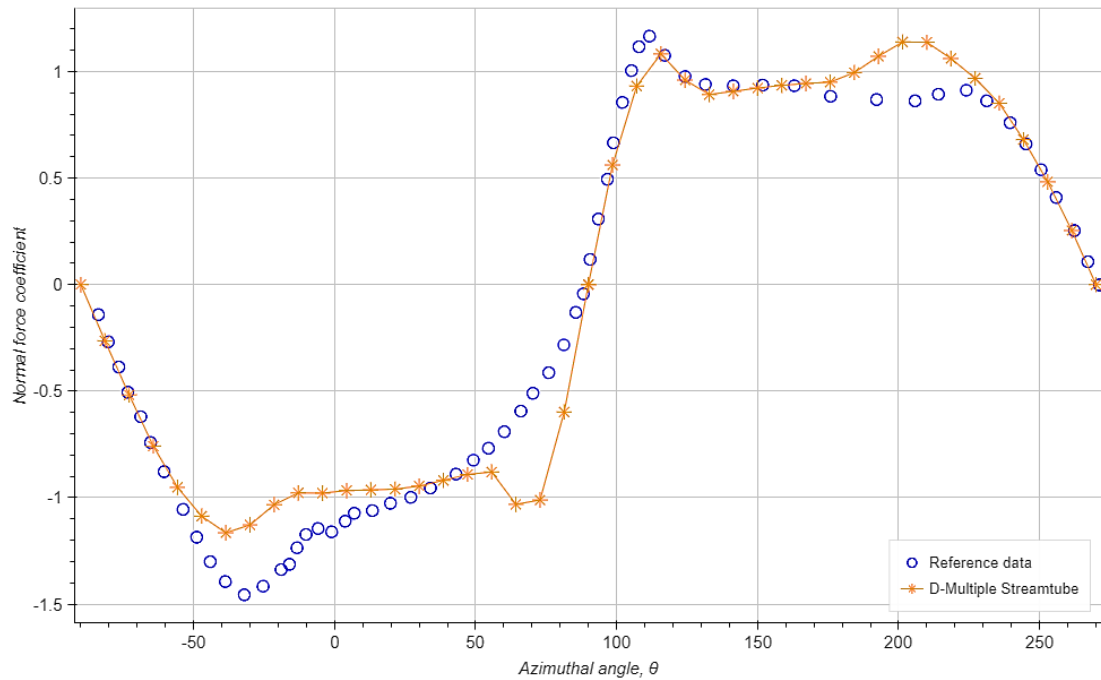


Figure 4.6. Normal force coefficient from two calculation at $TSR = 2.49$

In terms of normal force coefficient, at all tip speed ratio, two sources of data produce a very good agreement. And the similarity of two graph increase as the tip speed ratio getting larger.

VAWT H-260

In the UK VAWT Ltd constructed 20 m diameter VAWT-260 turbine that operated on the Scilly Isles with a rated power of 105 kW. Aerodynamics parameters of this turbine is evaluated using double multiple streamtube by L.H. Trong in his thesis. [11].

Table 4.2. VAWT H-260 parameters [11], [15]

VAWT Ltd 260H	
Rated power (kW)	105
Rotational speed (rpm)	33
Rated wind speed (m/s)	10
Rotor diameter (m)	19.5
Swept area (m^2)	260
Blade airfoil	2 x NACA 0018
Blade chord (m)	1.02
Solidity	0.105
AR	13

Reference simulation data is obtain from [11] at $TSR = 4$ and rotational speed of 33 RPM are illustrated in the following graphs together with this thesis computation.

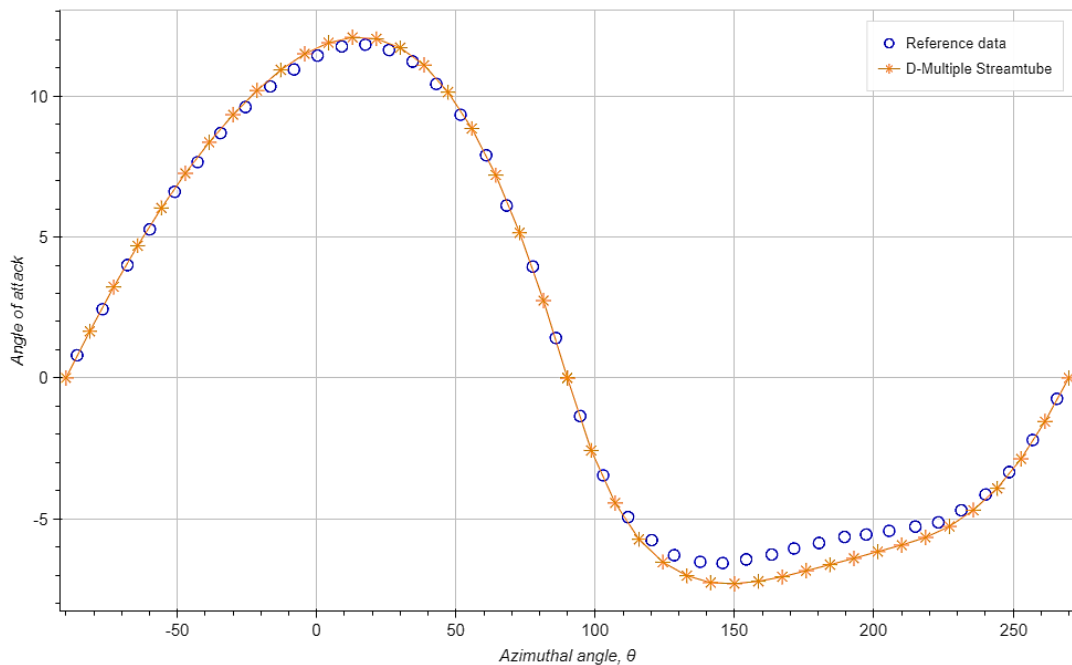
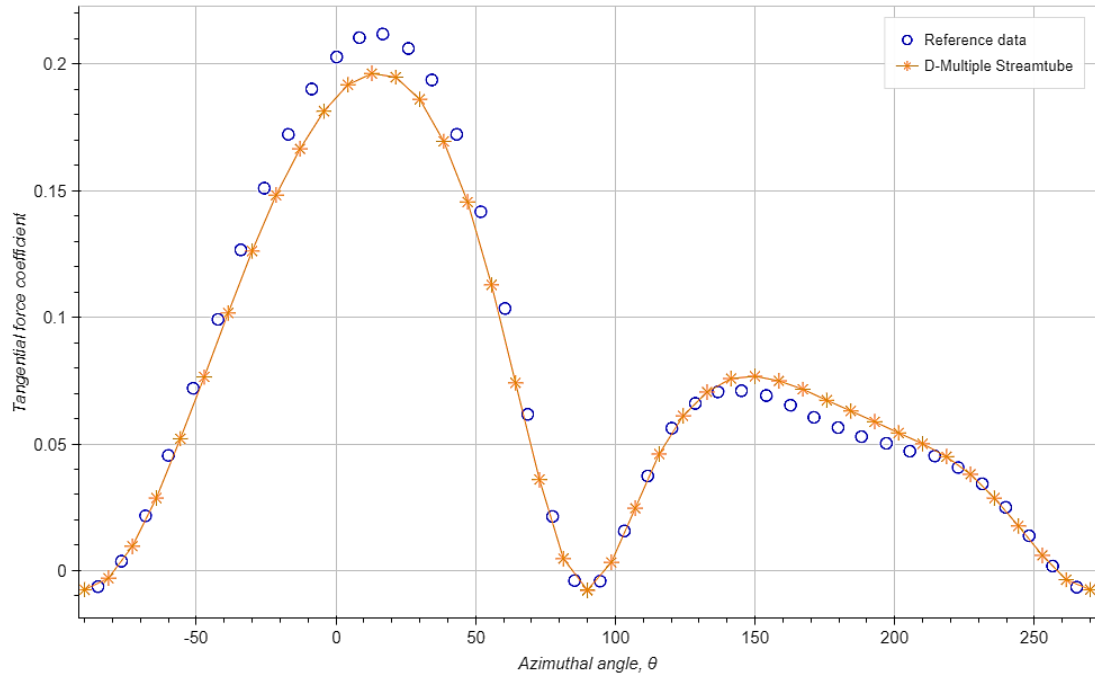


Figure 4.7. Local AOA from two calculation at $TSR = 4, \omega = 33 RPM$

Figure 4.8. Tangential force coefficient from two calculation at $TSR = 4, \omega = 33 RPM$

Both graph show that there is good agreement of the two graph in both tangential force and angle of attack. The biggest discrepancy of tangential force occurs in the azimuthal position of 20°

In a paper about numerical Investigation of VAWT from University of Belgrade [9], authors also use Double Streamtube Model to predict the power curves of a turbine to compare with 2D CFD simulation. As a result, the two the 2D CFD simulation produce a performance prediction that poorly agreeable with numerical simulation data.

Table 4.3. Turbine parameters [9]

Rated wind speed (m/s)	5
Rotor diameter (m)	4
Rotor height (m)	4
Swept area (m^2)	16
Blade airfoil	3 x NACA 0012
Blade chord (m)	0.2
Solidity	0.15

Reference numerical simulation data is obtain from [9] at different TSR are illustrated in the following graphs together with this thesis computation using two models.

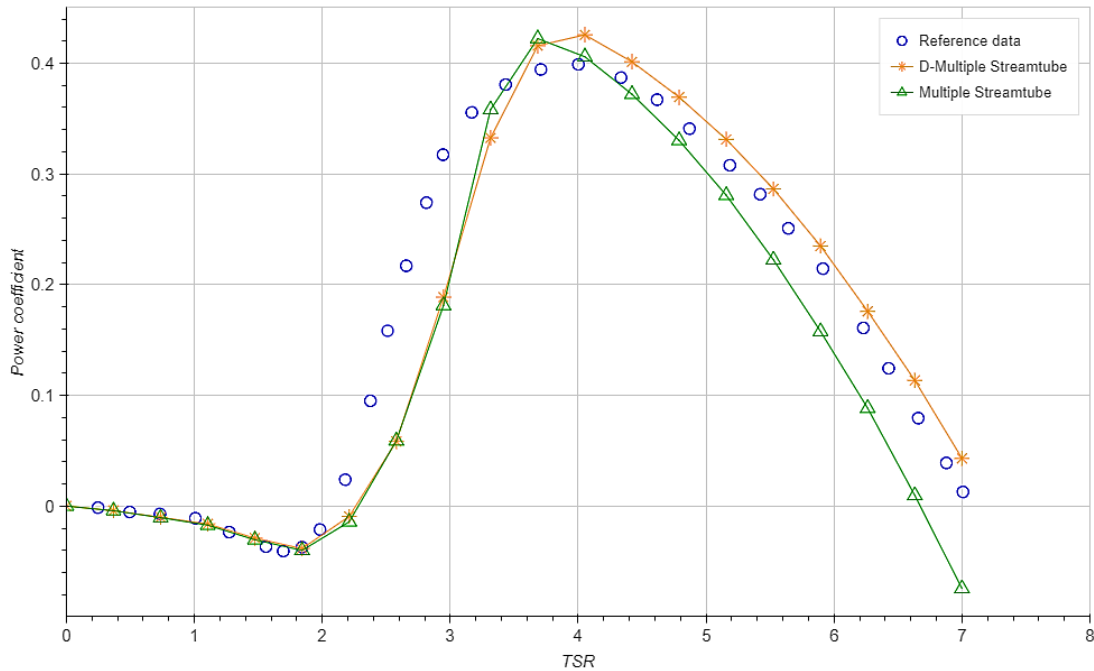


Figure 4.9. Power curves from reference data with thesis calculation with 2 model

It is evident that from 2 to 3.2 of TSR, both model of this thesis under predict power coefficient. DMST prediction agrees better than MST with reference data. This is understandable because these two set of data use the same DMST to predict. Nevertheless, DMST and MST both give a very similar trend of the power curve with reference data.

4.2 Comparison with CFD Simulation

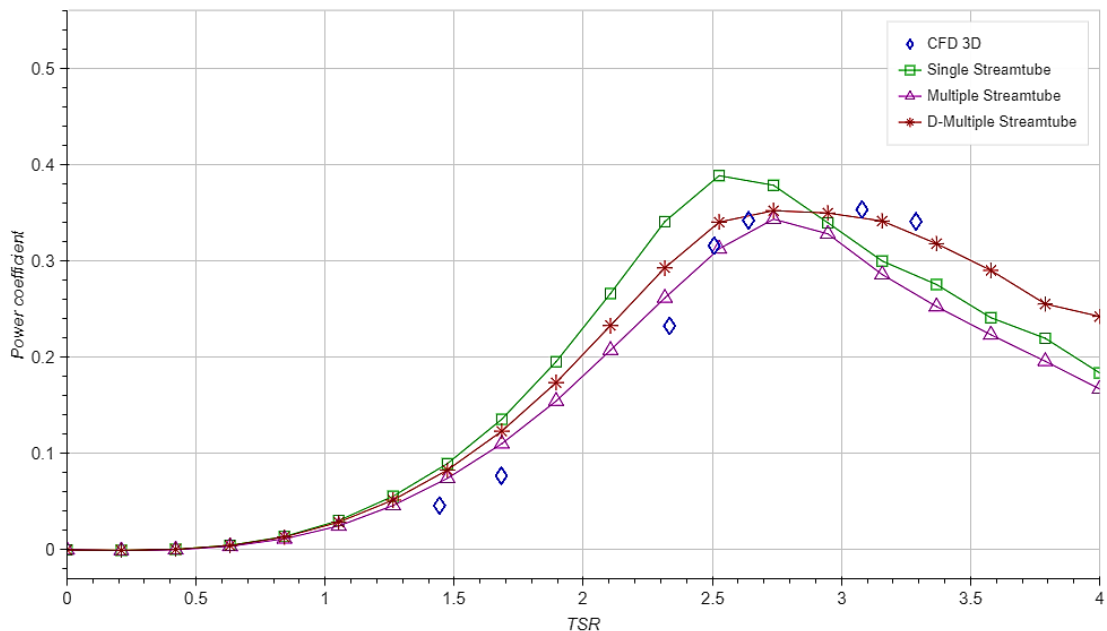
A three-bladed rotor was predicted the performance using 2D CFD method by Castelli in 2011 [16], which resulted in a very poor agreement with measured data obtained from wind tunnel. Later, Abdolrahim Rezaeihah with two other researchers did a work on the Effect of pitch angle on power performance of a vertical axis wind turbine [17], in which he used 3D CFD model to prediction the performance of the same turbine, and the research yielded a better agreement between prediction and experimental data.

Table 4.4. Three-bladed wind turbine model parameter [16]

Rated wind speed (m/s)	9
Blade airfoil	3 x NACA 0021
Rotor height (m)	1.45
Rotor diameter (m)	1.03
Blade chord (m)	0.086
Solidity	0.25
AR	16.8

Table 4.5. 3D CFD simulation data (digitized form [17])

<i>TSR</i>	<i>C_P</i>
1.443	0.046
1.682	0.077
2.334	0.232
2.507	0.316
2.640	0.342
3.080	0.353
3.289	0.341


Figure 4.10. Power curves comparision with CFD data

As TSR ranging from 1.5 to 2.5, all three model predict higher power coefficient. However, as TSR increase above 2.5, DMST yielded the best power curve with CFD data.

4.3 Comparison with Experimental Force Data

4.3.1 The 12 kW turbine

The wind power research at the Division of Electricity at Uppsala University has been conducted since 2002. Three H-rotor VAWTs have been built north of Uppsala. 1.5 kW, 10 kW and 12 kW turbines. And the 12 kW which built by Uppsala University in 2006 is a small-scale prototype designed for experimental purposes. The turbine has been used the most for experiments therefore there are available measurements of this turbine in particular. It is important to compare the simulations against both the normal and tangential forces, since the tangential force response from the 12 kW VAWT was distorted and so only the normal force could be used.



Figure 4.11. The 12 kW turbine, designed and built at the Division of Electricity at Uppsala University [13]

Table 4.6. Turbine parameters obtained from [13]

Uppsala University VAWT H-rotor	
Rated power (kW)	12
Rated rotational speed (rpm)	127
Rated wind speed (m/s)	12
Rotor diameter (m)	6.48
Swept area (m ²)	32
Blade airfoil	3 x NACA 0021
Blade chord (m)	0.25
Solidity	0.125
Blade pitch	2°
AR	20

Normal force coefficient experimental data are plotted together with thesis simulation at different TSR and rotational speed

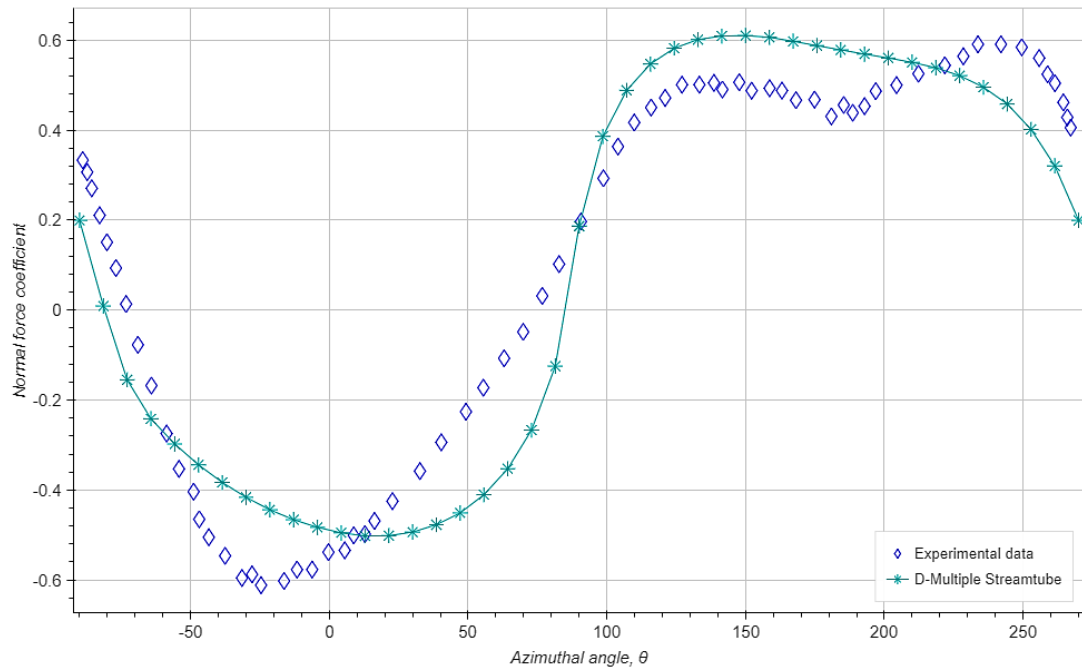


Figure 4.12. Comparison of measured data from [13] and simulations of C_{FN} at $TSR = 3.44, \omega = 64.8 \text{ RPM}$

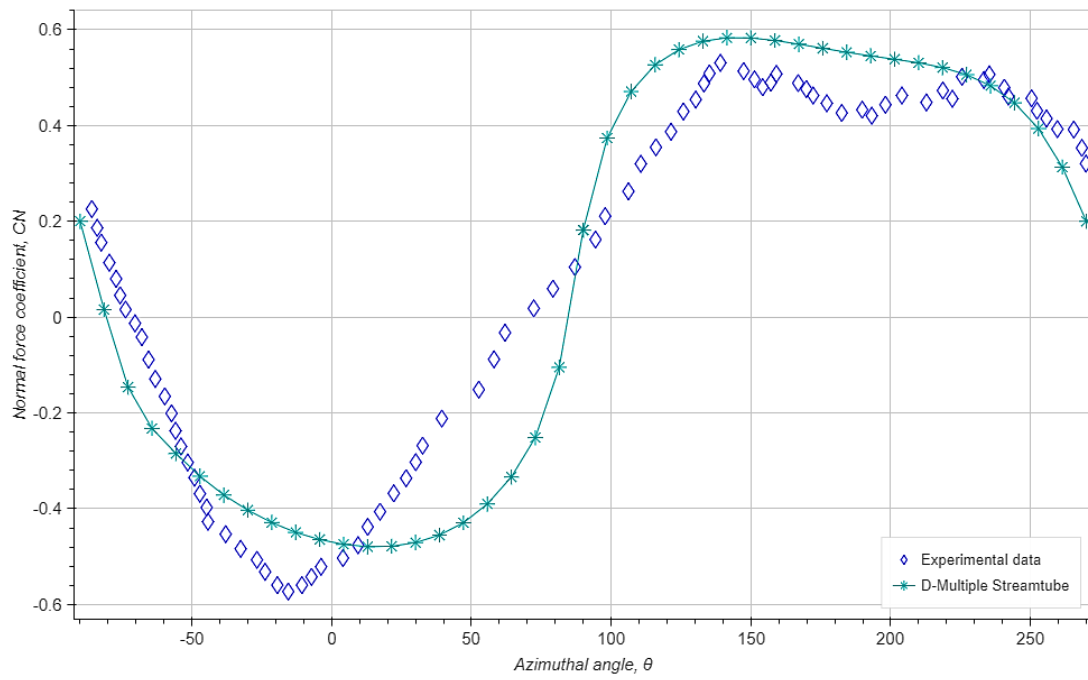


Figure 4.13. Comparison of measured data from [18] and simulations of C_{FN} at $TSR = 3.6, \omega = 50.6 \text{ RPM}$

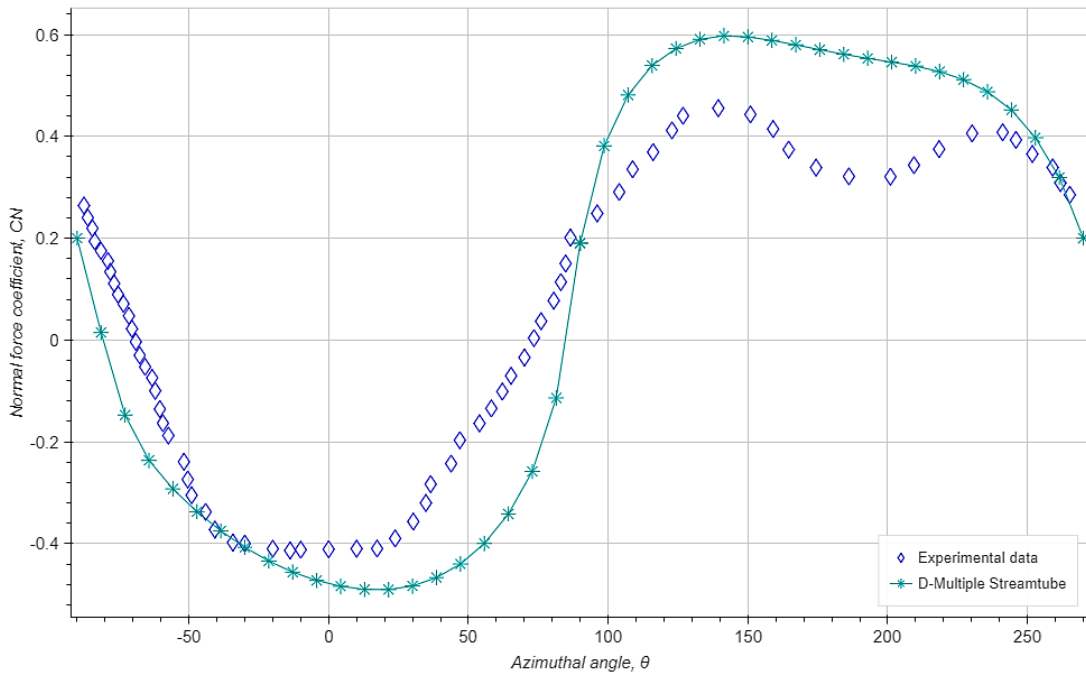


Figure 4.14. Comparison of measurement data from [18] and simulations of C_{F_N} at $TSR = 3.58, \omega = 64.67RPM$

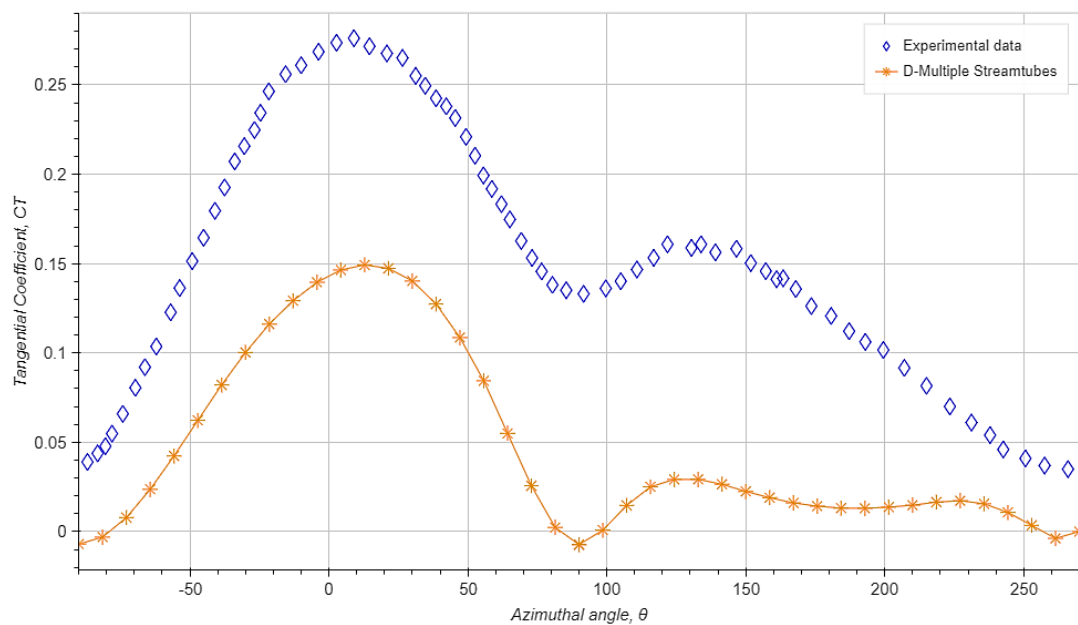
From the illustrations, simulation agree better with experimental data as TSR grow, upwind have better agreement with the data than downwind at the condition of $TSR = 3.58, \omega = 64.67RPM$, while downwind simulation at $TSR = 3.6, \omega = 50.6 RPM$ less difference than upwind half of the rotor.

4.3.2 Sandia 17-m VAWT

Several VAWTs with curved blades were studied by Sandia National Laboratories in the 1980s – 1990s in Albuquerque, New Mexico, USA and the Sandia 17-m was one of them. It is important to compare simulation results against experimental results, since the tangential force response from the 12 kW VAWT was distorted and only the normal force could be used. Thus, force data on the Sandia 17-m turbine [14] were used in this section. Pressure transducers for the force measurements were installed at the mid-2span of the blades. Thus, it is important to emphasize that the data on this turbine are in 2D

Table 4.7. Turbine parameters collected from [13], [14]

Sandia 17-m VAWT	
Rotor maximum diameter (m)	16.72
Rotor height (m)	16.72
Swept area (m^2)	187
Blade airfoil	2 x NACA0015
Blade chord (m)	0.612
Solidity	0.11
Rotational speed (rpm)	38.7
ω (rad/s)	4.05
Blade pitch	0


 Figure 4.15. Tangential force coefficient at $TSR = 4.6$

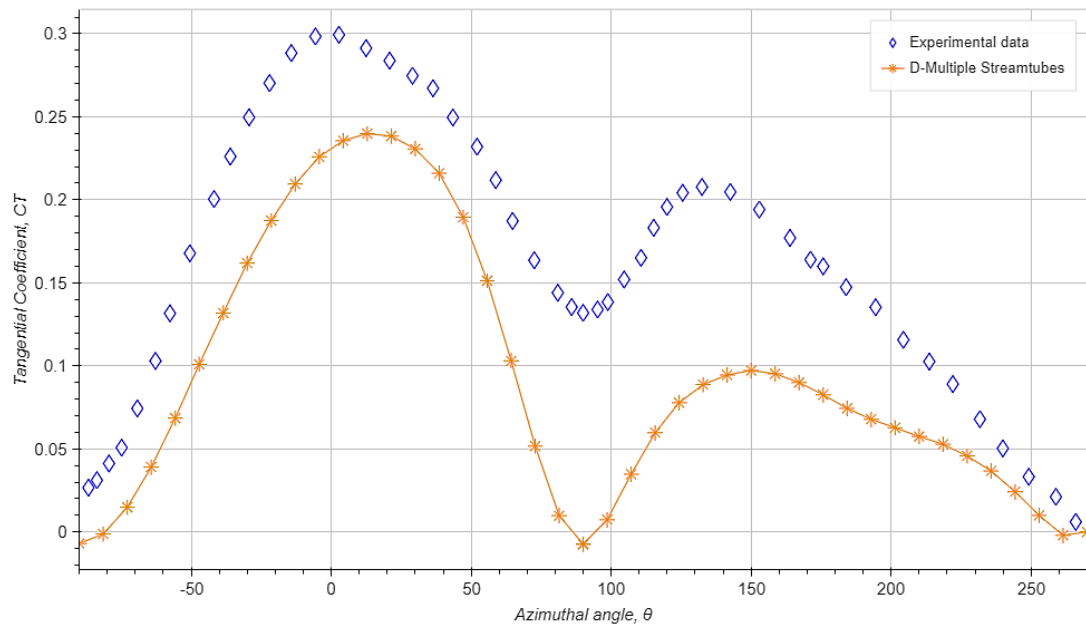


Figure 4.16. Tangential force coefficient at $TSR = 3.7$

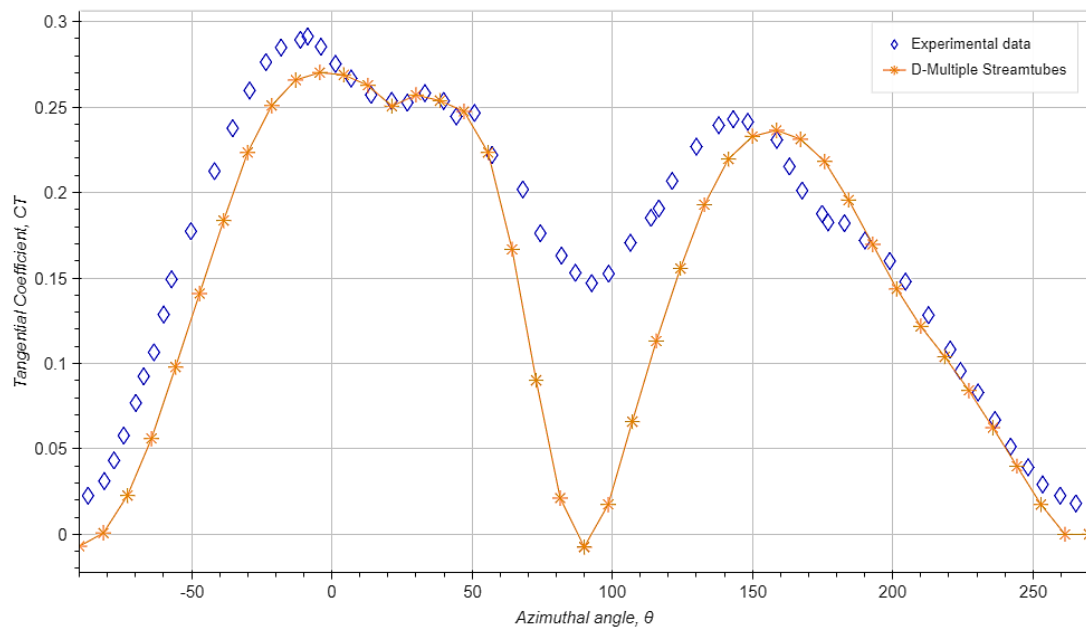


Figure 4.17. Tangential force coefficient at $TSR = 3.09$

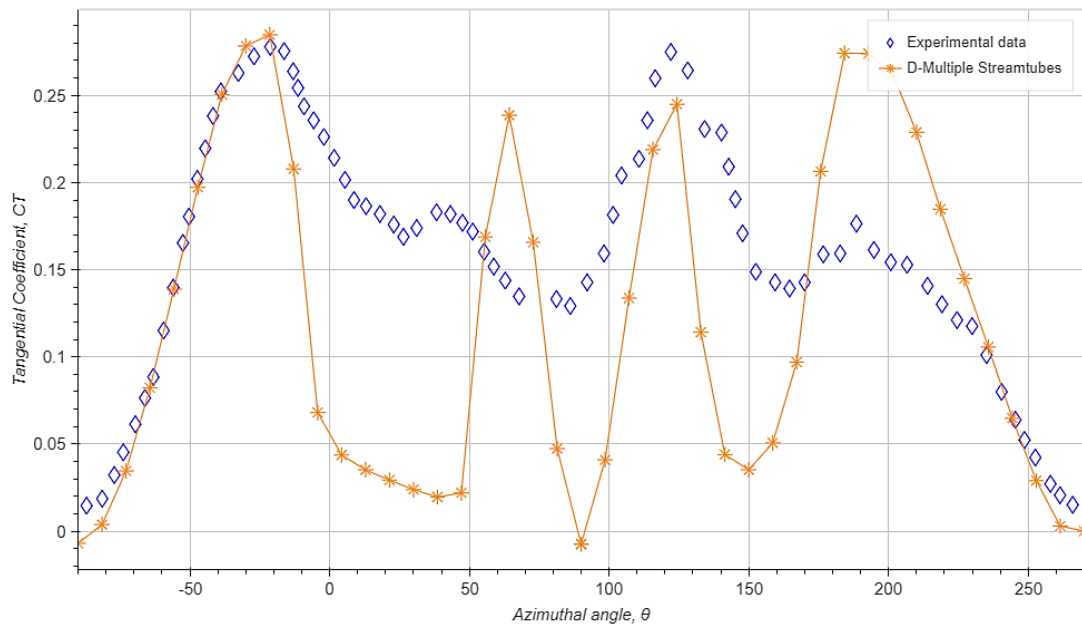


Figure 4.18. Tangential force coefficient at $TSR = 2.49$

Regarding tangential force coefficient, as TSR reduce from 4.6 to 3.09, trend of the graph is more similar in high TSR, while data difference reduces in low TSR. Comparison at $TSR=2.49$ present the lowest similarity.

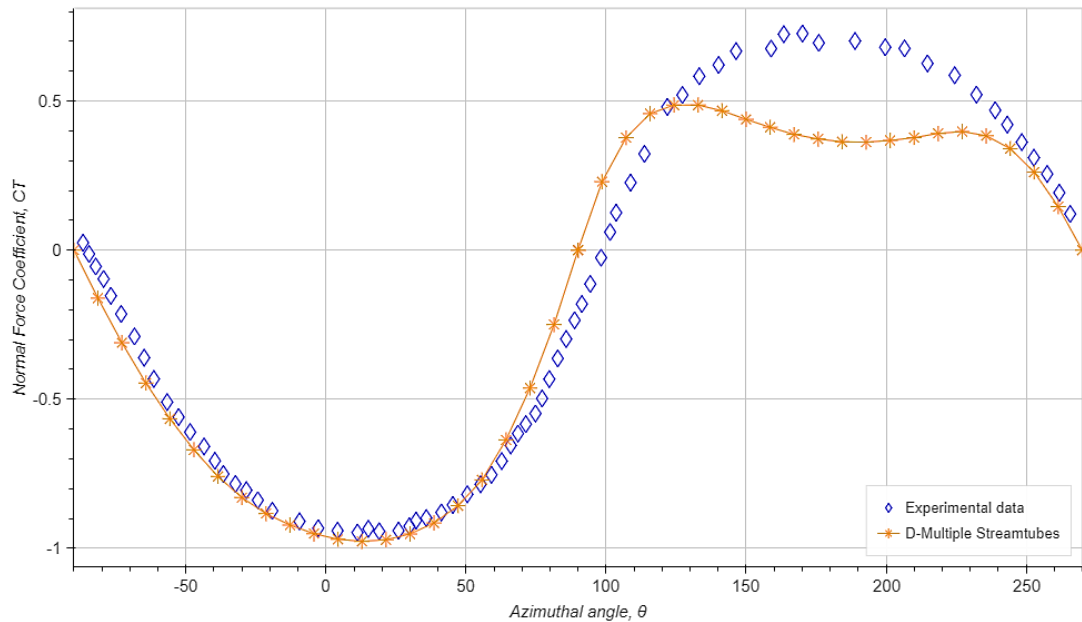


Figure 4.19. Normal force coefficient at $TSR = 4.6$

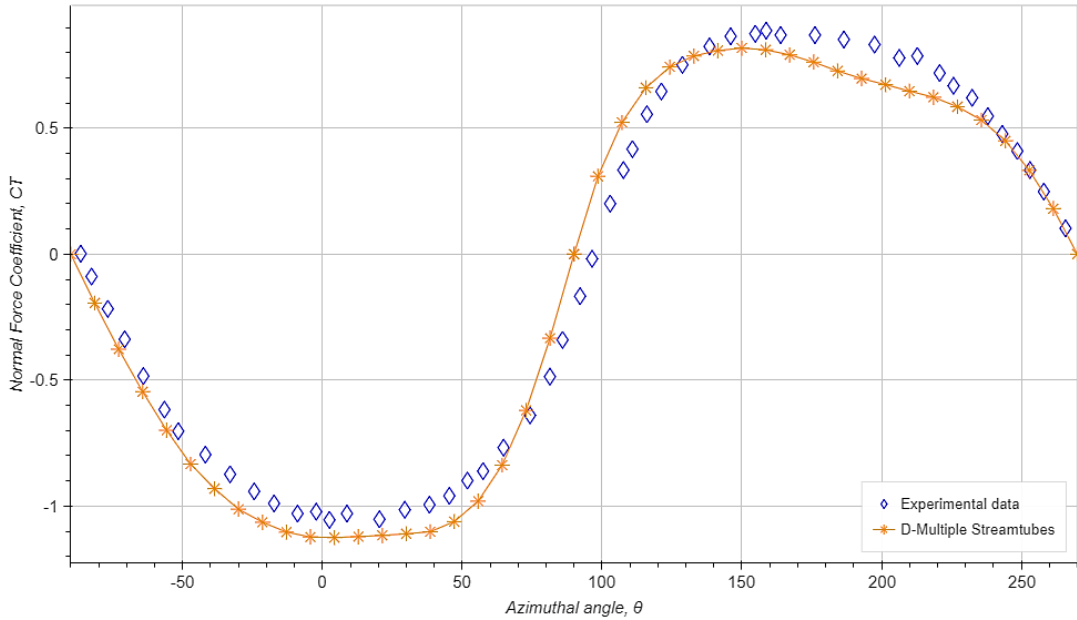


Figure 4.20. Normal force coefficient at $TSR = 3.7$

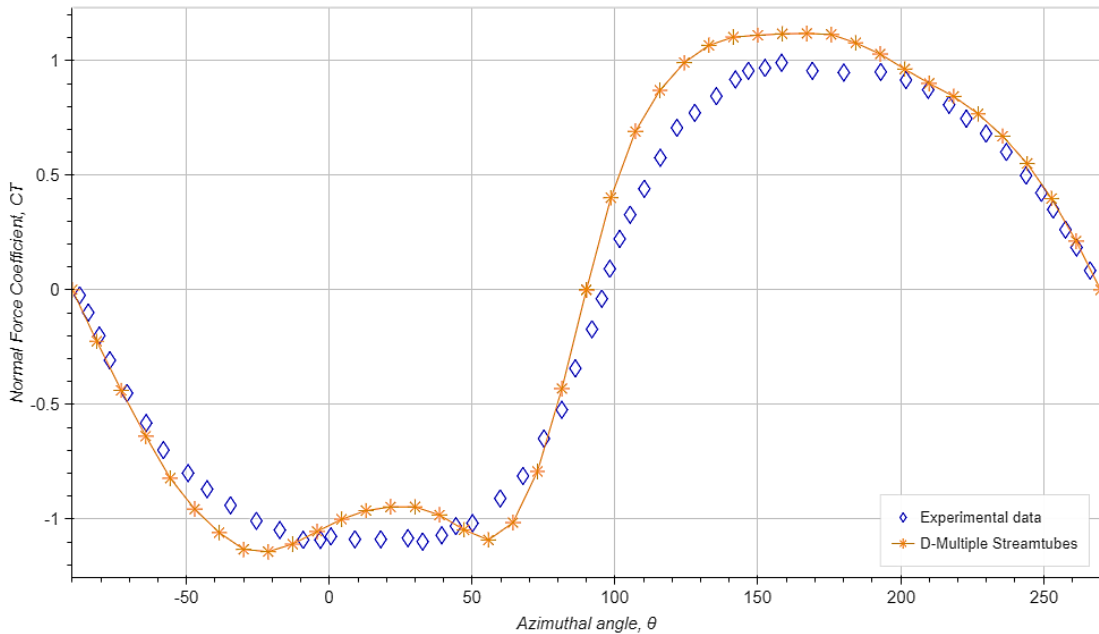


Figure 4.21. Normal force coefficient at $TSR = 3.09$

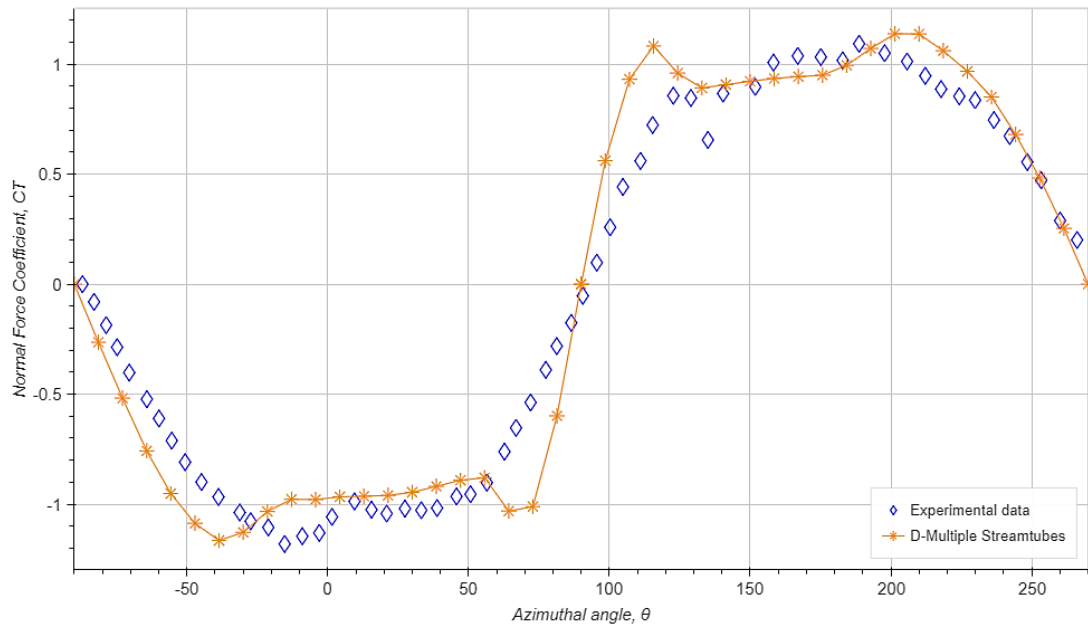


Figure 4.22. Normal force coefficient at $TSR = 2.49$

Different with the previous normal force comparison, at low TSR two set of data yielded very good agreement whereas at $TSR = 4.6$, two data set have a very high gap at $125^\circ < \theta < 225^\circ$.

4.4 Comparison with Experimental Performance Data

In this section, simulation results are compared with power coefficient data of 3 straight blade wind turbine namely VAWT Ltd 260H, VAWT Ltd 850H, and a 12kW H-rotor VAWT.

4.4.1 Uppsala University VAWT H-rotor

A 12 kW vertical axis H-rotor type wind turbine has been designed and constructed at Uppsala University. A measurement campaign has been performed to collect data to calculate the power coefficient using the method of bins. The measurement was performed at different constant rotational speeds on the turbine during varying wind speeds to observe the power coefficients

Table 4.8. Nominal properties of the wind turbines [19],[13]

Uppsala University VAWT H-rotor	
Rated power (kW)	12
Rotational speed (rpm)	127
Rated wind speed (m/s)	12
Rotor diameter (m)	6
Swept area (m ²)	30
Blade airfoil	3 x NACA 0021
Blade chord (m)	0.25
Solidity	0.116
AR	20



Figure 4.23. The 12 kW turbine, designed and built at the Division of Electricity at Uppsala University [13]

Table 4.9. Power coefficient experimental data (digitized from [19])

TSR	C_P	TSR	C_P
1.746	0.056	3.182	0.280
1.855	0.068	3.304	0.291
1.968	0.085	3.421	0.289
2.098	0.106	3.536	0.287
2.228	0.138	3.659	0.285
2.345	0.160	3.780	0.280
2.459	0.183	3.900	0.269
2.580	0.206	4.025	0.234
2.696	0.227	4.139	0.218
2.828	0.248	4.255	0.179
2.940	0.263	4.378	0.154
3.063	0.269	4.468	0.149

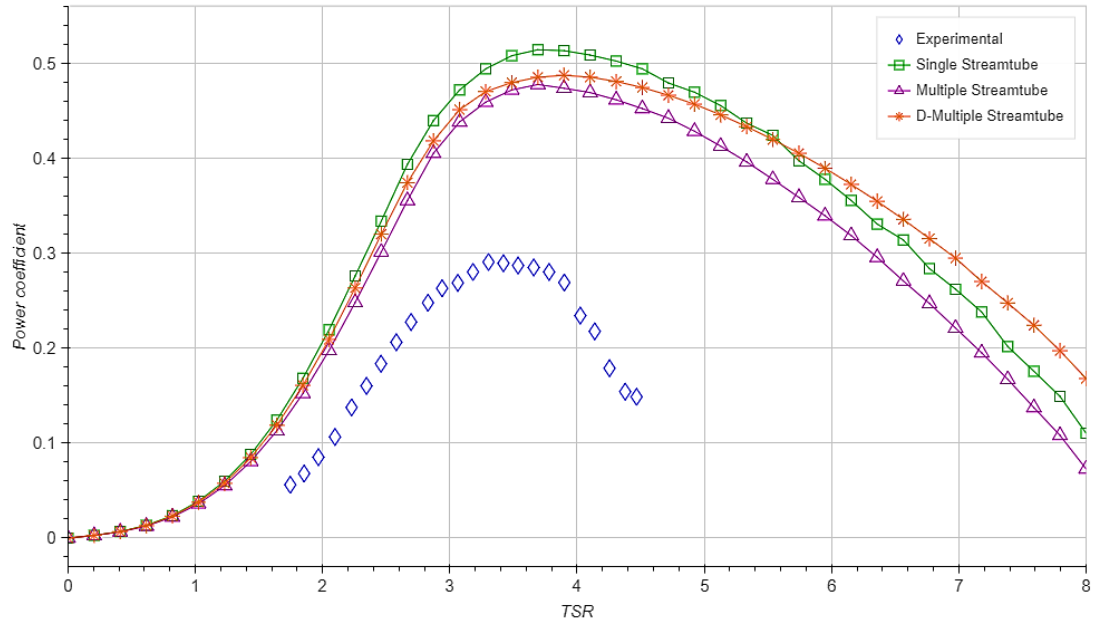


Figure 4.24. Power curves of Uppsala University VAWT H-rotor

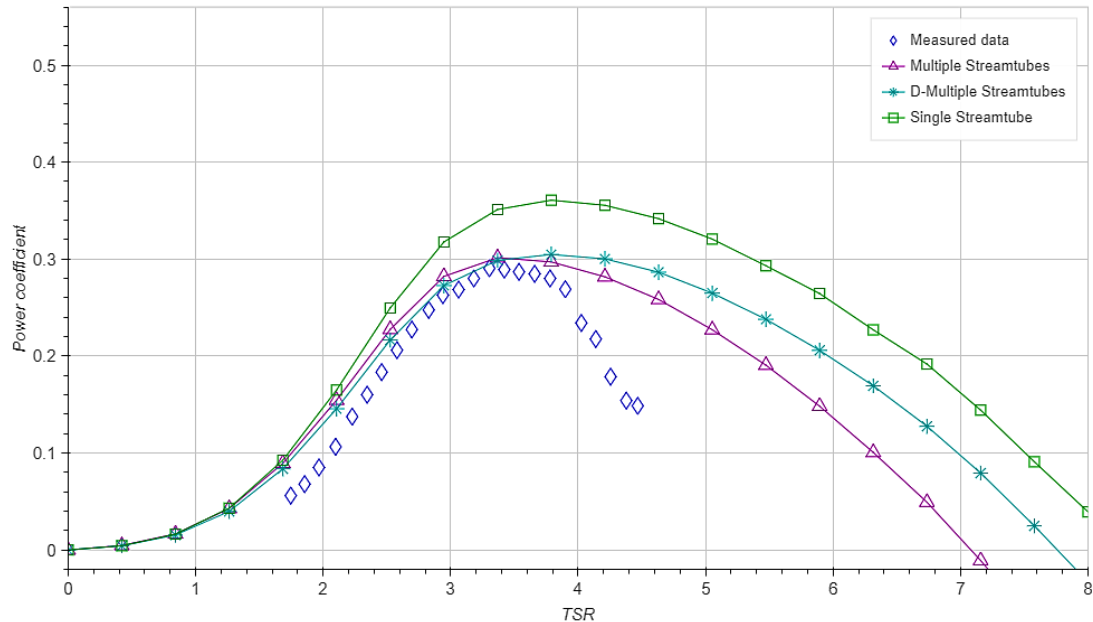


Figure 4.25. Power curves of Uppsala University VAWT H-rotor with finite AR effect

It can be seen that the single streamtube model (SST) always predict the highest power. As finite AR effect taken into account, prediction of DSMT and MST come closer to experiment graph. Although as TSR goes beyond 3.8, the data deviation goes up, the significance is that these two multiple streamtube model have the same trend with experiment data, which would give the designer the desired TSR to maximize performance of the turbine

4.4.2 VAWT Ltd 260H

VAWT Ltd. installed a commercial 20 m diameter VAWT-260 turbine that operated on the Scilly Isles from 1988 to 1992 with a rated power of 105 kW. Turbine geometry and measured power data is shown by Andrew Shires in [15].

Table 4.10. Geometry parameters of wind turbines [11],[15]

VAWT Ltd 260H	
Rated power (kW)	100
Rotational speed (rpm)	33
Rated wind speed (m/s)	10
Rotor diameter (m)	19.5
Swept area (m ²)	260
Blade airfoil	2 x NACA 0018
Blade chord (m)	1.02
Solidity	0.105
AR	13

Table 4.11. Power coefficient experimental data (digitized from [15])

TSR	C_P	TSR	C_P
1.718	0.089	2.882	0.303
1.775	0.100	3.011	0.323
1.818	0.105	3.132	0.342
1.862	0.113	3.277	0.365
1.929	0.121	3.429	0.380
1.973	0.130	3.612	0.390
2.040	0.141	3.816	0.393
2.095	0.152	4.076	0.386
2.159	0.163	4.290	0.389
2.240	0.177	4.580	0.361
2.316	0.192	4.913	0.359
2.384	0.209	5.280	0.370
2.494	0.225	5.748	0.346
2.573	0.244	6.282	0.316
2.670	0.265	6.955	0.233
2.779	0.280	7.830	0.087

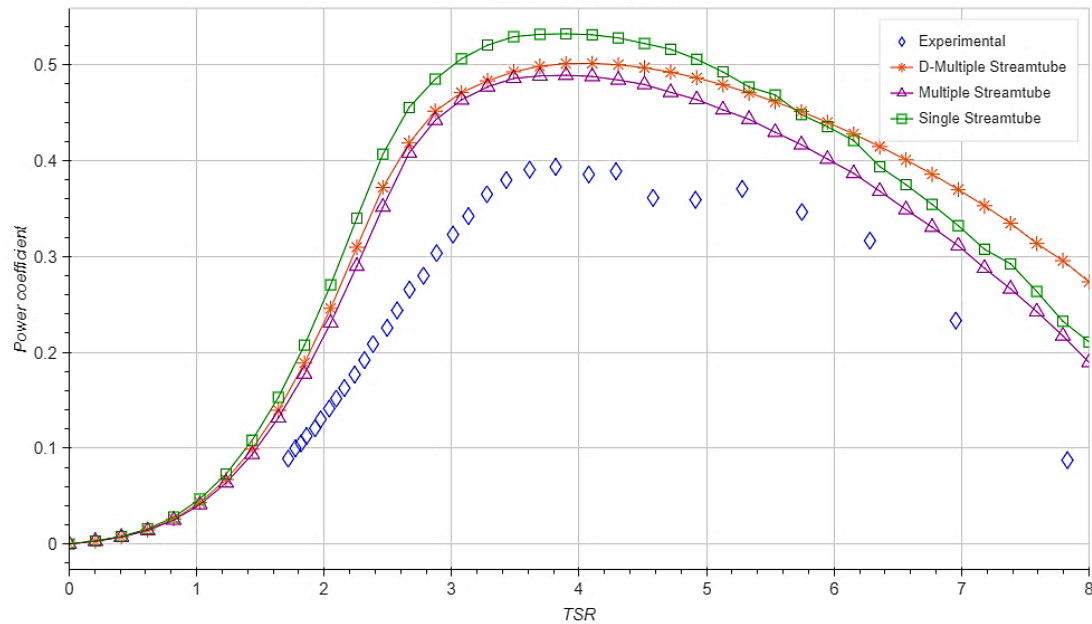


Figure 4.26. Power curves of VAWT Ltd 260H

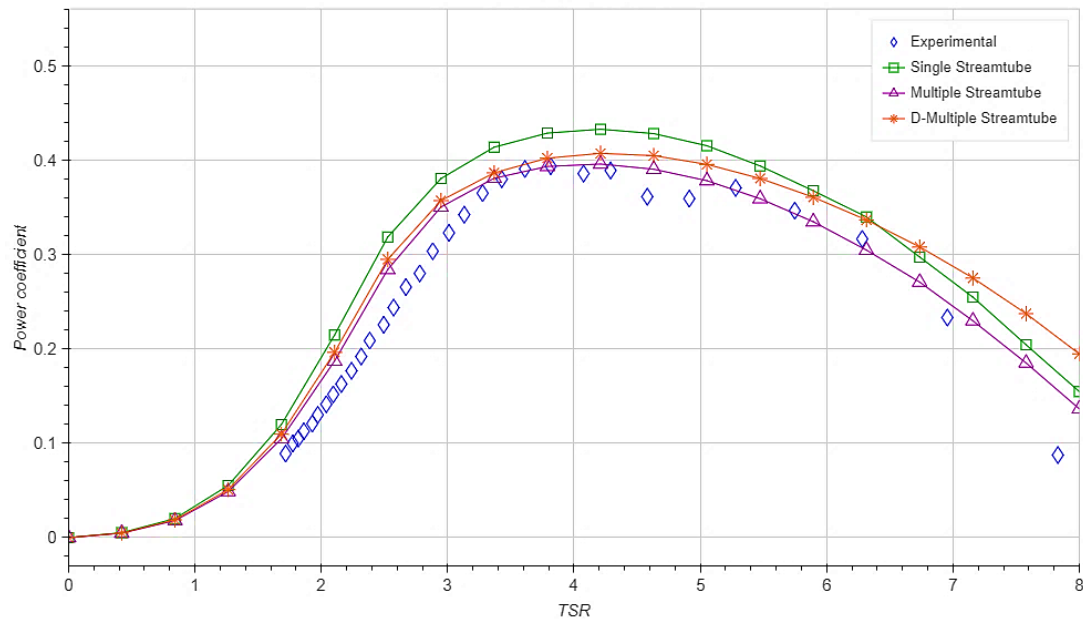


Figure 4.27. Power curves of VAWT Ltd 260H with finite AR effect

With this turbine, after integrating AR effect, DMST give the best agreement with experimental data. Although MST over predict the data, it also has the similar trend with experimental data and DMST.

4.4.3 VAWT Ltd 850H

VAWT Ltd also constructed a larger 35m diameter VAWT-850 H-rotor at the Carmarthen test site with a rated power of 500 kW which operated between 1990 and 1991. Turbine geometry and measured power data is shown by Andrew Shires in [15].

Table 4.12. Geometry parameters of wind turbines [11],[15]

VAWT Ltd 850H	
Rated power (kW)	500
Rotational speed (rpm)	13.6
Rated wind speed (m/s)	13.5
Rotor diameter (m)	35
Swept area (m ²)	850
Blade airfoil	2 x NACA 0018
Blade chord (m)	1.84
Solidity	0.105
AR	13.2

Table 4.13. Power coefficient experimental data (digitized from [15])

TSR	C_P	TSR	C_P
1.475	0.075	2.255	0.243
1.518	0.084	2.368	0.264
1.564	0.090	2.480	0.275
1.615	0.099	2.621	0.295
1.667	0.109	2.767	0.329
1.726	0.120	2.933	0.342
1.784	0.131	3.110	0.358
1.848	0.143	3.347	0.363
1.915	0.158	3.579	0.379
1.994	0.180	3.886	0.365
2.072	0.201	4.195	0.340
2.159	0.219	4.647	0.309

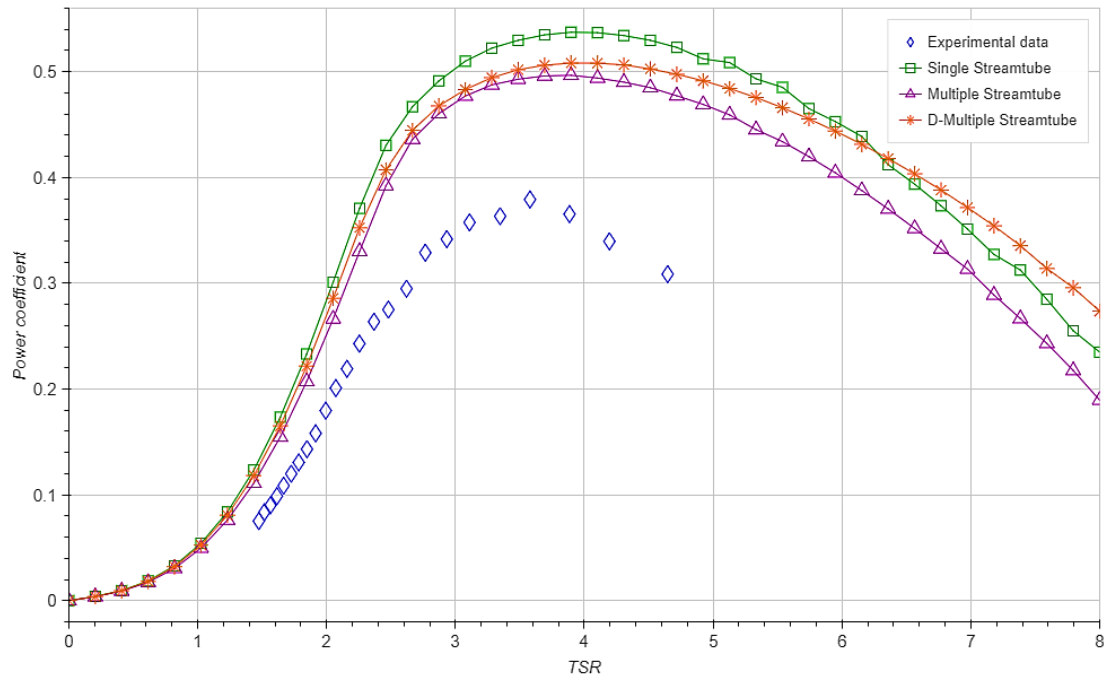


Figure 4.28. Power curves of VAWT Ltd 850H

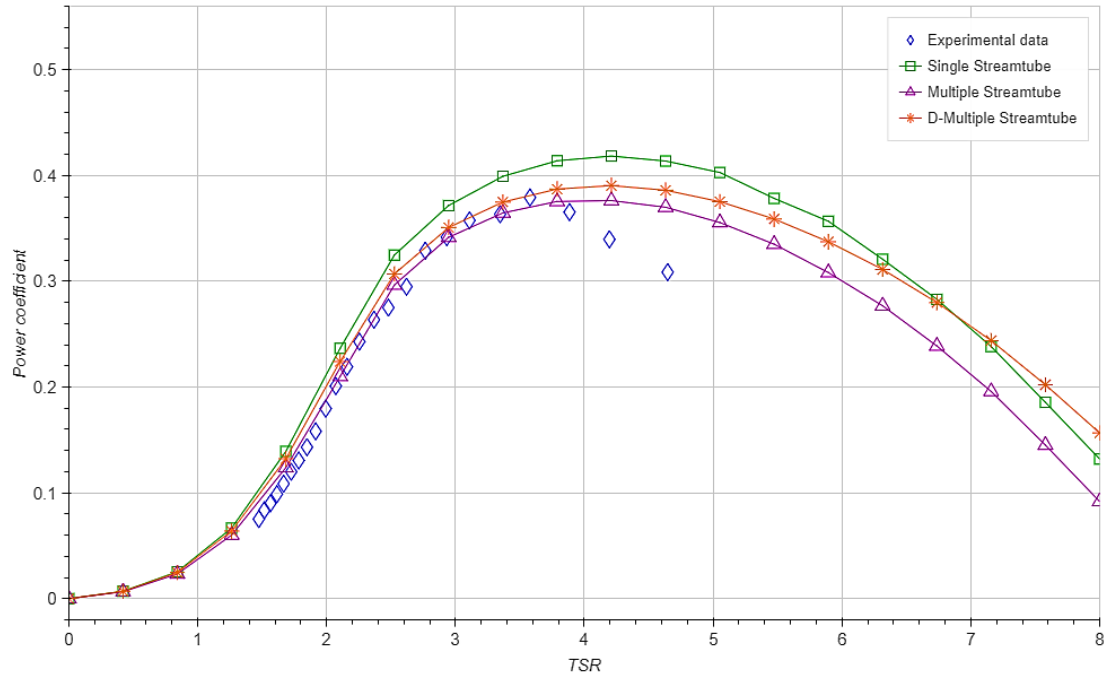


Figure 4.29. Power curves of VAWT Ltd 850H with finite AR effect

It is clear and lucid that, when using finite AR effect, the prediction's accuracy improves significantly. MST and DMST give much better agreement compared to SST. The performance prediction matched the best with experimental data at low TSR (1.5 – 3.5). As TSR becomes greater than 3.5, data difference between simulation and experiment grows.

Chapter 5. PREDICTION CALCULATION FOR DESIGNING

5.1 Prediction Using Single Streamtube with Betz Limit

Professor N.T.Tong in his lectures of Wind turbine course [20], suggest that from Betz's limit, maximum power coefficient occur at induced factor $a = 1/3$.

$$C_P = C_{P_{max}} = \frac{16}{27} \quad (5.1)$$

$$C_{Thrust} = \frac{8}{9} \quad (5.2)$$

Combining Single Streamtube model together with Betz limit to produce a straightforward and lucid prediction method at the very initial stage of the design process. For the sake of simplicity, airfoil characteristic as well as Reynolds number is left out.

Assume that airfoil is symmetric. Lift coefficient could be express as

$$C_L = 2\pi \sin \alpha \quad (5.3)$$

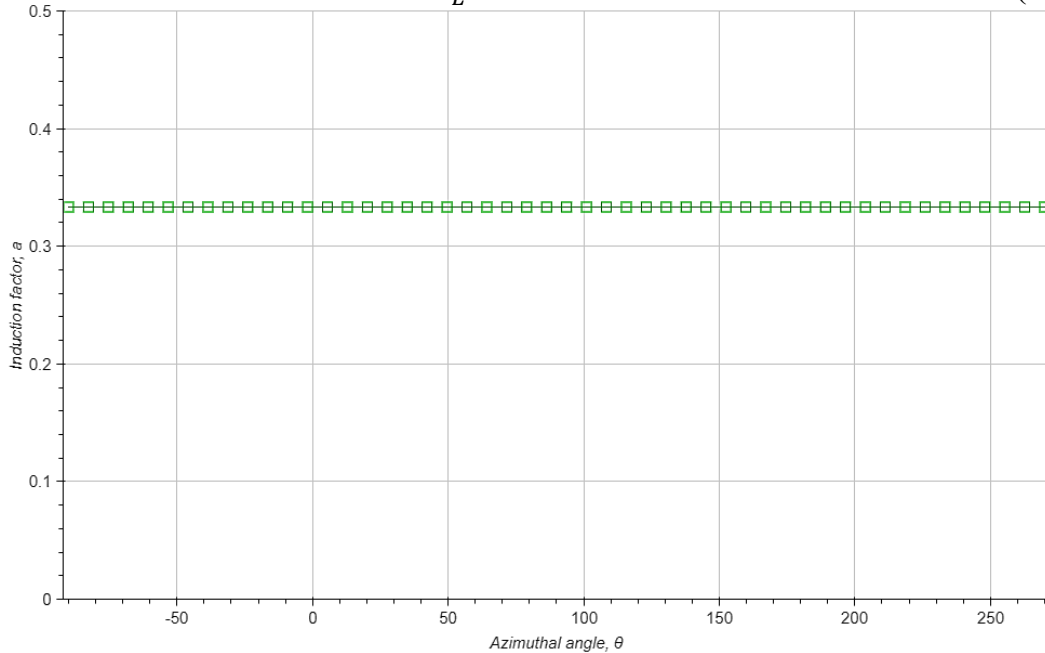


Figure 5.1. Induction factor a in Betz's limit at different azimuthal position

In this power prediction, blade chord is unknown, so that lift and drag coefficient are functions of angle of attack α

Table 5.1. Lift and drag coefficient characteristic

Blade element lift coefficient	$C_L = 2\pi \sin \alpha$
Blade element drag coefficient	$C_D = kC_L$
k	0.03
Induced factor a	1/3

Following the calculation process of Single Streamtube model in Section 3.6 with induced factor $a = 1/3$.

Optimum solidity.

$$\sigma_{op} = \frac{8/9}{\frac{1}{2\pi} \left(\frac{W}{V_\infty} \right)^2 \int_0^{2\pi} C_{Ti} d\theta} \quad (5.4)$$

Predicted maximum power coefficient.

$$C_P = \frac{\sigma_{op}}{2\pi} \left(\frac{W}{V_\infty} \right)^3 \int_0^{2\pi} C_{Pi} d\theta \quad (5.5)$$

At TSR = 4, the solidity found is $\sigma = 0.108$, and maximum power coefficient $C_P = 0.456$. Similar calculation for other TSR gives respective power coefficient and solidity.

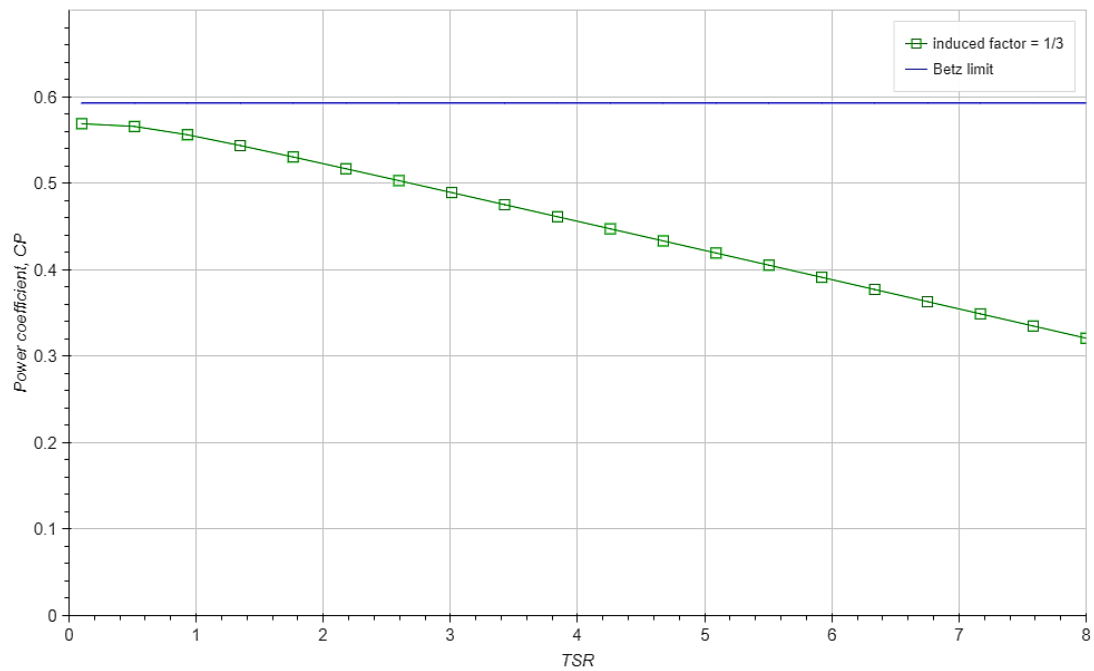


Figure 5.2. Optimum power coefficient at different TSR using Betz assumption

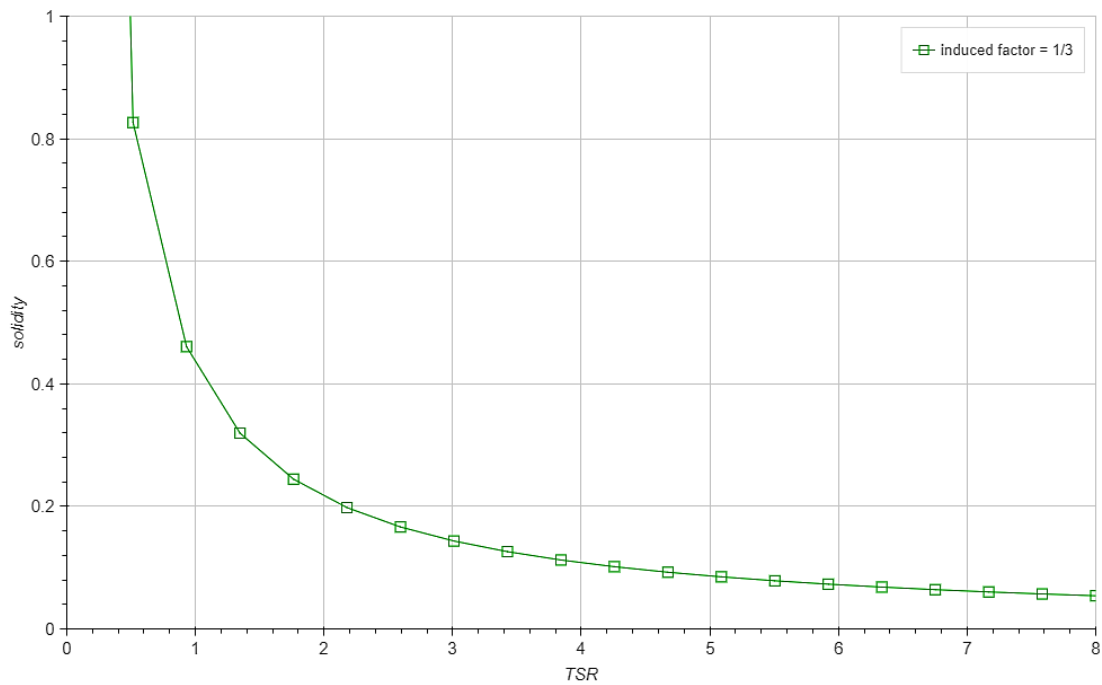


Figure 5.3. Optimum solidity at different TSR using Betz assumption

Impact of drag force on power prediction

In this section, drag coefficient characteristic is changed by changing k

$$C_D = k C_L \quad (5.6)$$

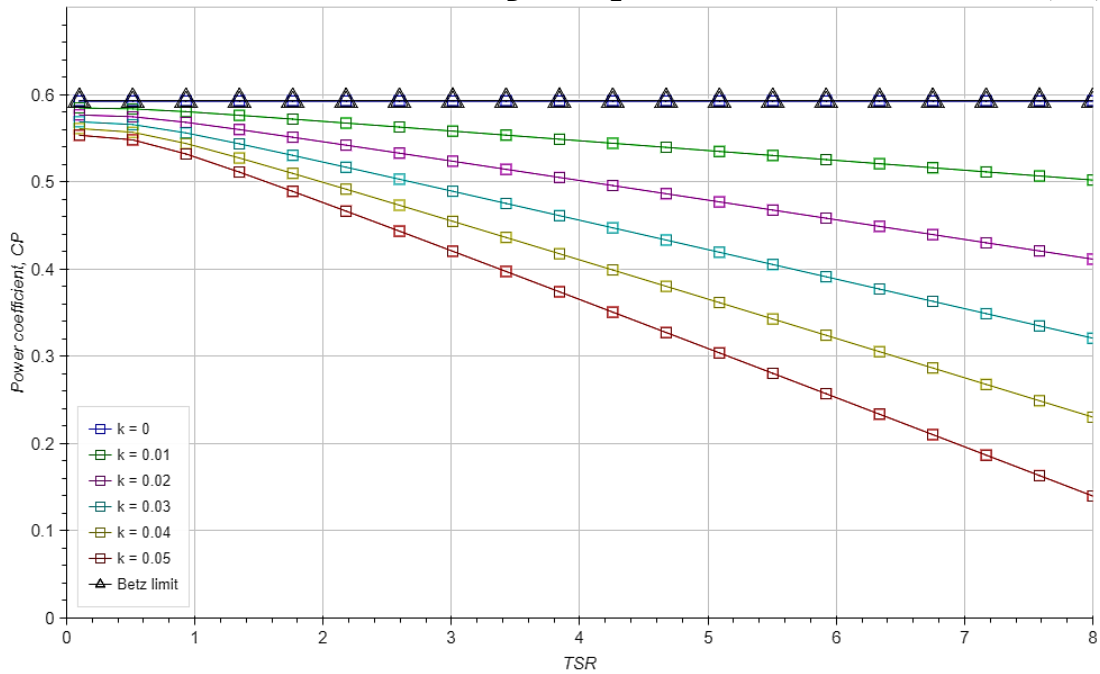


Figure 5.4. C_p curves with different C_D characteristic

It is evident that, as k down to 0, C_p curves shift up to Bezt's limit power coefficient. Which means the power loss of the rotor is fundamentally caused by drag force.

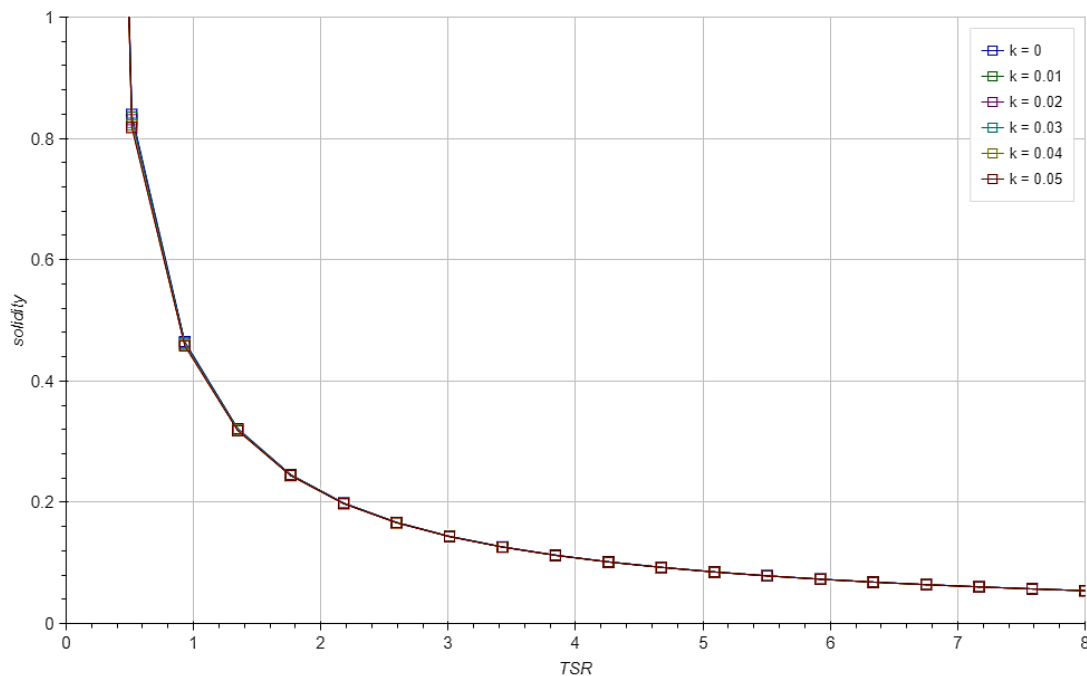


Figure 5.5. Solidity graphs wth different C_D chacteristic

Surprisingly, solidity graph remains almost the same with different C_D chacteristic, which show that solidity depends only on TSR

5.2 Power Prediction Using Two Multiple Streamtube Models

For this operating regime, the scripts are run for a range of TSR by varying blade chord as well as shifting up TSR of each running solidity to get one power curves. As a result, a number of power curves are produced. Input data

Table 5.2. Input parameters of designing turbine

Design wind speed (m/s)	6
Swept area (m^2)	5
Blade airfoil	3 x NACA 0021
Rotor height (m)	2.5
Rotor diameter (m)	2

For this mode. An optimum solidity is given out, and TSR by varying chord and TSR to give out a set of power curves

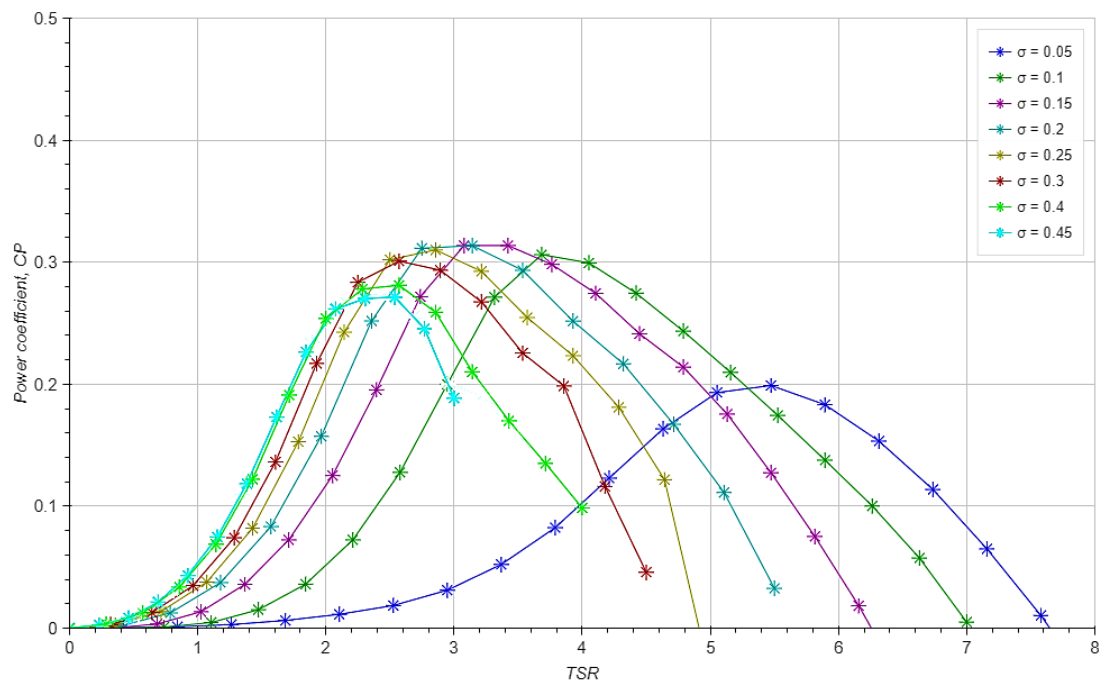


Figure 5.6. Power curves prediction with Double Multiple Streamtube model

From the graph, with Double Multiple Streamtube model, the optimum value of solidity and TSR are:

$$\sigma_{optimum} = 0.15 - 0.2 \quad (5.7)$$

$$TSR_{optimum} = 2.8 - 3.8 \quad (5.8)$$

$$C_{P_{optimum}} = 0.32 \quad (5.9)$$

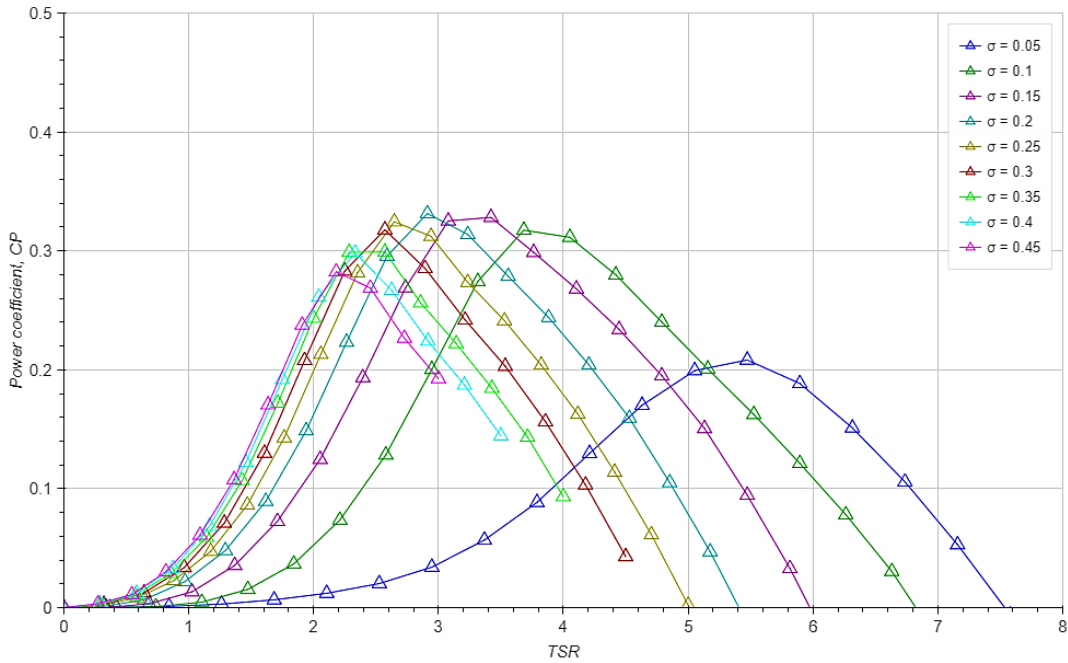


Figure 5.7. Power curves prediction with Multiple Streamtube model

From the graph, with Multiple Streamtube model, optimum value of solidity and TSR are:

$$\sigma_{optimum} = 0.15 - 0.2 \quad (5.10)$$

$$TSR_{optimum} = 2.8 - 3.8 \quad (5.11)$$

$$C_{P_{optimum}} = 0.33 \quad (5.12)$$

Although Multiple Streamtube model predict higher power coefficient than Double Multiple Streamtube model. From the two predictions, it is clear and lucid that both model produced similar optimum result for designer

Compare with prediction using single streamtube model with Betz's limit, with Tip speed ratio ranging from 2.8 to 3.8, from Figure 5.5, it can be inferred that optimum solidity is form 0.16 to 0.11, which show very poor agreement between two methods of prediction due to the simplicity of SST compared to DMST. Thus, to improved prediction using SST with Betz's Limit by integrating finite AR effect to the model. As a result, a new solidity versus TSR graph obtained.

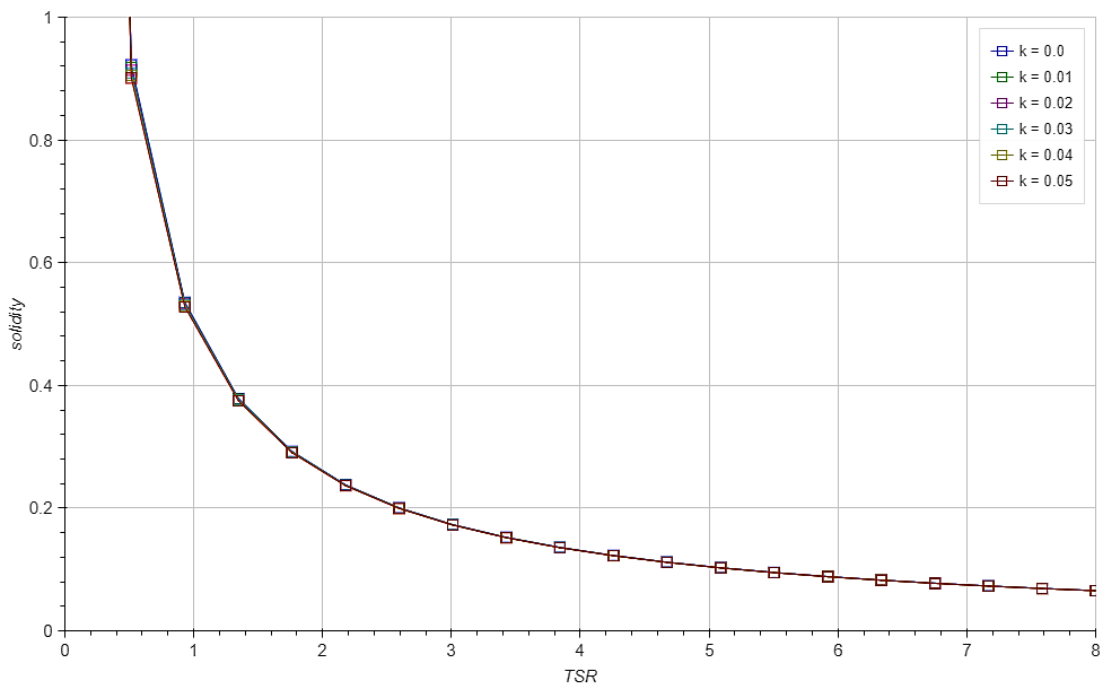

 Figure 5.8. Solidity graphs with different C_D characteristic with finite AR effect

Table 5.3. The result table for both methods

Suggested parameter	Multiple stream tube model	Double multiple stream tube model	SST with Betz's limit
Solidity	0.15 – 0.2	0.15 – 0.2	0.15 – 0.2
TSR	3.5 – 2.9	3.4 – 2.8	3.4 – 2.6
C_P	0.33	0.32	----

From the table above, it is obvious that three models reasonably consistent with each other. In conclusion, for maximizing turbine performance, the turbine should have a solidity from 0.15 – 0.2 and TSR from 3.4 – 2.8 correspondingly.

Table 5.4. Advisable parameters for the turbine

Design wind speed (m/s)	6
Swept area (m^2)	5
Blade airfoil	3 x NACA 0021
Rotor height (m)	2.5
Rotor diameter (m)	2
Solidity	0.15 – 0.2
Blade chord (m)	0.1 – 0.13
TSR	3.4 – 2.8
Rotational speed (rpm)	189 – 166

Drag force contribution of the power difference

Assume that from Table 5.7, designer decides the final turbine configuration as follow.

Table 5.5. Final design parameter

Design wind speed (m/s)	6
Swept area (m ²)	5
Blade airfoil	3 x NACA 0021
Rotor height (m)	2.5
Rotor diameter (m)	2
Solidity	0.2
Blade chord (m)	0.13
TSR	3
Rotational speed (rpm)	166

From Figure 5.6, power coefficient.

$$C_{P_{prediction}} = 0.3232 \quad (5.13)$$

Betz's maximum power coefficient

$$C_{P_{Betz}} = \frac{16}{27} = 0.59 \quad (5.14)$$

There is a huge gap between $C_{P_{prediction}}$ using Double Multiple Streamtube and Betz maximum C_P

From prediction using Single streamtube with Betz limit, it is explicit that power loss of the turbine mainly caused by drag force, so to investigate the difference between two values of power coefficient, the drag power of the turbine need to be calculated.

At each streamtube,

$$\text{Drag power of } = \text{Drag power upwind} + \text{Drag power downwind}$$

From section 3.8, drag power.

$$\text{Drag power} = \frac{\Delta\theta}{2\pi} \frac{1}{2} \rho W^3 C_D c \Delta h + \frac{\Delta\theta}{2\pi} \frac{1}{2} \rho W'^3 C'_D c \Delta h \quad (5.15)$$

Where,

$$\frac{\Delta\theta}{2\pi} = \text{time 1 blade spent in that stream tube} \quad (5.16)$$

For N blade.

$$\text{Drag power} = \frac{N\Delta\theta}{2\pi} \frac{1}{2} \rho W^3 C_D c \Delta h + \frac{N\Delta\theta}{2\pi} \frac{1}{2} \rho W'^3 C'_D c \Delta h \quad (5.17)$$

$$\text{Drag power} = \frac{N\Delta\theta}{4\pi} \rho c \Delta h (W^3 C_D + W'^3 C'_D) \quad (5.18)$$

For the whole turbine

$$\text{Drag power} = \frac{N\Delta\theta}{4\pi} \rho c H (W^3 C_D + W'^3 C'_D) \quad (5.19)$$

$$\text{Drag power} = \frac{1}{2} \frac{\sigma}{\pi} \rho c H (W^3 C_D + W'^3 C'_D) \quad (5.20)$$

$$\begin{aligned} \text{Drag power} &= \frac{1}{2} \frac{\sigma}{\pi} \rho c H \left(\left(\frac{W}{V_\infty} V_\infty \right)^3 C_D \right. \\ &\quad \left. + \left(\frac{W'}{V_w} V_\infty (1 - 2a) \right)^3 C'_D \right) \end{aligned} \quad (5.21)$$

$$\text{Drag power} = \frac{1}{2} \frac{\sigma}{\pi} \rho c H V_\infty^3 \left(\left(\frac{W}{V_\infty} \right)^3 C_D + \left(\frac{W'}{V_w} (1 - 2a) \right)^3 C'_D \right) \quad (5.22)$$

Drag power coefficient

$$\begin{aligned} C_{P_{drag}} &= \frac{\text{Drag power}}{\frac{1}{2} \rho V_\infty^3 D H} \\ &= \frac{\sigma c}{\pi D} \left(\left(\frac{W}{V_\infty} \right)^3 C_D + \left(\frac{W'}{V_w} (1 - 2a) \right)^3 C'_D \right) \end{aligned} \quad (5.23)$$

Take summation for all the streamtube to find the turbine power

From the calculation process,

$$\text{Drag power} = 160.6 \text{ W} \quad (5.24)$$

$$C_{P_{drag}} = \frac{\text{Drag power}}{\frac{1}{2} \rho V_\infty^3 D H} = \frac{160.6}{\frac{1}{2} \times 1.225 \times 6^3 \times 5} = 0.24 \quad (5.25)$$

And the difference of the two power coefficient is.

$$\Delta C_P = 0.59 - 0.32 = 0.27 \quad (5.26)$$

There are good agreement between the power loss due to drag force and the difference of power coefficient with Betz maximum C_P

5.3 Effect of Pitch Angle

From the previous conclusion, designer can opt the value of solidity for the turbine. However, the preset pitch angle of the turbine blades is shown to have a large impact on turbine performance. Thus, to enhance the turbine performance further as well as make use of the prediction model effectively, blade pitching angle β is taken into consideration.

There are a number of works done on the effect of blade pitch angle for power improvement. Klimas and Worstell (1981) tested preset pitch angles ranging from -7° (toe-out) to $+3^\circ$ (toe-in) experimentally and the finding was that the optimal pitch angle $\beta = -2^\circ$ (toe-out) [21]. Y-T. Lee et al. [22] did a research involving investigating the effects of toe in, toe out pitch angles on performance of a turbine. The varying pitch angle is from -6° (toe-out) to $+3^\circ$ (toe-in), and he explored that $\beta = -2^\circ$ (toe-out) also corresponding with highest power coefficient. Benjamin Strom at al. [23] set up experiments to unearth the influences of blade preset pitch angle β , which ranged from 0° to 12° (toe-out angle as their sign convention), on two turbines' performance (two and four-bladed turbines), and the optimal preset pitch angle was found to be 6° (toe-out) for both turbines. From the presented findings, it is notable that all the optimal preset pitching angle are toe-out.

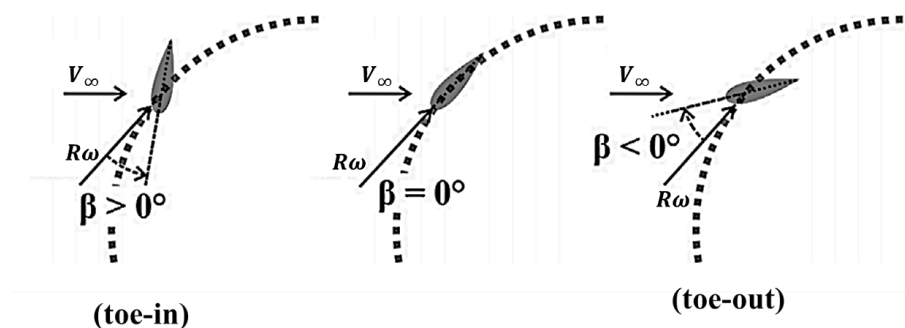


Figure 5.9. Blade pitch angle's sign convention (modified from [17])

For calculation, local angle of attack.

$$\alpha = \phi + \beta \quad (5.27)$$

Where

$$\phi = \tan^{-1} \frac{\frac{V}{V_\infty} \cos \theta}{TSR - \frac{V}{V_\infty} \sin \theta} \quad (5.28)$$

Normal and tangential force coefficient on blade element.

$$C_N = C_L \cos \phi + C_D \sin \phi \quad (5.29)$$

$$C_T = C_L \sin \phi - C_D \cos \phi \quad (5.30)$$

From Table 5.3, turbine would perform best at TSR from 2.8 to 3.5. However, in reality wind velocity changes and rotational speed is not constant, so that the analysis runs on a range of free stream velocity $V_\infty = 4 - 10 \text{ m/s}$ with TSR shifting from 2 to 4.

Table 5.6. Turbine parameters

Design wind speed (m/s)	6
Swept area (m^2)	5
Blade airfoil	3 x NACA 0021
Rotor height (m)	2.5
Rotor diameter (m)	2
Solidity	0.2
Blade chord (m)	0.13
TSR	3
Rotational speed (rpm)	166

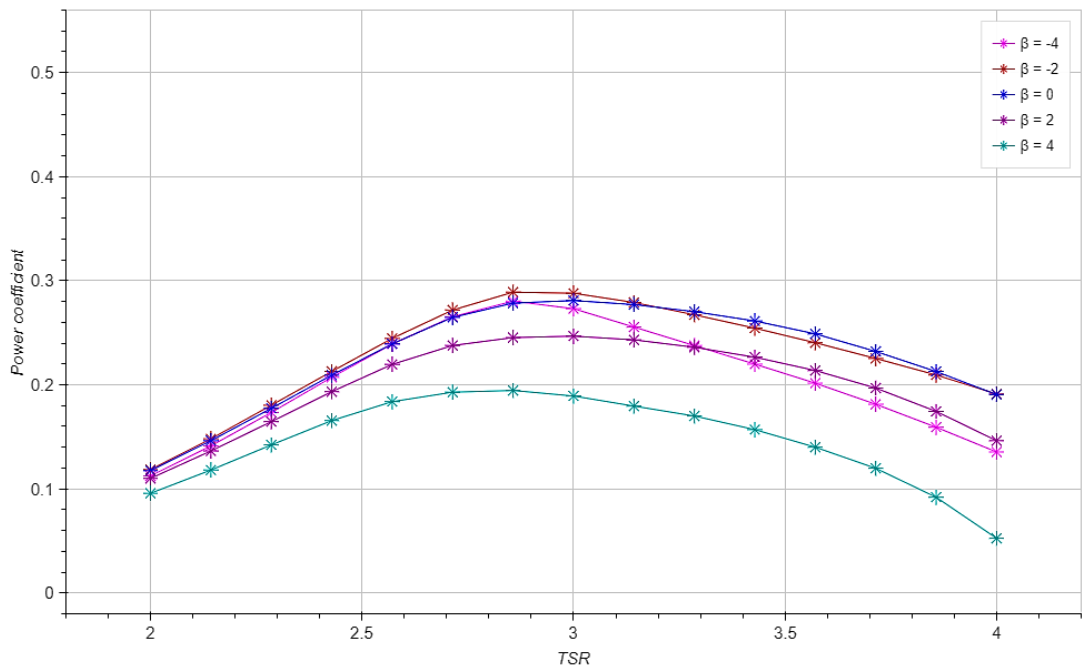


Figure 5.10. Performance curves for varied pitch angle at $V_{\infty} = 4 \text{ m/s}$

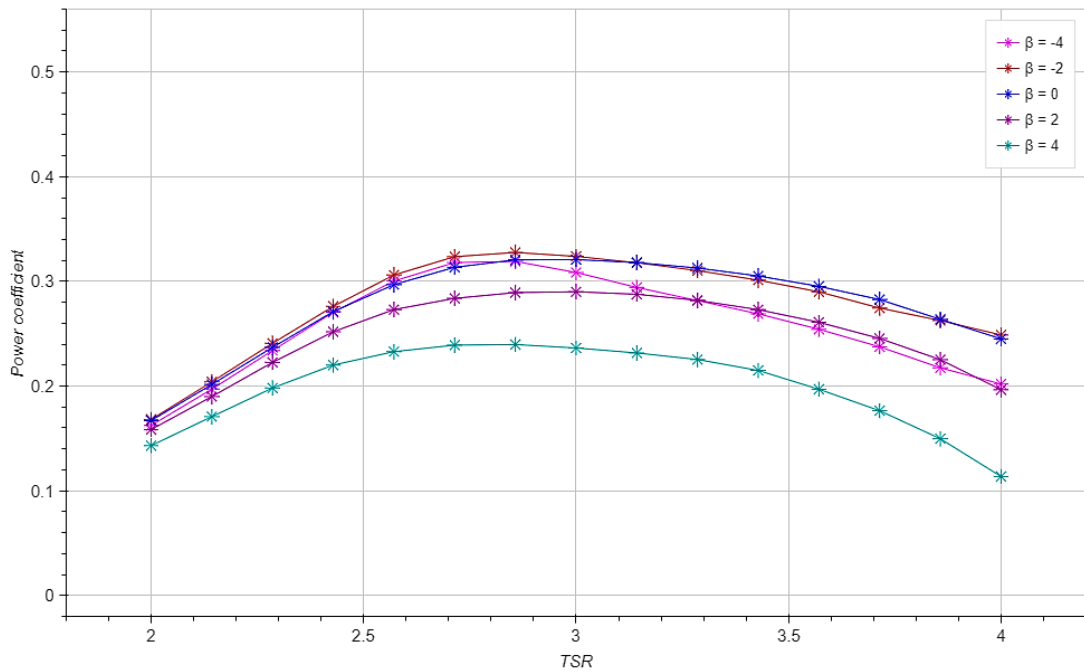


Figure 5.11. Performance curves for varied pitch angle at $V_{\infty} = 6 \text{ m/s}$

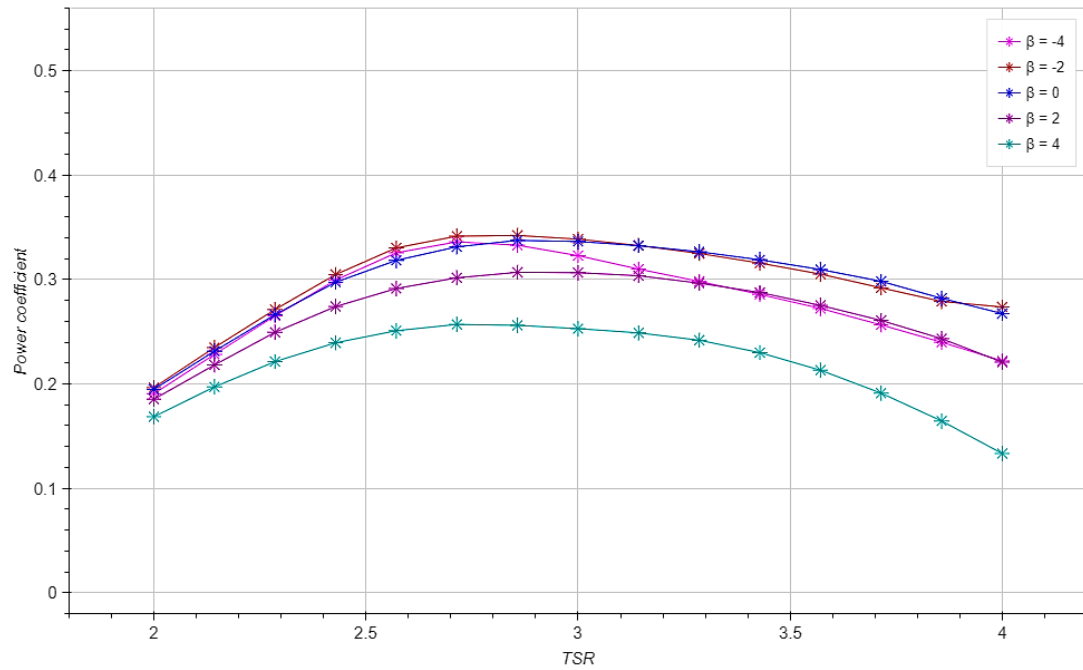


Figure 5.12. Performance curves for varied pitch angle at $V_\infty = 8 \text{ m/s}$

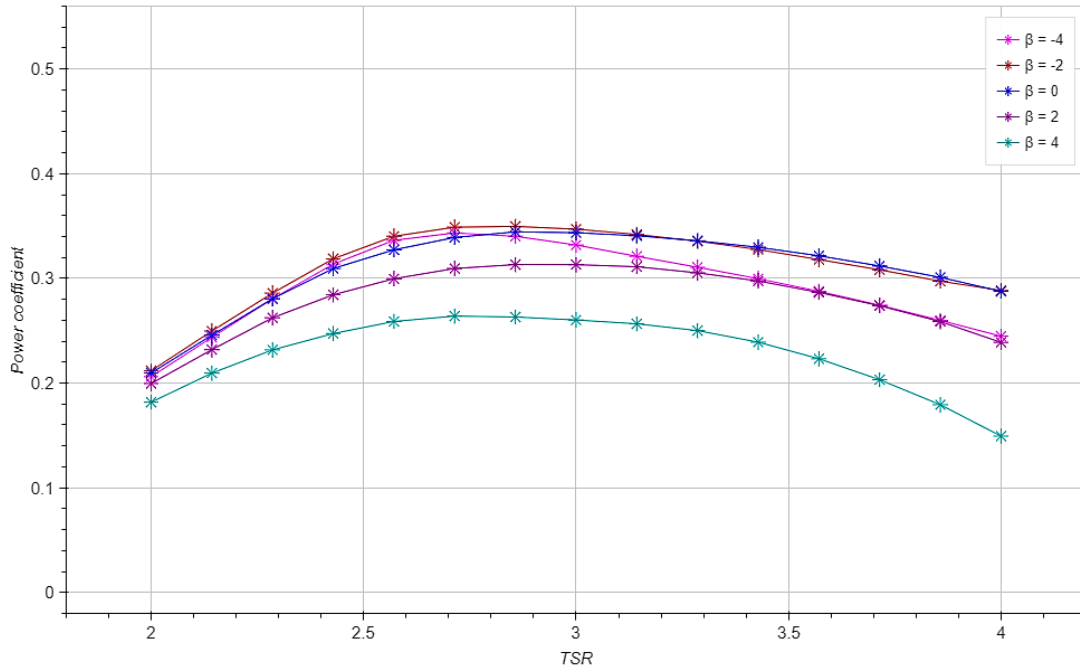


Figure 5.13. Performance curves for varied pitch angle at $V_\infty = 10 \text{ m/s}$

From the illustrations, when far-field velocity varies around design velocity value, preset pitching angle $\beta = -2^\circ$ (toe-out angle) produce the best performance when $TSR < 3$, and when $TSR > 3$, zero pitch angle $\beta = 0^\circ$ suggest a more decent power curve. Nonetheless, for $TSR > 3$, as free-stream velocity goes up to

10 m/s , the data gap between the graphs of $\beta = -2^\circ$ and $\beta = 0^\circ$ become marginal. Thus, with the fact that preset pitching angle β is fixed during the operation, $\beta = -2^\circ$ (toe-out) is the suggesting design blade pitching angle for the turbine.

Table 5.7. Final parameters for the turbine

Design wind speed (m/s)	6
Swept area (m ²)	5
Blade airfoil	3 x NACA 0021
Rotor height (m)	2.5
Rotor diameter (m)	2
Solidity	0.2
Blade chord (m)	0.13
TSR	3
Blade pitch angle (°)	-2 (toe-out)
Rotational speed (rpm)	166

Chapter 6. CONCLUSIONS

6.1 Achievements and Limitations

This thesis utilizes a straightforward and affordable approach to forecast the performance of VAWT by combining momentum theory with blade element method in three prevalent streamtube model. Finite aspect ratio effect is also taken into effect to enhance prediction accuracy. Beside the performance output, sub parameters of the turbine such as AOA, force coefficient, induction factor...could also available for structure analysis.

The results show decent agreement with experimental data to a certain degree, which would be beneficial for turbine designer for choosing turbine parameters and operating condition.

Besides accomplishments, there are still some limitations in the thesis.

- There only one secondary effect integrated in to the model
- The thesis doesn't have an alternative prediction model apart from streamtube models, so that there is no comparison between different kind of prediction model
- All the calculation process and stages are written in scripts of code so that it is require the user to have a specific amount of knowledge of coding and VAWT in order to utilize them.

6.2 Suggestions for Future Work

VAWT research direction is developing and the number of study into it is also rising. Thus improvement and advancement is always welcome and beneficial for the industry. Some of the thesis's suggestions for further work.

- Besides DMST, vortex model is known for its accuracy. Hence, vortex model should be study and compared with streamtube models.
- More comparisons with practical case test and other simulation to investigate the prediction models more comprehensive.
- There should be a User-friendly interface for the scripts to facilitate the utilization of the scripts

References

- [1] M. M. Bashar, “Computational and Experimental Study on Vertical Axis Wind Turbine in Search for an Efficient Design,” 2014.
- [2] GWEC, “Global Wind Report 2016,” 2017.
- [3] Embassy of the Kingdom of the Netherlands, “Renewable Energy in Vietnam,” no. Embassy of the Netherlands in Hanoi and Consulate General in Ho Chi Minh City, pp. 1–57.
- [4] F. M. for E. A. Energy, “Wind Energy in Vietnam,” no. Federal Ministry for Economic Affairs and Energy (BMWi) Public Relations, pp. 2014–2015, 2015.
- [5] S. Mathew, “Wind energy: Fundamentals, resource analysis and economics,” *Wind Energy: Fundamentals, Resource Analysis and Economics*. pp. 1–246, 2007.
- [6] M. M. Aslam Bhutta, N. Hayat, A. U. Farooq, Z. Ali, S. R. Jamil, and Z. Hussain, “Vertical axis wind turbine - A review of various configurations and design techniques,” *Renew. Sustain. Energy Rev.*, vol. 16, no. 4, pp. 1926–1939, 2012.
- [7] W. Tjiu, T. Marnoto, S. Mat, M. H. Ruslan, and K. Sopian, “Darrieus vertical axis wind turbine for power generation I: Assessment of Darrieus VAWT configurations,” *Renew. Energy*, vol. 75, pp. 50–67, 2015.
- [8] I. Paraschivoiu, *Wind Turbine Design with emphasis on Darrieus Concept*. Polytechnic International Press, 2002.
- [9] M. A. Biadgo, A. Simonović, D. Komarov, and S. Stupar, “Numerical and analytical investigation of vertical axis wind turbine,” *FME Trans.*, vol. 41, no. 1, pp. 49–58.
- [10] J. F. Manwell, J. G. McGowan, and A. L. Rogers, *Wind Energy Explained*.

2009.

- [11] L. H. Trong, “Development Of A Program For Designing Vertical Axis Wind Turbines,” Vietnam National University Ho Chi Minh City University Of Technology, 2016.
- [12] R. E. Sheldahl and P. C. Klimas, “Aerodynamic characteristics of seven symmetrical airfoil sections through 180-degree angle of attack for use in aerodynamic analysis of vertical axis wind turbines,” Albuquerque, NM, and Livermore, CA (United States), Mar. 1981.
- [13] E. Dyachuk, “Aerodynamics of Vertical Axis Wind Turbines - Development of Simulation Tools and Experiments,” Acta Universitatis Upsaliensis, 2015.
- [14] R. E. Akins, “Measurements of surface pressures on an operating vertical-axis wind turbine,” 1989.
- [15] A. Shires and Andrew, “Development and Evaluation of an Aerodynamic Model for a Novel Vertical Axis Wind Turbine Concept,” *Energies*, vol. 6, no. 5, pp. 2501–2520, May 2013.
- [16] M. Raciti Castelli, A. Englaro, and E. Benini, “The Darrieus wind turbine: Proposal for a new performance prediction model based on CFD,” *Energy*, vol. 36, no. 8, pp. 4919–4934, Aug. 2011.
- [17] A. Rezaeiha, I. Kalkman, and B. Blocken, “Effect of pitch angle on power performance and aerodynamics of a vertical axis wind turbine,” *Appl. Energy*, vol. 197, pp. 132–150, Jul. 2017.
- [18] M. Rossander *et al.*, “Evaluation of a Blade Force Measurement System for a Vertical Axis Wind Turbine Using Load Cells,” *Energies*, vol. 8, no. 6, pp. 5973–5996, Jun. 2015.
- [19] J. Kjellin, F. Bülow, S. Eriksson, P. Deglaire, M. Leijon, and H. Bernhoff, “Power coefficient measurement on a 12 kW straight bladed vertical axis wind turbine,” *Renew. Energy*, vol. 36, no. 11, pp. 3050–3053, Nov. 2011.

- [20] N. T. Tong, “Câu hỏi động cơ gió nộp trước khi thi - Lý thuyết tuabin gió trực đứng.” pp. 2–3, 2017.
- [21] P. C. Klimas and M. H. Worstell, “Effects of blade preset pitch/offset on curved-blade Darrieus vertical axis wind turbine performance,” *Sand-81-1762*, p. 15, 1981.
- [22] Y.-T. Lee and H.-C. Lim, “Power performance improvement of a 500W Vertical Axis Wind Turbine with salient design parameters,” *Int. J. Mech. Aerospace, Ind. Mechatron. Manuf. Eng.*, vol. 10, p. 40354, 2016.
- [23] B. Strom, S. Brunton, and B. Polagye, “Consequences of Preset Pitch Angle on Cross-Flow Turbine Hydrodynamics,” in *Proceedings of the 11th European Wave and Tidal Energy Conference*, 2015, no. 4, pp. 1–9.

Appendix

In this section, some scripts of code used for the calculation are presented. All the pieces of code were written in Python language.

Library required.

```
import numpy as np
from bokeh.plotting import output_file, show, figure
from bokeh.models import Title, Label, Legend
import bokeh.palettes as color
import xlwings as xw
from scipy import interpolate
from math import sqrt, degrees, pi, cos, sin, asin, tan, atan, radians, acos, e
from numpy import roots
from sympy.solvers import solve
from sympy import Symbol, simplify, expand, factor
```

Functions

```
# -*- coding: utf-8 -*-
"""
Created on Sat Nov 25 16:10:02 2017

@author: Mai Nguyen Van
"""
```

```
def newton(a,b,c,d):
    r1=0.1
    r2=0
    i=0
    Fa=lambda r:a**r**3+b**r**2+c*r+d
    fa=lambda r:3*a**r**2+2*b*r+c
    if d<-4: return 0
    elif d<-2: return 0.5
    elif d>0: return 0
    while abs(r2-r1)>0.001:
```

```

r1=r2
r2=r1- (Fa(r1) /fa(r1) )
#print(r2)
i+=1
if i>100:
    break
return r2
#####
###'
def bisec(a,b,c,d):
    i=0
    low=0
    high=1
    r1=0;r2=1
    while abs(r2-r1)>0.0001:
        r1=r2
        r2=(low+high)/2
        value=lambda x:a*x**3+b*x**2+c*x+d
        if value(r2)*value(low)<0:
            high=r2
        elif value(r2)*value(high)<0:
            low=r2
        else:
            if abs(value(low))<abs(value(high)):
                r2=low;break
            else: r2=high;break
    return r2
#####
##'
def cuctieuSMST(tta,z):
    a_range=np.linspace(0,1,200).tolist()
    Devi=[]
    for a1 in a_range:
        aoa=atan(( (1-a1)*cos(tta) ) / (TSR-(1-a1)*sin(tta)))+radians(beta)
        if (z*sin(abs(aoa)))==0 : F=1
        else:
            f=(N/2)*(1-z)/(z*sin(abs(aoa)))

```

```

F=2/pi*acos(e**(-f))

w7uinf=sqrt((TSR-(1-a1)*sin(tta))**2+((1-a1)*F*cos(tta))**2)
aoa=atan(((1-a1)*F*cos(tta))/(TSR-(1-
a1)*sin(tta)))+radians(beta)

re=w7uinf*uinf*c/v
cl=noisuyCL(re,degrees(abs(aoa)))
if aoa>0: cl=cl[0]
else: cl=-cl[0]
cl=cl/(1+a0/(pi*AR))
cd=noisuyCD(re,degrees(abs(aoa)))
cd=cd[0]+cl**2/(pi*AR)

cn=cl*cos(aoa)+cd*sin(aoa)
ct=cl*sin(aoa)-cd*cos(aoa)
cti=cn*cos(tta)+ct*sin(tta)
cpi=ct*TSR/w7uinf

d=(2*solidity/(1*pi))*w7uinf**2*(cti/abs(cos(tta)))
d1=(3*a1**3-5*a1**2+4*a1)*F
devi=abs(d-d1)
Devi.append(devi)
point=Devi.index(min(Devi))
return a_range[point]
#####
##'

def cuctieuDMSTup(tta,z):
    a_range=np.linspace(0,1,200).tolist()
    Devi=[]
    for a1 in a_range:
        aoa=atan(((1-a1)*cos(tta))/(TSR-(1-
a1)*sin(tta)))+radians(beta)

        if (z*sin(abs(aoa)))==0 : F=1
        else:
            f=(N/2)*(1-z)/(z*sin(abs(aoa)))
            F=2/pi*acos(e**(-f))

```

```

w7uinf=sqrt( (TSR-(1-a1)*sin(tta) )**2+( (1-a1)*F*cos(tta) )**2)
aoa=atan( ( (1-a1)*F*cos(tta) ) / (TSR-(1-
a1)*sin(tta) )+radians(beta)

re=w7uinf*uinf*c/v
cl=noisuyCL(re,degrees(abs(aoa)))
if aoa>0: cl=cl[0]
else: cl=-cl[0]
cl=cl/(1+a0/(pi*AR))
cd=noisuyCD(re,degrees(abs(aoa)))
cd=cd[0]+cl**2/(pi*AR)

cn=cl*cos(aoa)+cd*sin(aoa)
ct=cl*sin(aoa)-cd*cos(aoa)
cti=cn*cos(tta)+ct*sin(tta)
cpi=ct*TSR/w7uinf

d=(1*solidity/(1*pi))*w7uinf**2*(cti/abs(cos(tta)))
d1=(3*a1**3-5*a1**2+4*a1)*F
devi=abs(d-d1)
Devi.append(devi)
point=Devi.index(min(Devi))
return a_range[point]
#####
##'

def cuctieuDMSTdw(tta,z):
    a_range=np.linspace(0,1,200).tolist()
    Devi=[]
    for a1 in a_range:
        TSRdw=TSR/(1-2*a)
        aoa=atan( ( (1-a1)*cos(tta) ) / (TSRdw-(1-
a1)*sin(tta) )+radians(beta)

        if (z*sin(abs(aoa)) )==0 : F=1
        else:
            f=(N/2)*(1-z)/(z*sin(abs(aoa)))
            F=2/pi*acos(e**(-f))

    w7uw=sqrt( (TSRdw-(1-a1)*sin(tta) )**2+( (1-a1)*F*cos(tta) )**2)

```

```

aoa=atan( ((1-a1)*F*cos(tta)) / (TSRdw- (1-
a1)*sin(tta) ) )+radians(beta)

uw=uinf*(1-2*a)
re=w7uw*uw*c/v

cl=noisuyCL(re, degrees(abs(aoa)))
if aoa>0: cl=cl[0]
else: cl=-cl[0]
cl=cl/(1+a0/(pi*AR))
cd=noisuyCD(re, degrees(abs(aoa)))
cd=cd[0]+cl**2/(pi*AR)

cn=cl*cos(aoa)+cd*sin(aoa)
ct=cl*sin(aoa)-cd*cos(aoa)

cti=cn*cos(tta)+ct*sin(tta)
cpi=ct*TSRdw/w7uw

d=(solidity/pi)*(cti*w7uw**2)/(abs(cos(tta)))

d1=(3*a1**3-5*a1**2+4*a1)*F
devi=abs(d-d1)
Devi.append(devi)
point=Devi.index(min(Devi))
return a_range[point]
'#####
##'
def addlist(a,b):
    if len(a)==0 :return b
    c=[];
    for ind in range(len(a)):
        c.append(a[ind]+b[ind])
    return c
'#####
##'
def devlist(a,b):
    c=[]
    for ind in range(len(a)):
        c.append(a[ind]/b)

```

```

    return c

'#####
##'

def atube(a,b):
    c=[];
    for j in range(len(a)):
        ci=0.5-((1-2*a[j])*(1-2*b[j])/2)
        c.append(ci)
    return c

'#####
##'

def ghep(a,b):
    b[0]=a[0]
    b[-1]=a[-1]
    b.reverse()
    c=a+b

    return c

```

Single Streamtube model

```

# -*- coding: utf-8 -*-
"""

Created on Mon Nov 27 23:17:20 2017

@author: Mai Nguyen Van
"""

Ttaup=np.linspace(-pi/2, pi/2, 22).tolist()
Ttadw=np.linspace(pi/2, 3*pi/2, 22).tolist()
Ttadw.reverse();Ttadw.pop(0);Ttadw.pop(-1)
'#####

def run(tta,a1,TSR,z):
    global F

    w7uinf=sqrt((TSR-(1-a1)*sin(tta))**2+((1-a1)*cos(tta))**2)
    aoa=atan(((1-a1)*cos(tta))/(TSR-(1-
a1)*sin(tta)))+radians(beta)

    if (z*sin(abs(aoa)))==0 : F=1
    else:
        f=(N/2)*(1-z)/(z*sin(abs(aoa)))
        F=2/pi*acos(e**(-f))

```

```

w7uinf=sqrt( (TSR- (1-a1)*sin(tta) ) **2+ ( (1-a1)*F*cos (tta) ) **2)
aoa=atan( ((1-a1)*F*cos (tta) ) / (TSR- (1-
a1)*sin (tta) ) )+radians(beta)

re=w7uinf*uinf*c/v
cl=noisuyCL(re,degrees(abs(aoa)))
if aoa>0: cl=cl[0]
else: cl=-cl[0]
cl=cl/(1+a0/(pi*AR))
cd=noisuyCD(re,degrees(abs(aoa)))
cd=cd[0]+cl**2/(pi*AR)

cn=cl*cos(aoa)+cd*sin(aoa)
ct=cl*sin(aoa)-cd*cos(aoa)

cti=cn*cos(tta)+ct*sin(tta)
cpi=ct*TSR/w7uinf

cp=cpi*w7uinf**3
cf=cti*w7uinf**2

AOA.append(degrees(aoa))
Cti.append(cti)
Re.append(re)
CN.append(cn)
CT.append(ct)
W7uinf.append(w7uinf)
CP.append(cp)
CF.append(cf)
return

#####
# ITERATION #####
power=[];Loop=[];CFN=[]
for j in range(len(TSR_range)):
    TSR=TSR_range[j]
    print('TSR =',TSR)
    CP_tl=[]
    for alt in range(len(z_range)):
        a1=0.1
        a2=0
        loop=0
        z=z_range[alt]
        while abs(a2-a1)>0.0001:
            a1=a2
            CF=[];CP=[];AOA=[];Cti=[];W7uinf=[];Re=[];CN=[];CT=[]
            for i in range(len(Tta)):
                run(Tta[i],a1,TSR,z)
            CPn=solidity*sum(CP)/len(CP)
            CFn=solidity*sum(CF)/len(CF)
            a2=gpt(3,-5,4,-CFn/F)
            loop+=1
            if loop>100:
                a_range=np.linspace(0,1,200).tolist()
                Devi=[]
                for a1 in a_range:
                    CF=[ ] ; CP=[ ] #;AOA=[ ] ; Cti=[ ] ; W7uinf=[ ] ; Re=[ ] ; CN=[ ] ; CT=[ ]

```

```

        for i in range(len(Tta)):
            run(Tta[i],a1,TSR,z)
            CFn=solidity*sum(CF)/len(CF)
            d1=(3*a1**3-5*a1**2+4*a1)*F
            devi=abs(d1-CFn)
            Devi.append(devi)
        point=Devi.index(min(Devi))
        a1=a_range[point]
        CF=[];CP=[];AOA=[];Cti=[];W7uinf=[];Re=[];CN=[];CT=[]
        for i in range(len(Tta)):
            run(Tta[i],a1,TSR,z)
            CPn=solidity*sum(CP)/len(CP)
            CFn=solidity*sum(CF)/len(CF)
            break
        CP_tl.append(CPn)
        CPn=sum(CP_tl)/len(CP_tl)
        power.append(CPn)
        CFN.append(CFn)
        Loop.append(loop)
    
```

Multiple Streamtube Model

```
# -*- coding: utf-8 -*-
```

```
"""
```

Created on Tue Nov 28 13:09:14 2017

@author: Mai Nguyen Van

```
"""
```

```

Ttaup=np.linspace(-pi/2, pi/2, 22).tolist()
Ttadw=np.linspace(pi/2, 3*pi/2, 22).tolist()
' #####'
def runup(tta, TSR, solidity, z):
    a1=0.1
    a2=0
    loop=0
    while abs(a2-a1)>0.0001:
        a1=a2
        aoa=atan(((1-a1)*cos(tta))/(TSR-(1-
a1)*sin(tta)))+radians(beta)

        if (z*sin(abs(aoa)))==0 : F=1
        else:
            f=(N/2)*(1-z)/(z*sin(abs(aoa)))
            F=2/pi*acos(e**(-f))

        w7uinf=sqrt((TSR-(1-a1)*sin(tta))**2+((1-a1)*F*cos(tta))**2)
        aoa=atan(((1-a1)*F*cos(tta))/(TSR-(1-
a1)*sin(tta)))+radians(beta)

        re=w7uinf*uinf*c/v
        cl=noisuyCL(re, degrees(abs(aoa)))
    
```

```

if aoa>0: cl=cl[0]
else: cl=-cl[0]
cl=cl/(1+a0/(pi*AR))
cd=noisuyCD(re,degrees(abs(aoa)))
cd=cd[0]+cl**2/(pi*AR)

cn=cl*cos(aoa)+cd*sin(aoa)
ct=cl*sin(aoa)-cd*cos(aoa)
cti=cn*cos(tta)+ct*sin(tta)
cpi=ct*TSR/w7uinf

d=(2*solidity/(1*pi))*w7uinf**2*(cti/abs(cos(tta)))
a2=gpt(3*F,-5*F,4*F,-d)
loop+=1
if loop>100:
    a2=cuctieuSMST(tta,z)
    a1=a2
    aoa=atan(((1-a1)*cos(tta))/(TSR-(1-
a1)*sin(tta))+radians(beta))

    if (z*sin(abs(aoa)))==0 : F=1
    else:
        f=(N/2)*(1-z)/(z*sin(abs(aoa)))
        F=2/pi*acos(e**(-f))

w7uinf=sqrt((TSR-(1-a1)*sin(tta))**2+(1-
a1)*F*cos(tta)**2)
aoa=atan(((1-a1)*F*cos(tta))/(TSR-(1-
...a1)*sin(tta))+radians(beta))

re=w7uinf*uinf*c/v
cl=noisuyCL(re,degrees(abs(aoa)))
if aoa>0: cl=cl[0]
else: cl=-cl[0]
cl=cl/(1+a0/(pi*AR))
cd=noisuyCD(re,degrees(abs(aoa)))
cd=cd[0]+cl**2/(pi*AR)

cn=cl*cos(aoa)+cd*sin(aoa)
ct=cl*sin(aoa)-cd*cos(aoa)
cti=cn*cos(tta)+ct*sin(tta)
cpi=ct*TSR/w7uinf
break

cp=cpi*w7uinf**3
cf=cti*w7uinf**2

AOA.append(degrees(aoa))
CF.append(cf)
CT.append(ct)
CN.append(cn)
Loop.append(loop)
A.append(a2)
CP.append(cp)
D.append(d)
Re.append(re)

```

```

    return
'#####'
for soli in range(len(soli_range)) :
    solidity=soli_range[soli]
    CPn=[]
    for tsr in range(len(TSR_range)) :
        TSR=TSR_range[tsr]
        print('TSR =',TSR)
        CP_tl=[];CN_tl=[]
        for z in z_range:
            CN=[];CT=[];Loop=[];A=[];CP=[];CF=[];AOA=[];D=[];Re=[]
            for k in range(len(Ttaup)):
                runup(Ttaup[k],TSR,solidity,z)
                #Cp+=solidity*W7uinf[k]**3*Cpi[k]/len(Ttaup)
                Cf=solidity*(sum(CF)/len(CF))
                Cp=solidity*(sum(CP)/len(CP))
                CP_tl.append(Cp)
                CN_tl=addlist(CN_tl,CN)

            Cp=sum(CP_tl)/len(CP_tl)
            CN_tl=devlist(CN_tl,len(z_range))
            CPn.append(round(Cp,5))

'##### plots #####
colors=['blue','green','darkmagenta','darkcyan','olive','darkred','lime','cyan','magenta','black','brown','gold']
mau=colors[2]

p1.triangle(TSR_range,CPn,legend='Multiple Streamtube',line_color=mau,fill_color=None,alpha=3,size=13)
p1.line(TSR_range,CPn,legend='Multiple Streamtube',line_color=mau,alpha=3,line_width=1)
show(p1)

```

Double Multiple Streamtube

```

# -*- coding: utf-8 -*-
"""
Created on Tue Nov 28 14:32:30 2017

@author: Mai Nguyen Van
"""

Ttaup=np.linspace(-pi/2, pi/2, 30).tolist()
Ttadw=np.linspace(pi/2, 3*pi/2, 30).tolist()
Ttadw.reverse();'#####function tính upwind factor
#####
def upfactor(tta,TSR,solidity):
    i=0
    a1=0.1
    a2=0
    while abs(a2-a1)>0.0001:
        a1=a2
        aoa=atan(((1-a1)*cos(tta))/(TSR-(1-
a1)*sin(tta)))+radians(beta)

        if (z*sin(abs(aoa)))==0 : F=1
        else:
            f=(N/2)*(1-z)/(z*sin(abs(aoa)))

```

```

F=2/pi*acos(e**(-f))

w7uinf=sqrt((TSR-(1-a1)*sin(tta))**2+((1-a1)*F*cos(tta))**2)
aoa=atan(((1-a1)*F*cos(tta))/(TSR-(1-
a1)*sin(tta)))+radians(beta)

re=w7uinf*uinf*c/v
cl=noisuyCL(re,degrees(abs(aoa)))
if aoa>0: cl=cl[0]
else: cl=-cl[0]
cl=cl/(1+a0/(pi*AR))
cd=noisuyCD(re,degrees(abs(aoa)))
cd=cd[0]+cl**2/(pi*AR)

cn=cl*cos(aoa)+cd*sin(aoa)
ct=cl*sin(aoa)-cd*cos(aoa)

cti=cn*cos(tta)+ct*sin(tta)
cpi=ct*TSR/w7uinf

d=(1*solidity/(1*pi))*w7uinf**2*(cti/abs(cos(tta)))
a2=gpt(3*F,-5*F,4*F,-d)
i+=1
if i>100:
    a2=cuctieuDMSTup(tta,z)
    a1=a2
    aoa=atan(((1-a1)*cos(tta))/(TSR-(1-
a1)*sin(tta)))+radians(beta)

    if (z*sin(abs(aoa)))==0 : F=1
    else:
        f=(N/2)*(1-z)/(z*sin(abs(aoa)))
        F=2/pi*acos(e**(-f))

w7uinf=sqrt((TSR-(1-a1)*sin(tta))**2+((1-
a1)*F*cos(tta))**2)
aoa=atan(((1-a1)*F*cos(tta))/(TSR-(1-
...a1)*sin(tta)))+radians(beta)

re=w7uinf*uinf*c/v
cl=noisuyCL(re,degrees(abs(aoa)))
if aoa>0: cl=cl[0]
else: cl=-cl[0]
cl=cl/(1+a0/(pi*AR))
cd=noisuyCD(re,degrees(abs(aoa)))
cd=cd[0]+cl**2/(pi*AR)

cn=cl*cos(aoa)+cd*sin(aoa)
ct=cl*sin(aoa)-cd*cos(aoa)
cti=cn*cos(tta)+ct*sin(tta)
cpi=ct*TSR/w7uinf
break

dti=cti*w7uinf**2

```

```

dpi=cpi*w7uinf**3
AOA.append(aoa)
CN.append(cn)
CT.append(ct)
Aup.append(a2)
loop.append(i)
Dti.append(dt)
Dpi.append(dpi)
CD.append(cd)
W7uinf.append(w7uinf)
return

' ##### DOWN WIND #####
def dwfactor(tta,a,TSR,solidity):
    w7uw=0;aoa=0;cl=0;cd=0;cn=0;ct=0
    cti=0;cpi=0;d=0;i=0
    a1=0
    a2=a
    while abs(a2-a1)>0.0001:
        a1=a2
        TSRdw=TSR/(1-2*a)
        aoa=atan(((1-a1)*cos(tta))/(TSRdw-(1-
a1)*sin(tta)))+radians(beta)

        if (z*sin(abs(aoa)))==0: F=1
        else:
            f=(N/2)*(1-z)/(z*sin(abs(aoa)))
            F=2/pi*acos(e**(-f))

        w7uw=sqrt((TSRdw-(1-a1)*sin(tta))**2+((1-a1)*F*cos(tta))**2)
        aoa=atan(((1-a1)*F*cos(tta))/(TSRdw-(1-
a1)*sin(tta)))+radians(beta)

        uw=uinf*(1-2*a)
        re=w7uw*uw*c/v

        cl=noisyCL(re,degrees(abs(aoa)))
        if aoa>0: cl=cl[0]
        else: cl=-cl[0]
        cl=cl/(1+a0/(pi*AR))
        cd=noisyCD(re,degrees(abs(aoa)))
        cd=cd[0]+cl**2/(pi*AR)

        cn=cl*cos(aoa)+cd*sin(aoa)
        ct=cl*sin(aoa)-cd*cos(aoa)

        cti=cn*cos(tta)+ct*sin(tta)
        cpi=ct*TSRdw/w7uw

        d=(solidity/pi)*(cti*w7uw**2)/(abs(cos(tta)))
        a2=gpt(3*F,-5*F,4*F,-d)
        i+=1
        if i>100:
            a2=cuctieuDMSTdw(tta,z)
            a1=a2

```

```

TSRdw=TSR/(1-2*a)
aoa=atan(((1-a1)*cos(tta))/(TSRdw-(1-
...a1)*sin(tta)))+radians(beta)

if (z*sin(abs(aoa)))==0 : F=1
else:
    f=(N/2)*(1-z)/(z*sin(abs(aoa)))
    F=2/pi*acos(e**(-f))

w7uw=sqrt((TSRdw-(1-a1)*sin(tta))**2+((1-
a1)*F*cos(tta))**2)
aoa=atan(((1-a1)*F*cos(tta))/(TSRdw-(1-
...a1)*sin(tta)))+radians(beta)

uw=uinf*(1-2*a)
re=w7uw*uw*c/v

cl=noisuyCL(re,degrees(abs(aoa)))
if aoa>0: cl=cl[0]
else: cl=-cl[0]
cl=cl/(1+a0/(pi*AR))
cd=noisuyCD(re,degrees(abs(aoa)))
cd=cd[0]+cl**2/(pi*AR)

cn=cl*cos(aoa)+cd*sin(aoa)
ct=cl*sin(aoa)-cd*cos(aoa)

cti=cn*cos(tta)+ct*sin(tta)
cpi=ct*TSRdw/w7uw
break

dti=cti*(w7uw*(1-2*a))**2
dpi=cpi*(w7uw*(1-2*a))**3
AOAdw.append(aoa)
CNDw.append(cn)
CTdw.append(ct)
Adw.append(a2)
loopdw.append(i)
Dtiddw.append(dti)
Dpidw.append(dpi)
CDDdw.append(cd)
W7uw.append(w7uw)
return

#####
# tinh toán upwind #####
for soli in range(len(soli_range)):
    solidity=soli_range[soli]
    CPtt=[]
    for tsr in range(len(TSR_range)):
        TSR=TSR_range[tsr]
        print('TSR =',TSR)
        CP_tl=[];CT_tl=[];CTdw_tl=[];
        CN_tl=[];CNDw_tl=[]

        CD_tl=[];W7uinf_tl=[];Aup_tl=[];
        CDDdw_tl=[];W7uw_tl=[];Adw_tl=[];

```

```

for z in z_range:
    AOA=[];CN=[];CT=[];Aup=[];loop=[];Dti=[];Dpi=[];
    W7uinf=[];CD=[];
    for i in range(len(Ttaup)):
        upfactor(Ttaup[i],TSR,solidity)
    CF1=solidity*(sum(Dti)/len(Dti))
    CP1=solidity*(sum(Dpi)/len(Dpi))

    CT_tl=addlist(CT_tl,CT)
    CN_tl=addlist(CN_tl,CN)
    W7uinf_tl=addlist(W7uinf_tl,W7uinf)
    CD_tl=addlist(CD_tl,CD)
    Aup_tl=addlist(Aup_tl,Aup)

    ' ##### tinh toán downwind ######'

AOAdw=[];CNDw=[];CTdw=[];Adw=[];loopdw=[];Dtiddw=[];Dpidw=[]
W7uw=[];CDdw=[];
for j in range(len(Ttadw)):
    tta=Ttadw[j]
    a=Aup[j]
    dwfactor(tta,a,TSR,solidity)
    CF2=solidity*(sum(Dtidw)/len(Dtidw))
    CP2=solidity*(sum(Dpidw)/len(Dpidw))

    CFn=(CF1+CF2)/2
    CPn=(CP1+CP2)/2

    CP_tl.append(CPn)
    CTdw_tl=addlist(CTdw_tl,CTdw)
    CNDw_tl=addlist(CNDw_tl,CNDw)
    W7uw_tl=addlist(W7uw_tl,W7uw)
    CDdw_tl=addlist(CDdw_tl,CDdw)
    Adw_tl=addlist(Adw_tl,Adw)

    CT_tl=devlist(CT_tl,len(z_range))
    CTdw_tl=devlist(CTdw_tl,len(z_range))
    CN_tl=devlist(CN_tl,len(z_range))
    CNDw_tl=devlist(CNDw_tl,len(z_range))

    W7uinf_tl=devlist(W7uinf_tl,len(z_range))
    CD_tl=devlist(CD_tl,len(z_range))
    Aup_tl=devlist(Aup_tl,len(z_range))

    W7uw_tl=devlist(W7uw_tl,len(z_range))
    CDdw_tl=devlist(CDdw_tl,len(z_range))
    Adw_tl=devlist(Adw_tl,len(z_range))

    CPn=sum(CP_tl)/len(CP_tl)
    CPtt.append(CPn)

```

```
colors=['blue','green','darkmagenta','orangered','darkcyan','olive','darkred','lime','cyan','magenta','black','brown','gold']
mau=colors[3]
p1.asterisk(TSR_range,CPtt,legend='D-Multiple Streamtube',line_color=mau,fill_color=None,alpha=3,size=13)
p1.line(TSR_range,CPtt,legend='D-Multiple Streamtube',line_color=mau,alpha=3,line_width=1)
show(p1)
```

Data Visualization

```
output_file("Visualization.html")
p1=figure(x_range=(0, 8),
           y_range=(-0.02, 0.56),
           plot_width=1000)
p1.title.align="center"
p1.title.text_font_size = "25px"
p1.xaxis[0].axis_label = 'TSR'
p1.yaxis[0].axis_label = 'Power coefficient'

p1.xaxis[0].axis_label_text_font_size ="15px"
p1.yaxis[0].axis_label_text_font_size ="15px"
p1.xaxis[0].major_label_text_font_size ="15px"
p1.yaxis[0].major_label_text_font_size ="15px"

p3=figure(x_range=(0, 8),
           y_range=(0, 1),
           plot_width=1000)
p3.title.align="center"
p3.title.text_font_size = "25px"
p3.xaxis[0].axis_label = 'TSR'
p3.yaxis[0].axis_label = 'solidity'

p3.xaxis[0].axis_label_text_font_size ="15px"
p3.yaxis[0].axis_label_text_font_size ="15px"
p3.xaxis[0].major_label_text_font_size ="15px"
p3.yaxis[0].major_label_text_font_size ="15px"
```